Charles University in Prague

Faculty of Mathematics and Physics

DOCTORAL THESIS

Mgr. Zuzana Rulfová

Frequency analysis of precipitation amounts

Department of Atmospheric Physics

Supervisor of the doctoral thesis: RNDr. Jan Kyselý, Ph.D.

Study programme: Physics

Specialization: Meteorology and Climatology

Praha 2016

I declare that I carried out this doctoral thesis independently, and only with the cited sources, literature and other professional sources.

I understand that my work relates to the rights and obligations under the Act No. 121/2000 Coll., the Copyright Act, as amended, in particular the fact that the Charles University in Prague has the right to conclude a license agreement on the use of this work as a school work pursuant to Section 60 paragraph 1 of the Copyright Act.

In Prague date May 26, 2016 Mgr. Zuzana Rulfová

Název práce: Frekvenční analýza srážkových úhrnů

Autor: Mgr. Zuzana Rulfová

Katedra: Katedra fyziky atmosféry

Vedoucí disertační práce: RNDr. Jan Kyselý, Ph.D., Ústav fyziky atmosféry

AV ČR, v.v.i.

Abstrakt: Práce se zabývá studiem charakteristik průměrných a extrémních srážek v pozorovaných datech a regionálních klimatických modelech s ohledem na jejich konvekční a vrstevnatý původ. Na základě informací o stavu počasí a typu oblačnosti z dat SYNOP byl navržen a otestován algoritmus na rozlišení srážek na převážně konvekční a vrstevnaté. Časové řady 6-hodinových úhrnů konvekčních a vrstevnatých srážek pro oblast České republiky z let 1982–2010 byly použity pro analýzu základních klimatologických charakteristik srážek, včetně extrémů, a pro validaci regionálních klimatických modelů pocházejících z projektu ENSEMBLES. Budoucí změny konvekčních a vrstevnatých srážek ve střední Evropě (v České republice) byly analyzovány na základě regionálních klimatických modelů z projektu EURO-CORDEX. V poslední části práce je zaveden nový statistický model pro analýzu extrémů srážek, který využívá informaci o původu extrémů, tedy zda se jedná o srážky z konvekční nebo vrstevnaté oblačnosti. Do budoucna lze očekávat nárůst konvekčních a vrstevnatých srážek ve všech sezónách kromě léta, kdy podle simulací klimatických modelů mají vrstevnaté srážky klesat. Extrémní srážky budou intenzivnější bez ohledu na jejich původ a větší nárůst intenzity se očekává v případě vyššího nárůstu teploty. Nárůst podílu konvekčních srážek v létě a obecně vyšší intenzita srážek může mít významné důsledky pro půdní erozi nebo výskyt bleskových povodní.

Klíčová slova: konvekční srážky, vrstevnaté srážky, regionální klimatické modely, extrémy, střední Evropa

Title: Frequency analysis of precipitation amounts

Author: Mgr. Zuzana Rulfová

Department: Department of Atmospheric Physics

Supervisor: RNDr. Jan Kyselý, Ph.D., Institute of Atmospheric Physics CAS

Abstract: This thesis deals with analysing characteristics of mean and extreme precipitation in observations and regional climate models (RCMs) with respect to their convective and stratiform origin. An algorithm for subdivision of precipitation amounts into predominantly convective and stratiform using station weather data is proposed and evaluated. The time series of convective and stratiform precipitation from the Czech Republic over 1982–2010 are used for analysing basic climatological characteristics of precipitation, including extremes, and evaluating RCMs from the ENSEMBLES project. Projected changes of convective and stratiform precipitation in Central Europe (the Czech Republic) are analysed using data from RCM simulations from the EURO-CORDEX project. The last part of the thesis introduces a new statistical model for analysing precipitation extremes. This model takes advantage from knowledge of origin of precipitation extremes. In future climate we could expect more convective and stratiform precipitation amounts in all seasons except summer, when climate models project decline in amounts of stratiform precipitation. Extreme precipitation is projected to increase for both convective and stratiform precipitation, and more extremes are expected with a larger increase of temperature. An increasing proportion of convective precipitation in summer and generally growing intensity of precipitation may have important implications for soil erosion and occurrence of flash floods.

Keywords: convective precipitation, stratiform precipitation, regional climate models, extremes, Central Europe

First of all, I am grateful to my supervisor, Jan Kyselý, for the careful scientific guidance of my work. I thank the Institute of Atmospheric Physics for creating excellent conditions for my scientific work. The study was supported under projects GAP209/10/2045 and GA14-18675S funded by the Czech Science Foundation, by the European Social Fund and the Ministry of Education of the Czech Republic under project CZ.1.07/2.3.00/20.0086, and by GAUK No. 851713. Part of the work was carried out while working in a Visiting Scientist position at Royal Netherlands Meteorological Institute (KNMI). I would like, therefore, to give special thanks to Adri Buishand and Martin Roth from KNMI. Finally, I am grateful to Mykhaylo for his support and patience.

Contents

Introduction

Motivation

Characteristics of precipitation extremes are important in many practical applications, including hydrological modelling, design of hydraulic structures, urban planning, and others. Numerous studies have examined the distributions of precipitation extremes in observed data and climate model simulations, using methods of local or regional frequency analysis of different complexity (e.g., Stewart et al., 1999; Hanel et al., 2009; Svensson and Jones, 2010a). One of the main assumptions of extreme value theory is that the maxima belong to the same population (e.g., Coles, 2001). This assumption is not fulfilled for extreme precipitation in mid-latitudes, however, as this is caused by different physical mechanisms. Precipitation extremes arise from convective processes at small spatial scales (convective precipitation) or from cloud belts associated with cyclones and atmospheric fronts at larger scales (stratiform precipitation).

The classification of precipitation into convective and stratiform is useful not only in the analysis of extremes but also in a variety of meteorological and climatological applications. It is important in understanding cloud physics, for instance, as these types are associated with different precipitation growth mechanisms. Furthermore, subdivided precipitation data can be used for evaluating climate models which simulate convective (subgrid) and stratiform (large-scale) precipitation separately through cumulus and large-scale precipitation parameterizations (Dai, 2006), as well as for analysing climate change effects on precipitation patterns.

Many studies focusing on European precipitation changes agree with the general intensification of precipitation, predominantly increasing trends in mean precipitation in northern Europe, and decreasing trends in the south (e.g., Frei et al., 2006; Boberg et al., 2010; Heinrich and Gobiet, 2012; Rajczak et al., 2013). Central Europe (and the Czech Republic) lies in a transition zone between increasing and decreasing precipitation trends.

The possible influence of global warming on change in the ratio of convective and stratiform precipitation has been discussed in many studies (e.g., Lenderink and van Meijgaard, 2008, 2010; Haerter and Berg, 2009; Fischer et al., 2015). Convective precipitation increases with temperature faster than does stratiform precipitation, as

shown, for example, by Berg et al. (2013) for observed data in Germany, and the ratio of seasonal convective precipitation amount to the total precipitation amount tends to be higher in future climate projections in all seasons when convective precipitation plays an important role (i.e., spring, summer, and autumn), as shown by Fischer et al. (2015) for Switzerland.

Extreme precipitation is thought to increase with warming at rates similar to or greater than that of the water vapour holding capacity of air, which is ~ 7% per 1°C, the so-called Clausius–Clapeyron (CC) rate (Trenberth et al., 2003). This rate seems to be dependent on the time scale corresponding to the origin of precipitation extremes. Analyses of precipitation data at sub-daily resolution generally show higher (so called super-CC) rates of increase in intensity with temperature (e.g., Allan and Soden, 2008; Lenderink and van Meijgaard, 2008, 2010; Lenderink et al., 2011; Loriaux et al., 2013). These super-CC rates are caused by a mixing of storm types, with stratiform lower-intensity precipitation at low temperatures and convective higher-intensity precipitation at high temperatures (Haerter and Berg, 2009; Berg et al., 2013). Molnar et al. (2015) showed for observed data in Switzerland that extreme precipitation events accompanied by lightning (convective events) exhibit consistently higher rates of increase with air temperature (8–9% per 1°C) than do stratiform events (6–7% per 1°C) for mean and peak 10 min intensity. However, both storm types have lower rates than do all events combined (11–13% per 1°C).

These results imply that the increase of precipitation extremes in future climate will depend on air temperature and the relative proportions of convective and stratiform precipitation at a given temperature. Furthermore, the intensification of extreme precipitation seems to depend not only on temperature but also on moisture availability (Panthou et al., 2014; Westra et al., 2014). Lenderink et al. (2011) have studied hourly precipitation extremes in Hong Kong and the Netherlands and found that precipitation intensity increases up to about 24°C but thereafter rises more slowly or even diminishes. This change is probably associated with moisture deficits.

Structure of the thesis

This thesis is organized as follows: In Chapter 1, an algorithm for subdivision of observed precipitation amounts into convective and stratiform is proposed and evaluated. The algorithm is based on SYNOP (surface synoptic observations) reports

from weather stations in the Czech Republic. Time series of 6-hour convective and stratiform precipitation amounts over 1982–2010 obtained using the algorithm are analysed in Chapter 2 with respect to such of their basic climatological characteristics as annual cycle of precipitation amounts, dependence on altitude and temperature, and trends in precipitation amounts and the number of wet days.

Ability of regional climate models (RCMs) to reproduce properties of convective (subgrid) and stratiform (large-scale) precipitation for recent climate over the Czech Republic, including extremes, is investigated in Chapter 3. The simulations from 11 RCMs with horizontal resolution of 0.22° driven by the ERA-40 reanalysis originate from the ENSEMBLES project database. Projected changes of convective (subgrid) and stratiform (large-scale) precipitation characteristics (for 2071–2100 vs. 1971–2000) are analysed in Chapter 4. For this purpose, RCM simulations with finer horizontal resolution (0.11°) from the EURO-CORDEX project are examined.

In Chapter 5, a new statistical model for analysing precipitation extremes is introduced. A two-component generalized extreme value (TCGEV) distribution is based on an assumption that the annual maxima for convective and stratiform precipitation follow two separate GEV distributions. The regional TCGEV model is applied to analyse 6-hour precipitation data for stations in the Czech Republic over 1982–2000. The return levels from the regional TCGEV distribution are compared with those obtained using the common method of fitting a regional GEV distribution to the overall annual maxima, thus ignoring their convective or stratiform origins.

The thesis is based on three papers published in peer-reviewed international journals (Atmospheric Research, Climate Dynamics, and Journal of Hydrology), and a fourth which is currently under review at International Journal of Climatology. I am first author of three of the papers and second author of one paper for which my supervisor, J. Kyselý, is first author. I am responsible for all calculations and the preparation of all figures and tables used in all papers, and I was a principal participant in interpreting the results. I drafted the manuscripts of all papers for which I am the first author, and I was responsible for revisions of the manuscripts. I participated actively also in preparation of the manuscript of which I am not the first author, including interpretation of the results.

1 Algorithm for subdivision of convective and stratiform precipitation*

1.1 Introduction

Several works have aimed at discriminating convective and stratiform precipitation on the basis of different instruments and techniques. Many methods originate from studies of ground-based measurements. Some authors have used subjective criteria for subdivision of precipitation based on analysis of synoptic maps for extreme precipitation (e.g., Štekl et al., 2001). Others subdivide precipitation from the viewpoint of relative spatial distribution. For example, Ungewitter (1970) distinguished widespread precipitation (occurring at 90–100% of stations in a study area), which corresponds with long-lasting rain or snow; isolated precipitation (occurring at 1–50% of stations); and precipitation-poor day (0–20% of stations), corresponding with rain or snow showers. An analogous method was used by Brázdil and Štekl (1986) for the Czech Republic (using data from 1972–1974). Some authors have used quantitative criteria for subdivision of long-lasting precipitation and rain showers based on the precipitation amount, average and maximum intensity, and area affected by precipitation (Kurejko, 1978; Orlova, 1979; Alibegova, 1985). A big disadvantage of these criteria has been their subjectivity and applicability only for specific data and areas for which they had been designed.

More recent methods devised for subdivision of rainfall often use data from radar and satellite measurements (e.g., Sempere-Torres et al., 2000; Anagnostou, 2004; Lam et al., 2010; Thurai et al., 2016). These methods originate from studies of rain gauge data (e.g., Austin and Houze, 1972; Houze, 1973) in which those gauge rainfall rates exceeding a specified threshold were classified as convective, which may not always be justified. This background-exceeding technique (BET) generally identifies the core of convection. The technique has been extended to two dimensions using radar reflectivity observations, where convective cores were identified by BET

* This chapter is based on:
Rulfová Z, Kyselý J. 2013. Disaggregating convective and stratiform precipitation from station weather data. *Atmospheric Research* **134**: 100–115.

and then a fixed radius of influence was taken to assign convective areas (Churchill and Houze, 1984). Steiner et al. (1995) improved this approach and used a variable radius of influence along with a variable threshold while both the radius and the threshold were functions of the area-averaged background reflectivity. Alder and Negri (1988) applied a variation of BET to subdivide convective and stratiform precipitation using infrared satellite data. Instead of searching for local maxima, they looked for local minima in the cloud-top temperatures to determine the location of a convective core. Methods using information about cloud water content and vertical motion (e.g., Tao and Simpson, 1989; Tao et al., 1993, 2000) are based on a principle similar to the methods described above and identify the convective core as an area with values above a given threshold.

The main advantage of the methods based on radar and satellite data is that they are spatially more homogeneous than station data and are easily comparable with model outputs which are in spatial grid form too. On the other hand, precipitation amounts are not directly measured by radar and satellite and are estimated on the basis of empirical formulae. Furthermore, relatively short time series and inhomogeneities make these data unsuitable for analyses of trends and extremes and for validating characteristics from climate model outputs.

Ruiz-Leo et al. (2013) presented a relatively new method based on the study of Tremblay (2005). The distribution of cumulative precipitation (in a given intensity class) versus intensity follows a near exponential law, albeit with anomalies. They suggest that the exponential term is associated with the stratiform precipitation predominating for smaller intensities, whereas the term expressing positive anomalies of the curve is related to the convective precipitation which is more important for larger intensities. Furthermore, they found a threshold of intensity separating precipitation into predominantly stratiform (i.e. intensity below a given threshold) and predominantly convective (i.e. intensity above a given threshold) origin. This method is based on 6-hour precipitation amounts from stations (standard synoptic data) and provides the opportunity to acquire long time series of convective and stratiform precipitation for analyses of changes in precipitation regimes. The disadvantage of this method is that extreme precipitation cannot be determined as stratiform in principle, which contradicts reality inasmuch as precipitation extremes may occur also in the form of widespread heavy rains from stratiform clouds even without embedded convection.

In this study, we propose an alternative algorithm for subdivision of precipitation into predominantly convective and stratiform on the basis of SYNOP reports (surface synoptic observations) at weather stations. Unlike most radar and satellite data, these data are long term and allow analysing trends and estimating high quantiles and design values of precipitation amounts as well as validating climate model outputs. Our approach is based on the same type of data as used in the method proposed by Ruiz-Leo et al. (2013), but we relax their simplifying assumption that heavy precipitation is of convective origin only. The algorithm we propose and test is based on different criteria, allowing also for subdivision of heavy precipitation into predominantly convective or stratiform.

The stations and data used are described in section 1.2. A detailed overview of the algorithm for subdivision of precipitation and its performance are presented in section 1.3 and 1.4, respectively. A discussion and summary follow in section 1.5.

1.2 Data

Observed precipitation data used in this study originate from SYNOP reports at 11 stations operated by the Czech Hydrometeorological Institute (CHMI). Table 1.1 shows the station names, locations and altitudes; their geographical positions are depicted in Figure 1.1. The altitudes of the stations range from 241 to 1322 m a.s.l., and the stations cover different climatological regions from lowlands to high mountains. The observations span from 1982 to 2010. The dataset includes 6-hour precipitation amounts, codes of present and past weather (weather state) during the 6-hour interval, and hourly data on cloud cover, cloud type, air pressure and temperature.

The quality of the data was checked in a standard manner to uncover possible errors and suspicious 6-hour precipitation records. Some missing and incorrect readings were filled in by comparing daily totals from climatological measurements (aggregated 24-hour amounts). The majority of stations have a negligible percentage of missing 6-hour precipitation data (less than 0.1%). Exceptions were the stations 11698 Kuchařovice, with 4 months of missing values (January–April 1989), and 11406 Cheb, with 3 months of missing values (October–December 1993).

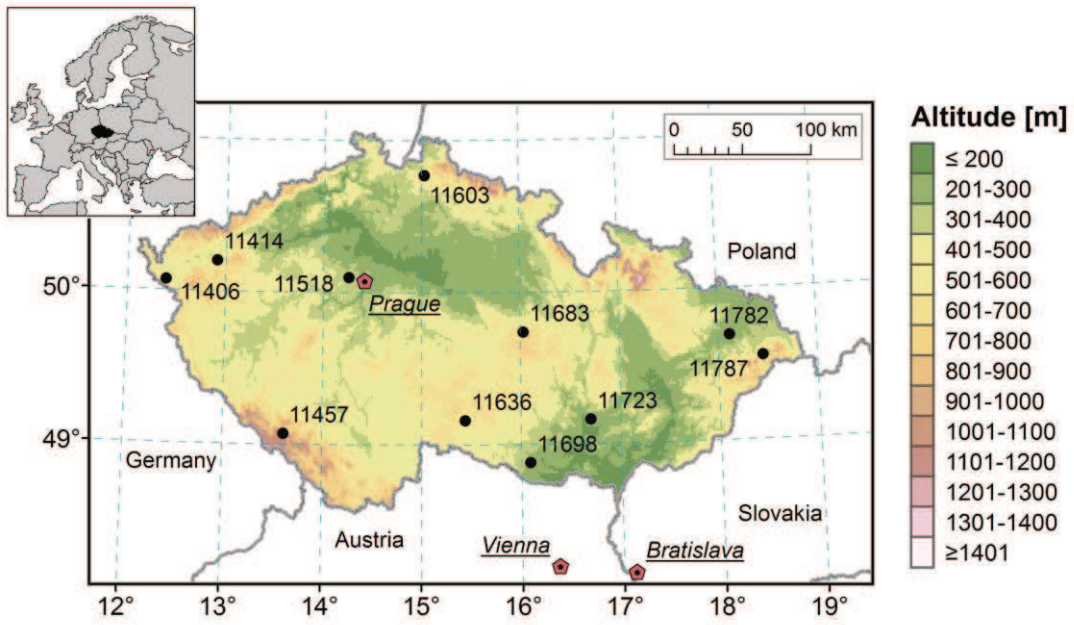

Figure 1.1: Location of stations.

Table 1.1: Characteristics of stations analyzed.

WMO code	Station name	Longitude [°E]	Latitude [°N]	Altitude [m a.s.l.]
11723	Brno-Tuřany	16.70	49.16	241
11782	Ostrava-Mošnov	18.12	49.69	251
11698	Kuchařovice	16.09	48.88	334
11518	Praha-Ruzyně	14.26	50.10	364
11603	Liberec	15.03	50.77	398
11406	Cheb	12.39	50.07	471
11636	Kostelní Myslová	15.44	49.16	569
11414	Karlovy Vary	12.91	50.20	603
11683	Svratouch	16.03	49.74	737
11457	Churáňov	13.61	49.07	1118
11787	Lysá hora	18.45	49.55	1322

1.3 Methodology

Convective and stratiform precipitation fall from different clouds and are characterized by different types of weather events, coded as weather state in the SYNOP reports (e.g., thunderstorm, rain shower, drizzle). Therefore, present and past weather (weather state, which is the main criterion) and cloud type (the

secondary criterion) are the variables employed in the algorithm for subdivision of precipitation into predominantly convective and stratiform.

The codes of weather states associated with convective and stratiform precipitation are summarized in Tables A.1 and A.2 (see Attachment A.1), respectively. The two main groups of weather states typical for convective precipitation (Table A.1) are showers (codes 80–90) and thunderstorms (codes 91–99). We include also codes that report thunderstorm or shower without precipitation at the station at the time of observation, corresponding to a situation wherein the precipitation event ends before the observation term or occurs in the station's vicinity (codes 17–19, 25–27, and 29). The three main groups of weather states typical for stratiform precipitation (Table A.2) are drizzle (codes 50–59), rain (not in the form of showers; 60–69) and snow (not in the form of showers; 70–79). No weather state codes other than those included in Tables A.1 and A.2 report precipitation events.

The secondary criterion used in the algorithm for subdivision of precipitation into convective and stratiform is information on cloud type. Convective precipitation is associated with cumulonimbus and cumulus clouds while stratiform precipitation with nimbostratus, stratocumulus, stratus and altostratus. We use this information as an auxiliary criterion, as explained below.

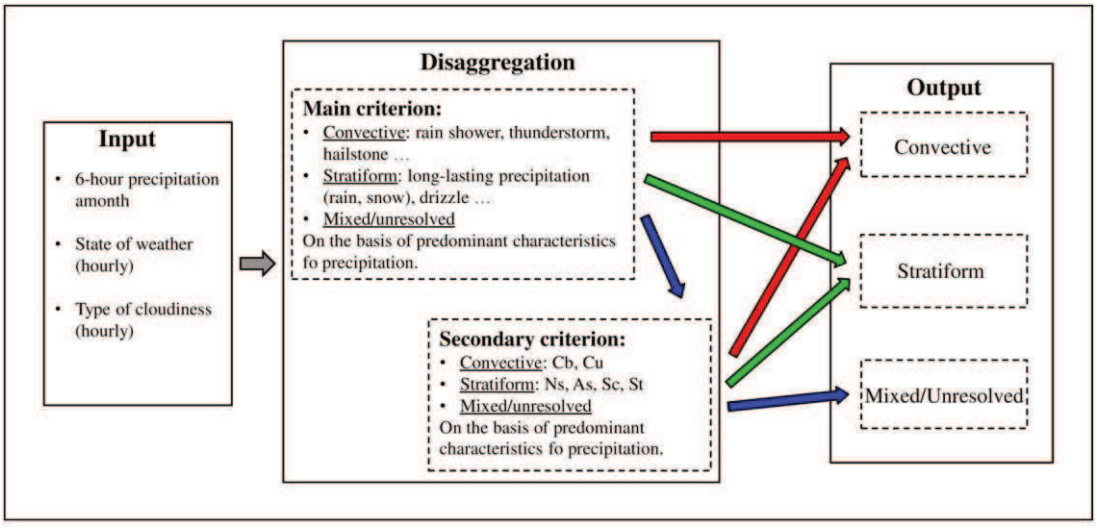

Figure 1.2: Scheme of the algorithm.

The algorithm is structured into three main steps (Figure 1.2). First, it searches for non-zero 6-hour precipitation amounts and reads all hourly data for weather state and cloud type during the 6-hour period. Second, it subdivides precipitation into

convective and stratiform using the main criterion. If the precipitation amount is classified as mixed/unresolved at this stage (occurrence of codes of weather state associated with both convective and stratiform precipitation within the 6-hour interval, or data on weather state is missing), the secondary criterion based on the cloud type is used. This leads to additional subdivision. Finally, time series of convective, stratiform and mixed/unresolved 6-hour precipitation amounts are created.

In section 1.4, we compare performance of three versions of the algorithm. In the first, precipitation is subdivided into convective and stratiform only in cases when codes of weather state (main criterion) or cloud type (if secondary criterion is applied) associated with *only one type of precipitation* (convective or stratiform) occurred through the 6-hour period (hereafter termed 'strict' subdivision). If this is not the case, the 6-hour precipitation amount is always classified as mixed/unresolved.

The second tested version of the algorithm, leading to 'maximum' subdivision of precipitation, is based on prevailing counts of values (of weather state or cloud type) associated with convective and stratiform precipitation within the 6-hour period, and so a part of the mixed/unresolved precipitation is further subdivided. The main criterion is adjusted to reflect that heavy convective precipitation contributes more to precipitation amounts by giving larger weights to codes associated with heavy precipitation (codes 91–99 and 29, Table A.1). For example, if there is a thunderstorm with heavy rain (convective event) and drizzle and rain (stratiform event) during the 6-hour period, the whole 6-hour precipitation amount is classified as convective. Although such an assumption is reasonable and leads only to negligible errors in most cases, we use this 'maximum' subdivision only for purposes of comparison with the other two versions of the algorithm.

The final algorithm is a compromise between the 'strict' and 'maximum' subdivision. First, precipitation is subdivided using the algorithm for 'strict' subdivision. Precipitation classified as mixed/unresolved is then further subdivided on the basis of whether there are codes of weather state corresponding to *heavy* convective precipitation in combination with codes corresponding to *light* stratiform precipitation only, and vice versa. For example, if codes of weather state denoting a moderate to heavy shower (convective event) are combined with light drizzle or light rain (stratiform event) during the 6-hour period, as is sometimes the case, and there

are no codes of weather state for moderate or heavy rain (corresponding to stratiform precipitation), then the 6-hour precipitation is classified as convective. This is a reasonable approach given the fact that precipitation rates for light drizzle or rain are negligible compared to those for moderate to heavy showers or thunderstorms. In cases when both convective and stratiform precipitation occurred within the 6 hours, on the other hand, and there is no indication that contribution from one of the types is negligible, then these 6-hour amounts are classified as mixed/unresolved.

1.4 Performance of the algorithm

Comparison of the results of the final algorithm with those for the 'strict' and 'maximum' subdivision is shown in Figure 1.3 for stations 11723 Brno-Tuřany (241 m a.s.l.), 11683 Svratouch (737 m a.s.l.) and 11787 Lysá hora (1322 m a.s.l.), which correspond with lowland, highland and mountain location, respectively.

The final version of the algorithm subdivides about 95% of precipitation amounts, compared to 78–90% for the 'strict' subdivision and about 99% for the 'maximum' subdivision. An even slightly higher subdivision rate is achieved in the final algorithm for the number of heavy precipitation events, defined as 6-hour precipitation amounts $\geq$ 5 mm (last column in Figure 1.3), while the algorithm is somewhat less successful for the total number of events with non-zero 6-hour precipitation. It follows that the proposed algorithm, as expected, subdivides larger precipitation amounts (which are linked to more distinct weather conditions) better than light precipitation, which means that it is particularly suitable for analysis of extremes. Comparing the results from the 'strict' subdivision and the final algorithm shows that the majority of initially mixed precipitation is ultimately classified as predominantly convective (Figure 1.3).

In annual data, precipitation of stratiform origin represents 54–77% and convective 19–37% of total precipitation amounts (Figure 1.3, Table 1.2). The percentage of mixed/unresolved precipitation is similar in all seasons, between 5% and 7% if averaged over the stations. It is largest at mid-elevated stations (about 600–800 m a.s.l.), probably because the ratio of convective and stratiform precipitation is most balanced here, and 6-hour events with both convective and

stratiform precipitation are most common (the percentage of convective precipitation increases with altitude first and then declines, so the dependence is not monotonous).

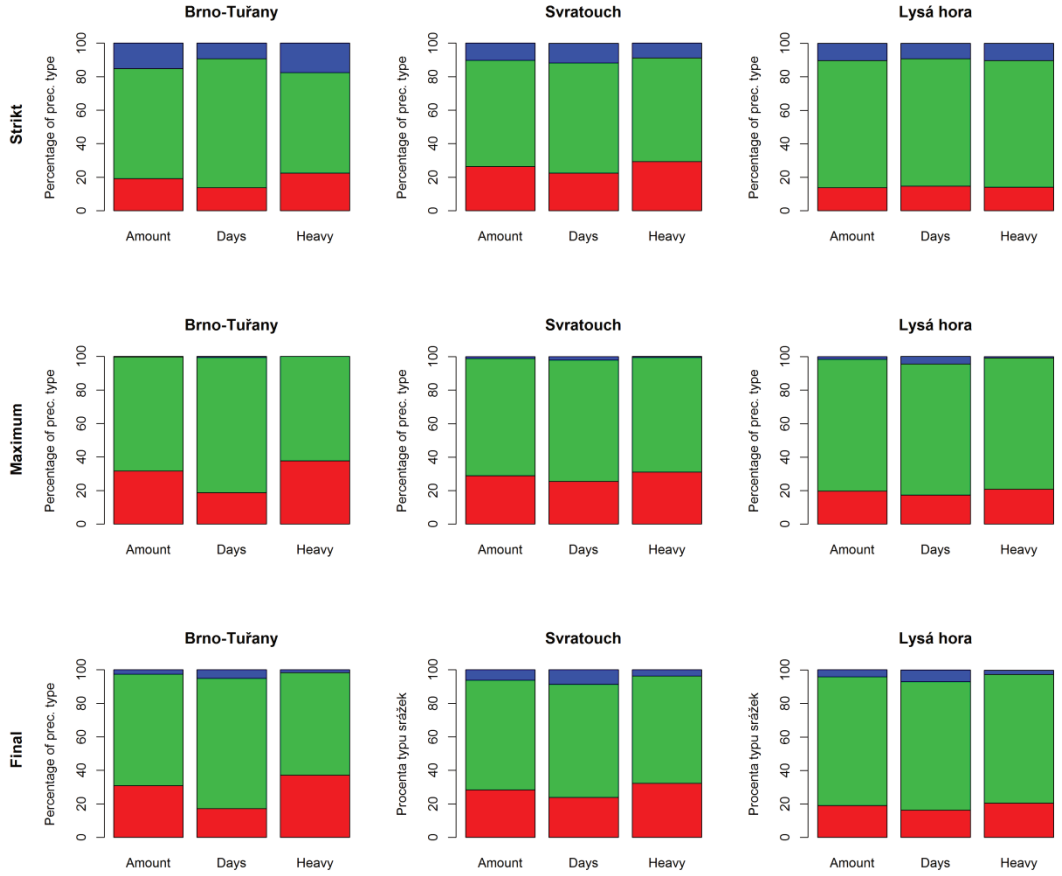

Figure 1.3: Percentage of precipitation amounts, number of non-zero precipitation events and number of heavy precipitation events (6-hour precipitation ≥ 5 mm) of convective (red), stratiform (green) and mixed/unresolved (blue) precipitation: 'strict' subdivision (top), 'maximum' subdivision (middle) and the final algorithm (bottom).

Table 1.2: Percentage of convective, stratiform and mixed precipitation amounts in all-year data and individual seasons: average (minimum – maximum) over 11 stations.

	Spring	Summer	Autumn	Winter	All year
Convective	28.5 (17.8 – 38.3)	48.8 (35.0 – 57.7)	13.9 (8.9 – 20.9)	6.2 (1.5 – 10.6)	29.1 (19.0 – 36.7)
Stratiform	64.2 (53.2 – 77.7)	45.0 (33.4 – 60.8)	79.8 (66.9 – 86.7)	88.6 (79.4 – 96.6)	64.6 (54.0 – 77.0)
Mixed	7.1 (3.1 – 11.5)	6.2 (3.3 – 8.9)	6.3 (1.8 – 12.1)	5.2 (1.2 – 9.9)	6.3 (2.6 – 10.4)

1.5 Discusion and summary

Methods utilizing radar and satellite data are widely used for subdivision of convective and stratiform precipitation (e.g., Lam et al., 2010; Sokol and Bližňák, 2009). Although they provide useful tools for such meteorological applications as predicting precipitation and analysing development of precipitation systems (e.g., Yu et al., 2010), they are not applicable for climatological studies because of the short records of available data. From this point of view, the methodology proposed by Ruiz-Leo et al. (2013) was a step forward, because it was able to provide long time series of convective and stratiform precipitation (although they applied it to an 11-year time series only). However, this method classifies heavy 6-hour precipitation as convective by definition, which may be reasonable for the specific study area (north-eastern coast of Spain) but this is not the case in other mid-latitudinal regions. Another simplifying assumption was that all precipitation amounts can be classified as either convective or stratiform.

While the algorithm we propose is based on 6-hour precipitation amounts as well, it makes use also of additional hourly weather data from SYNOP reports (information on weather state and cloud type during the 6-hour interval). Therefore, it allows for subdivision of precipitation into convective and stratiform on the basis of other weather characteristics, not the precipitation rate itself. In this way, heavy precipitation amounts, too, are subdivided into convective and stratiform (or mixed/unresolved), which is in contrast to the method proposed by Ruiz-Leo et al. (2013). We note that heavy precipitation associated with several recent major floods in Central Europe was stratiform (Řezáčová et al., 2005a; Bissolli et al., 2011), so it is important to relax the assumption that all 6-hour precipitation amounts exceeding a given threshold are of convective origin. The proposed method therefore has great potential also for the analysis of extremes, both as to their statistical distributions and analysis of their long-term variability and change (the time series available in the present study cover almost 30 years).

The proposed algorithm subdivides about 95% of precipitation amounts into convective and stratiform. Inasmuch as it is more successful in subdivision of moderate and heavy precipitation than light precipitation, it is particularly suitable for applications to analyse precipitation extremes.

In annual data, approximately one-quarter to one-third of precipitation amount is convective and the rest is stratiform. In all seasons, 5–7% of precipitation is classified as mixed/unresolved. This finding is not unexpected, as the two basic types of precipitation may both occur within the 6-hour interval (and both may contribute significantly to the 6-hour amount), and they can even occur simultaneously. We note that the concepts of stratiform and convective precipitation are simplified and there is no clear borderline between the two (for example in the case of embedded convection within large-scale stratiform clouds and related spatial patterns of precipitation). In spite of these limitations, the algorithm may be useful in follow-up applications, including for evaluating regional climate models which simulate convective and stratiform precipitation through separate parameterizations (Dai, 2006), but only aggregated precipitation amounts are usually evaluated in their outputs, which yields limited insight into sources of model biases.

Acknowledgements

The study was supported by the Czech Science Foundation, project P209/10/2045. We are grateful for useful discussions and help with preparation of data to P. Pešice and P. Sedlák. All calculations were made in statistical software R. This software is available at http://www.r-project.org.

2 Characteristics of convective and stratiform precipitation*

2.1 Introduction

When studying characteristics of precipitation in mid-latitudes, it is appropriate to focus on the basic types, convective and stratiform. Stratiform precipitation is large-scale precipitation from stratiform clouds (mainly nimbostratus, but also altostratus, stratocumulus and stratus). It is usually long-lasting, has smaller intensity and, due to relatively small updraft movements (~10^{-2}–10^{-1} m.s^{-1}), its precipitation elements are smaller (Houze, 1993). Convective precipitation is that from convective clouds (cumulus congestus and cumulonimbus). It occurs predominantly in the form of more localized rain showers and thunderstorms, it may have larger intensity, and its precipitation elements may grow to large sizes (e.g., hailstones several centimetres in diameter; Houze, 1993) due to strong updraft movements (~1–10 m.s^{-1}).

Although the concepts of stratiform and convective precipitation are simplified and there is no clear borderline between the two (for example in the case of embedded convection within large-scale stratiform clouds and related spatial patterns of precipitation), these two types are associated with different precipitation growth mechanisms and both play important roles in precipitation amounts falling during warm half-year in Central Europe.

After a short description of the data and methods in section 2.2, basic characteristics of convective and stratiform precipitation are presented in section 2.3. Section 2.4 contains a discussion of the results, and summary of results follow in section 2.5.

* This chapter is based on:
Rulfová Z, Kyselý J. 2013. Disaggregating convective and stratiform precipitation from station weather data. *Atmospheric Research* **134**: 100–115.

2.2 Data and methods

The data and the algorithm for subdivision of observed precipitation into convective and stratiform was described in Chapter 1. Time series of 6-hour convective and stratiform precipitation amounts obtained using the final version of the algorithm are analysed in this chapter with respect to their basic climatological characteristics such as annual cycle of precipitation amount, dependence on altitude and temperature.

Furthermore we analyse trends in precipitation amounts and the number of wet days (defined as days with precipitation ≥ 1.0 mm; Moberg and Jones 2005) over 1982–2010, separately for total, convective and stratiform precipitation. Seasonal precipitation characteristics are analysed. We exclude winter season, however, as then convective precipitation amounts are very small (cf. Table 1.2) and thus lead to inconclusive results as to temporal changes and trends.

Since precipitation has large random spatial variability and the study area is relatively small, we evaluate time series obtained by averaging data from all stations. The averages are calculated from scaled stations' data in order to give the same weight to all stations (notwithstanding the observed precipitation amount and number of wet days, which are larger at higher-elevated stations). Characteristics at individual stations were first divided by their mean values over the studied period and then averaged over all 11 stations.

Trends of indices were estimated using non-parametric Sen's estimator of slope, also known as the 'median of pair-wise slopes' or Theil-Sen estimator (Sen, 1968; Kyselý, 2009). The statistical significance of the trends was tested using the Mann–Kendall test (Mann, 1945; Kendall, 1975). This is a rank-based test that is robust to outliers and does not depend on the assumption of Gaussian distribution of residuals. The statistical significance of precipitation trends is usually lower compared with other climate elements due to large spatial and temporal variability of precipitation. Therefore, we evaluate the results at lower significance levels of $p = 0.1$ and $p = 0.2$.

Since most climate series are serially correlated due to the multi-year nature of natural climate variability, an approach to computing trends and their significance described in Wang and Swail (2001) or Zhang et al. (2000) was used, as it is able to remove autocorrelation from the time series. This method produces a slightly smaller magnitude of trend than does the traditional linear model, and, therefore, some trends

identified as statistically significant using linear regression are, in this case, not significant due to positive autocorrelations in the data. All trend magnitudes were expressed as relative changes of the examined characteristics in %/10 years, allowing easier comparison among all indices and seasons.

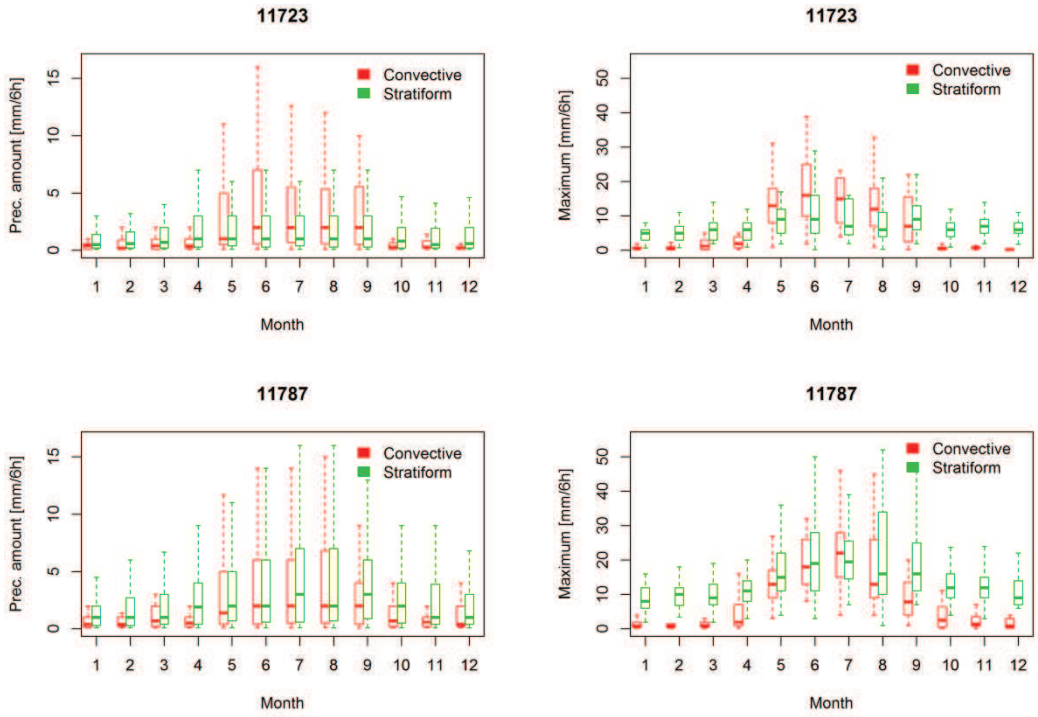

Figure 2.1: Example of boxplots of convective and stratiform precipitation for each month: all non-zero 6-hour precipitation amounts (left), and maximum monthly 6-hour precipitation amounts (right).

2.3 Results

2.3.1 Annual cycle of precipitation

Boxplots of non-zero 6-hour precipitation amounts and their monthly maxima (Figure 2.1) at lowland station 11723 Brno-Tuřany show that larger 6-hour precipitation amounts occur in summer for both convective and stratiform precipitation, and that there is greater variance of the 6-hour precipitation amounts in summer than in winter. In summer and May, maximum precipitation is predominantly convective; in the cold half of the year, maximum precipitation is stratiform. The differences between characteristics of convective and stratiform

precipitation are smaller for all non-zero precipitation amounts than the monthly maxima. Similar behaviour of 6-hour precipitation is found at all stations (see Attachment A.2) except for the highest-elevated one, 11787 Lysá hora (Figure 2.1). This mountain station has stratiform precipitation maximum greater than convective in all months except July.

Precipitation has a clear annual cycle in Central Europe, with the monthly maximum occurring between June and August at all stations (Figure 2.2). This annual cycle is determined by the annual cycle of convective precipitation only (with its maximum in June/July and its minimum in January/February), while the contribution of stratiform precipitation is relatively constant during the year at all stations (Figure 2.2).

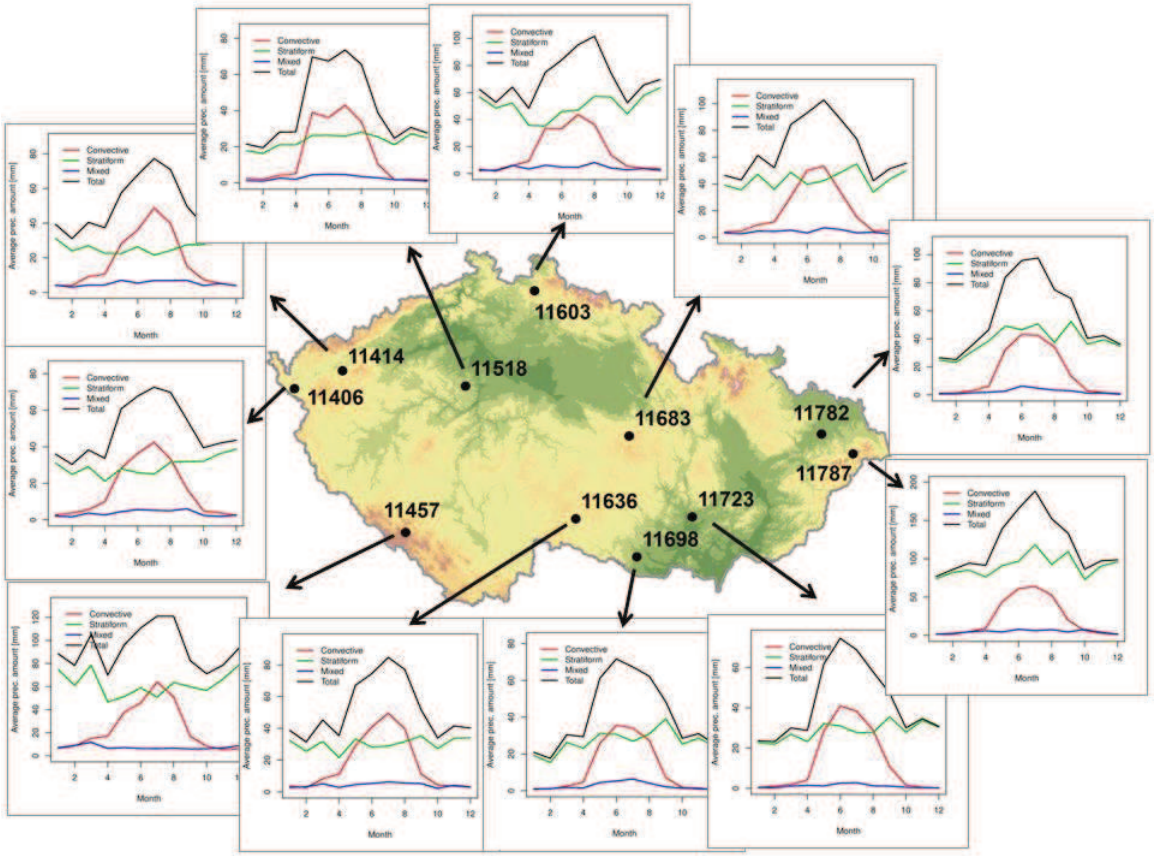

Figure 2.2: Annual regime of monthly precipitation amounts by different type.

In year-round data, stratiform precipitation predominates at all stations and the fraction of convective precipitation is very small in winter (5% of total precipitation if averaged over the stations; Table 1.2). On average, the contribution of convective and stratiform precipitation to summer amounts is almost balanced: 49% and 45% of

precipitation is of convective and stratiform origin, respectively, and the remaining 6% is mixed/unresolved. Convective precipitation tends to prevail at lower-elevated stations and in the south-western part of the country in summer, while stratiform precipitation dominates throughout the year at higher-elevated stations and in the northeast (Figure 2.2). The contribution of convective precipitation is by far the smallest at the highest-elevated station, 11787 Lysá hora.

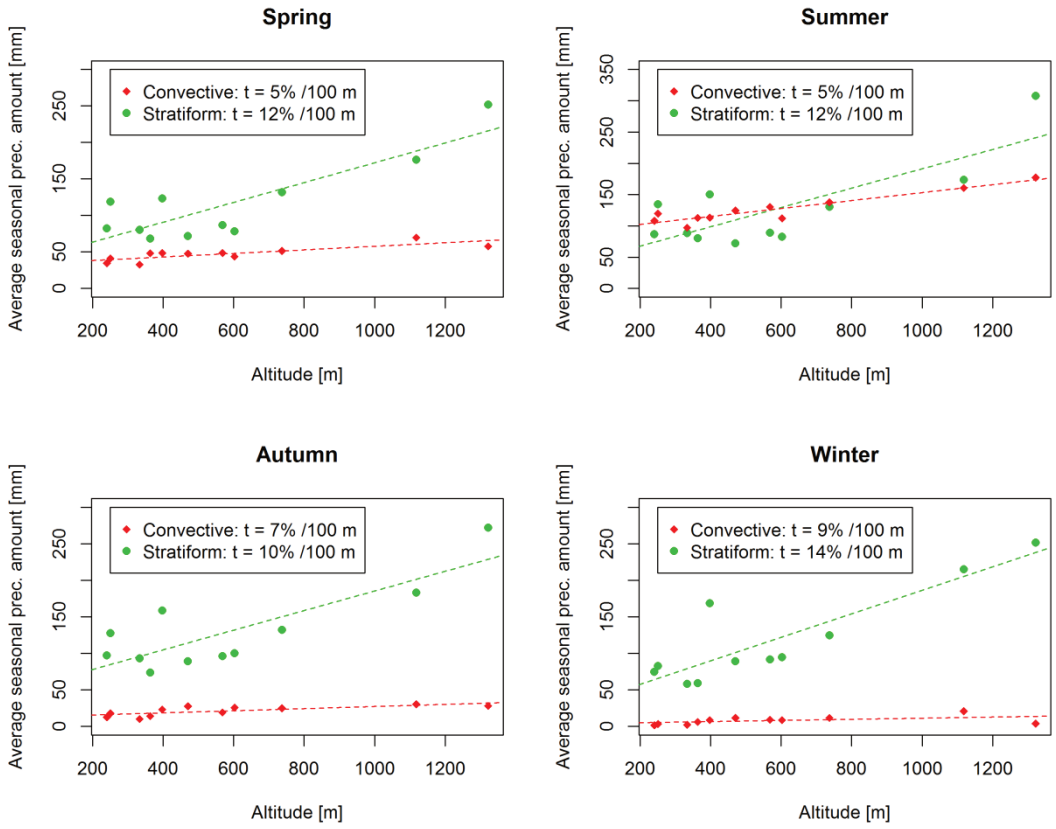

Figure 2.3: Dependence between mean seasonal precipitation amount and altitude (t represents relative change of convective or stratiform precipitation amount in %/100 m).

2.3.2 Dependence on altitude

Precipitation amounts increase with altitude, and this dependence is found for both precipitation types (Figure 2.3). There is, however, a large difference in the slopes of the dependence on altitude between stratiform and convective precipitation, with dependence of stratiform precipitation on altitude being much stronger. Particularly noteworthy is that very similar slopes are found in all seasons (increase by 10–14% per 100 m for stratiform, and by 5–9% per 100 m for convective precipitation). The

slopes are the same in summer and spring (12% per 100 m for stratiform and 5% per 100 m for convective precipitation), when the contribution of convective precipitation is largest (Table 1.2). This suggests a robust feature of the dependence on altitude and different roles of orography for the two components.

Dependence of mean seasonal 6-hour precipitation maxima on altitude is much weaker than is that of total seasonal precipitation amount (Figure 2.4), particularly in the case of convective precipitation, and it is again consistently stronger for stratiform precipitation in all seasons.

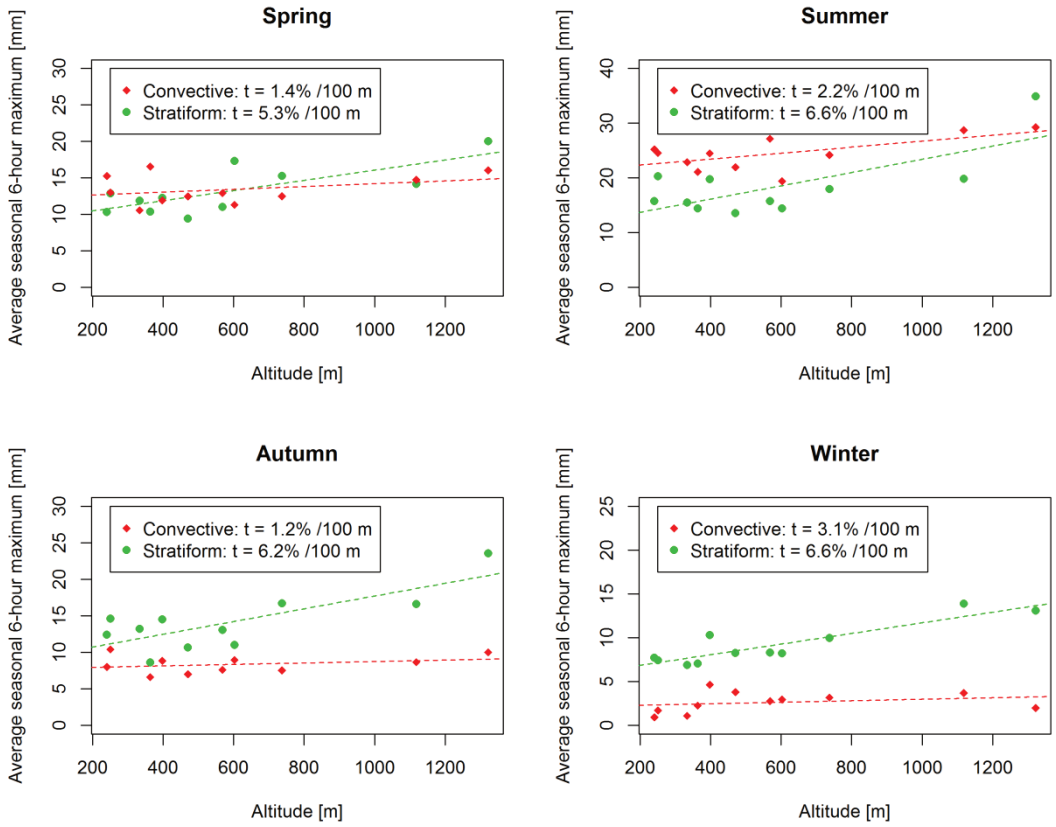

Figure 2.4: Same as in Figure 2.3 but for mean seasonal 6-hour precipitation maxima.

In summer, when proportion of convective and stratiform precipitation is almost balanced on average, we can study dependence of this proportion on precipitation rates (Figure 2.5). The fraction of convective precipitation tends to increase with rising precipitation rates, yet again except for the highest-elevated station 11787, where precipitation of all rates is predominantly of stratiform origin and even heavy

precipitation is more likely stratiform than convective. The percentage of mixed/unresolved precipitation declines with precipitation rates at most stations.

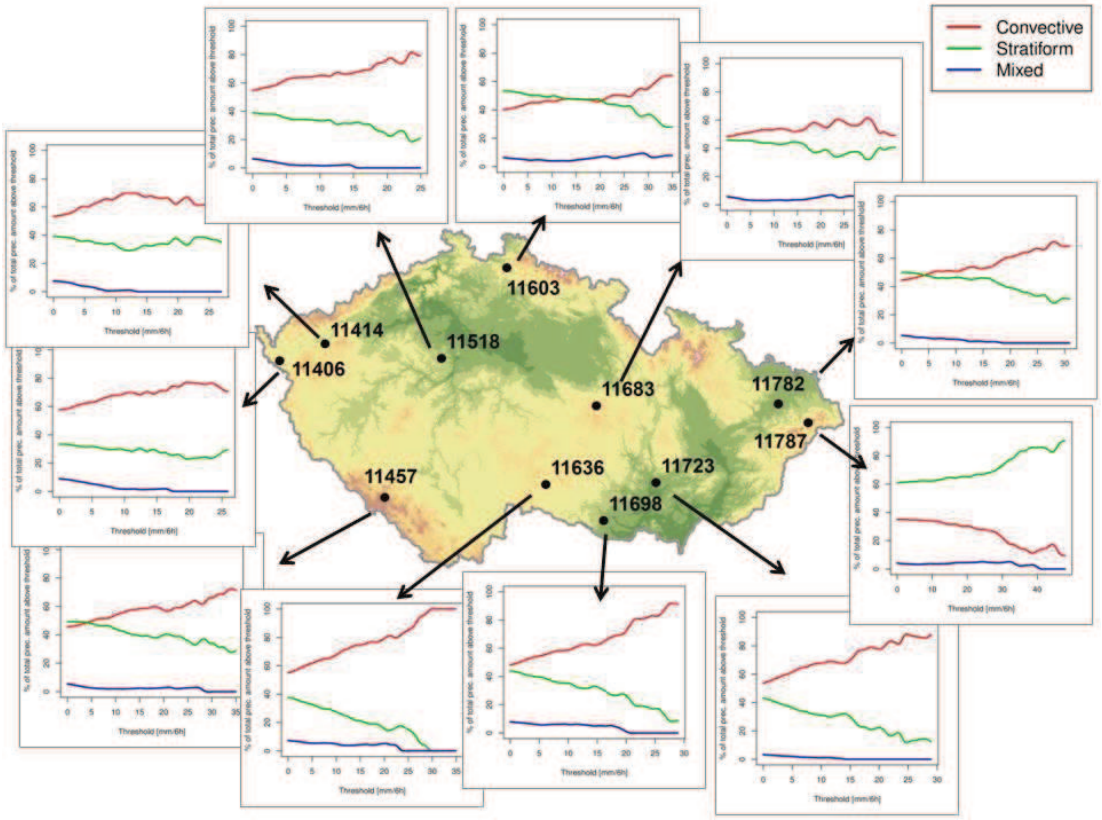

Figure 2.5: Dependence between precipitation amount and type of precipitation in summer. Percentage of the total precipitation amount above given threshold is shown on the vertical axis; threshold (6-hour precipitation amount) is shown on the horizontal axis.

2.3.3 Dependence on temperature

The relationship of convective and stratiform precipitation to mean daily temperature in summer is shown in Figure 2.6. We stratified the precipitation data based on the mean daily temperature into 1°C wide bins, and computed the percentage of convective and stratiform precipitation in each bin. At all stations, stratiform precipitation prevails for lower mean daily temperatures (to about 15°C at lowland stations and 10°C at the highest-elevated stations) and convective for higher temperatures. This relationship becomes much weaker at the seasonal time scale, however, if the fraction of convective and stratiform precipitation is evaluated against mean summer temperature anomaly (Figure 2.7).

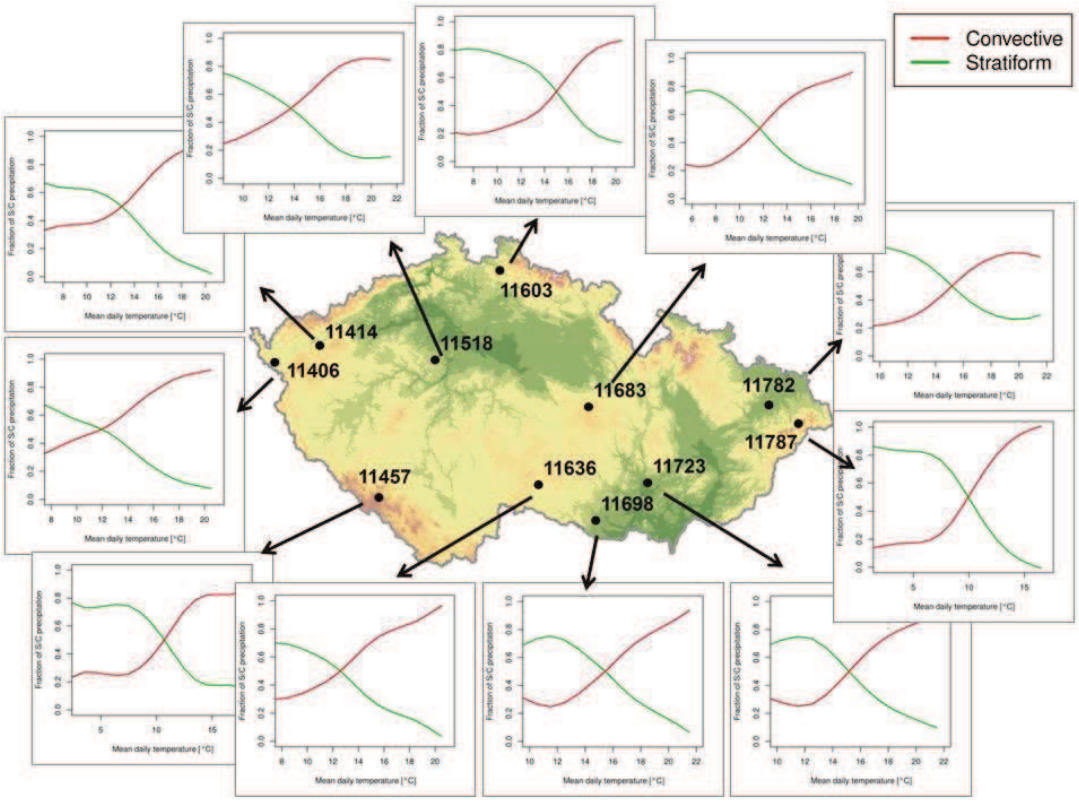

Figure 2.6: Dependence between precipitation amounts of different type and mean daily temperature in summer. Precipitation amounts were divided into 1°C wide bins and the data were fitted by polynomial function. Bins with less than 20 precipitation events at the margins were disregarded.

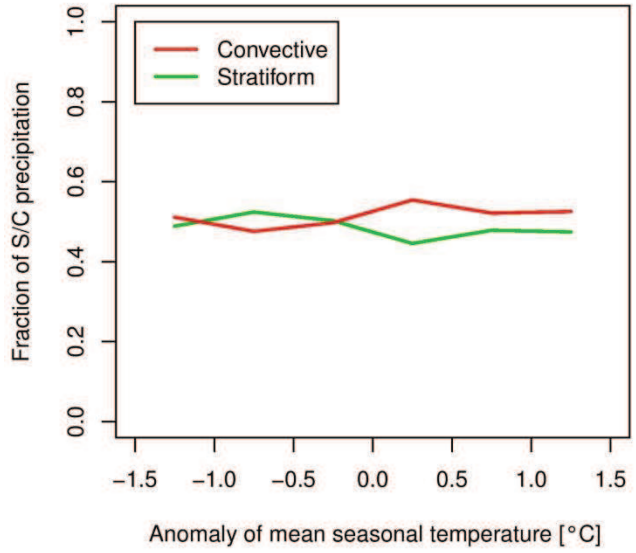

Figure 2.7: Dependence between precipitation amounts of different type (averaged over the stations) and anomaly of mean summer temperature (with respect to the station mean over 1982–2010). Precipitation amounts were divided into 0.5°C wide bins.

2.3.4 Trend analysis

In all three examined seasons and for both precipitation characteristics, convective precipitation increases more than stratiform (Table 2.1, Figure 2.8). The increase is largest in autumn (16–20%/10 years in both characteristics of convective precipitation, significant at p = 0.1) and far exceeds the increase in stratiform precipitation in this season (5–11%/10 years). Since there is a clear tendency to positive trends in both convective and stratiform precipitation in autumn, the increases in total precipitation characteristics are largest in this season.

Table 2.1: Trend magnitudes (expressed as relative changes of the examined characteristics in %/10 years) of averaged precipitation characteristics over 1982–2010 in spring, summer and autumn. The data obtained by the algorithm were scaled for individual stations by their long-term mean and then averaged over the stations. * (**) denotes trend significant at the 0.2 (0.1) level.

	Spring			**Summer**			**Autumn**		
	Total	Convective	Stratiform	Total	Convective	Stratiform	Total	Convective	Stratiform
Precipitation amount	2.6	8.0*	-3.0	5.2	7.4*	2.7	11.5**	15.9**	10.7**
Number of wet days	1.5	14.5**	-3.7	1.9	6.3*	-9.4	5.7*	20.2**	4.4

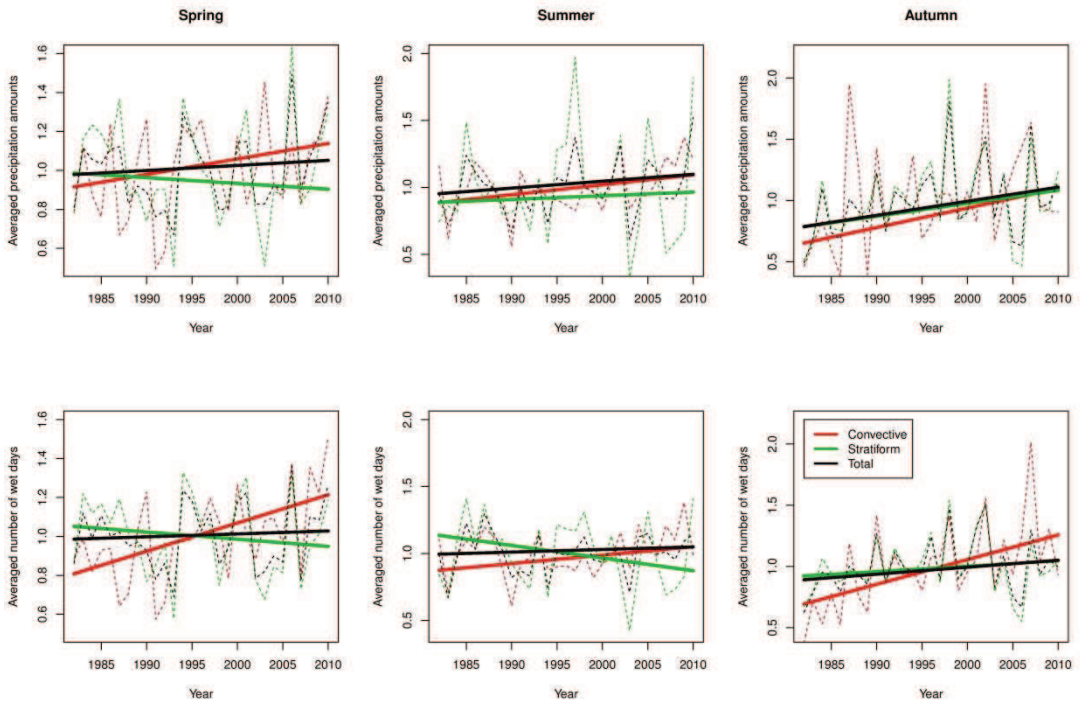

Figure 2.8: Time series of precipitation amounts (top) and number of wet days (bottom) for total, convective and stratiform precipitation over 1982–2010 in spring, summer and autumn. The data obtained by the final algorithm were scaled for

individual stations by their long-term mean and then averaged over the stations. Linear trends estimated by the non-parametric method are plotted.

In spring, by contrast, only characteristics of convective precipitation increase (significant at $p = 0.1$ for the number of wet days and $p = 0.2$ for precipitation amounts) while those of stratiform precipitation decline. A similar pattern is found in summer when trends of convective precipitation are significant at $p = 0.2$. These counterbalancing trends of convective and stratiform precipitation lead to the fact that trends in characteristics of total precipitation are relatively small (but increasing for both precipitation amounts and the number of wet days) in spring and summer.

Trend analysis of precipitation characteristics was supplemented by trend analysis of mean seasonal temperatures, calculated again by averaging temperature data from the 11 stations. Trends of mean seasonal temperatures over 1982–2010 are increasing in all seasons, notwithstanding whether seasonal means are calculated from daily maximum, minimum or mean temperature. The trends are statistically significant in summer ($p = 0.05$) and spring ($p = 0.1$, for mean and maximum temperatures only; Table 2.2). Except for autumn, the trends are stronger for seasonal temperatures calculated from daily maxima (which are more closely linked to conditions suitable for convection) than minima. This points to a possible link of increasing convective precipitation to warming surface temperatures.

Table 2.2: Trend magnitudes (expressed in °C/10 years) of averaged daily maximum, minimum and mean temperature over 1982–2010 in spring, summer and autumn. * (**) denotes trend significant at the 0.1 (0.05) level.

	Spring	Summer	Autumn
Mean daily temperature	0.43*	0.75**	0.19
Tmin	0.26	0.66**	0.29
Tmax	0.55*	0.70**	0.06

2.4 Discussion

2.4.1 Annual cycle of precipitation

In Central Europe, the annual precipitation cycle has a single maximum in June and July and minimum in January and February (Tolasz et al., 2007). We find that this is

entirely due to the annual cycle of convective precipitation while stratiform precipitation is almost constant throughout the year.

Stratiform precipitation dominates at all stations in all seasons except summer. In summer, the fraction of convective precipitation is largest as a result of optimal weather conditions supporting the formation of convective cells. Convective precipitation does not prevail in summer at all stations, however, and this contradicts previous assessments (Tolasz et al., 2007) based on qualitative analysis only. This is the case of several higher-elevated stations and stations in the eastern part of the Czech Republic, where cloud belts associated with Mediterranean cyclones play a more important role in inducing precipitation (Hanslian et al., 2000). This precipitation falls usually from widespread stratiform clouds, so the fact that convective precipitation does not dominate even in summer at these stations has a climatological interpretation.

2.4.2 Spatial patterns of convective and stratiform precipitation and dependence on altitude

In summer, low and moderate precipitation rates are associated with stratiform and convective precipitation whereas heavy precipitation is predominantly of convective origin at all stations except for mountain station 11787 Lysá hora. The peculiarity of this station probably relates to the relatively common occurrence of stratiform precipitation associated with Mediterranean cyclones in the eastern part of the Czech Republic, and the prevailing flow from the northern quadrant leads to orographically enhanced precipitation at the windward side of the Beskydy mountains (Hanslian et al., 2000; Řezáčová et al., 2005a). We also find that stratiform precipitation has much stronger dependence on altitude than does convective, and the slopes of the dependence are consistent among seasons for both types of precipitation. The dependence is weaker for mean seasonal maxima of 6-hour precipitation of both stratiform and convective origin. The latter agrees with the results of Sokol and Bližňák (2009), who studied the precipitation–altitude relationship of short-term precipitation from radar data divided into total and convective. They showed that 6-hour total precipitation depends on altitude for low and high precipitation rates while 6-hour convective precipitation depends on altitude for low rates only. The slopes of

the fitted lines were smaller for heavy precipitation in the cases of both total and convective precipitation.

Our findings support to some extent the general concept that heavier convective precipitation is more likely to arise at lower-elevated stations while heavier stratiform precipitation is more likely at higher-elevated stations. Although convective precipitation is more frequent at higher-elevated stations (Bek et al., 2010) due to conditions suitable for its formation (topographically triggered convection; Frei and Schär, 1998), it is mostly weaker than is heavy convective precipitation at lower-elevated stations (Bek et al., 2010), which is mostly associated with atmospheric fronts. On the contrary, heavy stratiform precipitation is more likely at higher-elevated stations where influences of altitude, declination and prevailing wind direction affect the precipitation amount (Karagiannidis et al., 2012). Despite these facts, the spatial distribution of precipitation in the mountains can vary to a large extent. For instance, during strong winds and due to redistribution processes over the mountainous ridges, the largest amount of precipitation can appear in the valley and the smallest on the exposed windward slopes (Sevruk, 1997).

2.4.3 Dependence on temperature

There is ongoing discussion concerning possible changes in precipitation rates and relative contributions of convective and stratiform precipitation with increasing surface temperatures. Our analyses as to the dependence of convective and stratiform precipitation on mean daily temperature in summer shows results similar to those reported by Haerter and Berg (2009) for simulated data in the Netherlands, namely increase of convective precipitation and decrease of stratiform precipitation with surface air temperature at the daily scale. Convective precipitation prevails over stratiform at mean daily temperatures higher than about 15°C at lowland stations and 10°C at the highest-elevated stations. At the seasonal scale, however, there is only weak dependence of the proportions of convective and stratiform precipitation on mean summer temperature. Therefore, the data suggest that possible climate change and increase of mean seasonal temperature may have weaker influence on changes in the proportions of convective and stratiform precipitation in warm season.

2.4.4 Trends of convective and stratiform precipitation

For all three examined seasons in which convective precipitation represents an important part of total precipitation (spring, summer and autumn), convective precipitation is increasing over time more than stratiform. The sign of the trends in characteristics of total precipitation (precipitation amounts and number of wet days) are governed by trends in convective precipitation. Increasing trends in convective precipitation correspond with increasing trends in mean seasonal temperatures, which support conditions suitable for the formation of convective precipitation. This topic deserves further investigation to determine whether similar patterns for trends in seasonal temperature and convective precipitation are to be found also in other regions, as well as whether these represent manifestations of a single underlying physical mechanism or happen by coincidence. Our results contrast with those of Ruiz-Leo et al. (2013), who found steeper (positive) trends for stratiform than convective precipitation in the eastern Spanish coast. They, however, had examined a much shorter time period (1998–2008) and used a different algorithm for subdivision of precipitation, as discussed above.

2.5 Summary

Based on analysis of station data in the Czech Republic over 1982–2010, we show that:

- Stratiform precipitation predominates at all stations in all seasons except summer, at which time the proportion of convective precipitation increases and leads to slightly higher precipitation amounts of convective than stratiform origin at most (but not all) stations. Stratiform precipitation is relatively constant throughout the year (and does not contribute to the annual cycle of total precipitation) while convective has a strong annual cycle.

- Stratiform precipitation amounts increase with altitude much faster than convective, and the slopes of the altitudinal dependence are consistent in all seasons for both stratiform and convective precipitation.

- Proportions of convective and stratiform precipitation strongly depend on mean daily surface air temperature in summer. Percentage of convective precipitation sharply increases and stratiform decreases with rising daily temperature. This relationship is much weaker at the seasonal scale, however, which indicates that climate change may have smaller influence on the ratio of convective and stratiform precipitation than suggested by the analysis at the daily scale.

- Increasing trends in convective precipitation are found in all three examined seasons (spring, summer, autumn) over 1982–2010, the slopes being larger than those for stratiform precipitation in each season and relating to both precipitation amounts and number of wet days. This suggests that the observed increases in total precipitation is primarily due to increases in convective precipitation, and this effect may also be related to an observed warming of surface air temperatures, which, in turn, may enhance instability and support conditions for stronger convection.

Acknowledgements

The study was supported by the Czech Science Foundation, project P209/10/2045. We are grateful for useful discussions and help with preparation of data to P. Pešice and P. Sedlák. All calculations were made in statistical software R. This software is available at http://www.r-project.org. Trend analyses were worked out using the packages ‘Kendall’ and ‘zyp’.

3 Convective and large-scale precipitation in regional climate models*

3.1 Introduction

Precipitation is one of the variables with the largest uncertainty in climate models, due to the large number of parameterized processes involved in its simulation. This is particularly the case for summer precipitation in mid-latitudes, which is controlled by convective processes at small spatial scales while cloud belts associated with cyclones and atmospheric fronts at larger scales. Although the two components may be comparable in their contribution to overall rainfall amounts (see Chapter 2), they differ substantially in manifesting spatial and temporal variability that is crucially related to the hydrological response. Uncertainty and errors associated with reproducing the convective processes in climate models are particularly large (e.g., Dai et al., 2006; Déqué et al., 2007; Brockhaus et al., 2008; Hohenegger et al., 2008; Kendon et al., 2012) and contribute significantly to uncertainty in climate change projections. Biases in the relative proportion of convective and stratiform precipitation are important also because associated processes affect other aspects of the simulated climate through different mass and heating profiles, which may have important implications for atmospheric circulation and thermodynamics (Houze, 1997). For an ensemble of 18 global climate models (GCMs), Dai et al. (2006) reported large overestimation of convective precipitation over tropical regions and generally smaller biases in the mid-latitudes.

While many studies have dealt with evaluation of precipitation characteristics in regional climate model (RCM) simulations over Europe (e.g., Fowler et al., 2007; Jacob et al., 2007; May, 2007; Boberg et al., 2010; Hanel and Buishand, 2010; Herrera et al., 2010; Kjellström et al., 2010; Kyselý et al., 2012), including dependence on horizontal resolution (e.g., Durman et al., 2006; Boyle and Klein, 2010; Rauscher et al., 2010; Li et al., 2011; Kendon et al., 2012) and links to

* This chapter is based on:
Kyselý J, **Rulfová** Z, Farda A, Hanel M. 2016. Convective and stratiform precipitation characteristics in an ensemble of regional climate model simulations. *Climate Dynamics* **46**(1): 227–243.

atmospheric circulation (Maraun et al., 2012; Plavcová et al., 2013), little attention has been devoted to investigating the ability of RCMs to reproduce basic properties of convective (subgrid) and stratiform (large-scale) precipitation that are simulated separately through deep (precipitating) convection and large-scale precipitation parameterizations. One reason is the lack of long-term series of observed precipitation data subdivided according to their origin into convective and stratiform, to which the simulated characteristics can be compared.

Precipitation in current climate models (except for very high-resolution convection-permitting RCMs) originates from two distinct parameterization schemes: the large-scale scheme, which deals with precipitation events affecting larger areas (typically on mesosynoptic and synoptic scales), and the subgrid scheme, typically capturing small-scale precipitation events usually associated with deep (moist) convection episodes. This dual approach roughly corresponds to processes in the real atmosphere, although, important differences exist between convection in the real atmosphere and its formulation in numerical weather prediction and climate models. The differences are related to model resolution that separates scales directly resolved by a model from subgrid scales for which parameterizations must be deployed. When grid spacing falls below about 50 km, it becomes increasingly likely that assumptions of the scale-separation will be violated (Molinari and Dudek, 1992).

The resolution in which convective clouds are partly resolved but convective parameterizations are still needed is termed “grey zone” in the modelling community. Both parameterized and unparameterized convective clouds may exist simultaneously in a grid column, and the separation of the large-scale and convective precipitation components becomes physically unsound as the resolution increases (cf. Williamson 2013). Although typical grey zone scales are in the range of 1–10 km (http://www.knmi.nl/samenw/greyzone/), some large convective storms may get resolved also at a coarser resolution of ~25 km used in the present study (see below). Organised convective systems may be captured directly in the form of large-scale vertical movements and attributed to large-scale (stratiform) precipitation, while on the other hand, stratiform precipitation within mesoscale convective systems may be treated partly by the convection parameterization (e.g., Gregory and Guichard, 2002; Hu et al., 2011). These effects may compensate for one another to some extent but add to the model convection/stratiform precipitation uncertainty.

In this study, we adopt the simplified assumption that the subgrid (large-scale) precipitation computed in climate models corresponds to convective (stratiform) precipitation in the real atmosphere, although the results have to be interpreted with respect to the above-mentioned caveats in the model separation of the two components. The same approach, in which the RCM-simulated convective and large-scale precipitation were considered proxies for precipitation types, has recently been employed by Fischer et al. (2015) to study projected changes in precipitation characteristics over Switzerland.

A number of studies mention the convective parameterization scheme as the main source of error in simulating precipitation in current climate models. This conclusion is often drawn, however, from inference based upon biases in daily or hourly precipitation extremes (Frei et al., 2003; Lenderink and van Meijgaard, 2008; Hanel and Buishand, 2010; Gregersen et al., 2013) or from comparison of climate models involving a convection parameterization scheme with cloud-resolving/convection-permitting models explicitly representing convection (Guichard et al., 2004; Hohenegger et al., 2008; Kendon et al., 2012). As shown by Kendon et al., (2014), the deficiencies in simulating convective precipitation may have severe consequences for the estimated changes in precipitation extremes. Although the results from convection-permitting climate models are promising, their high computational cost might impede wider availability of their simulations. Therefore, the identification of deficiencies in precipitation simulated by the convective parameterization schemes is relevant for further model development and assessment of future changes.

In this study, we evaluate characteristics of convective and stratiform precipitation in an ensemble of 11 ERA-40 driven RCM simulations for recent climate over the Czech Republic (Central Europe). We make use of a recently proposed algorithm for sudvivision of precipitation into predominantly convective and stratiform based on SYNOP reports described in Chapter 1.

The data and methods are introduced in section 3.2. The simulation of convective and stratiform precipitation in recent climate (1982–2000) is evaluated against observations in Section 3.3. The discussion and summary of results follow in sections 3.4 and 3.5, respectively.

3.2 Data and methods

3.2.1 Observed data

The observed precipitation data originate from SYNOP reports at 10 stations operated by the Czech Hydrometeorological Institute (for more details see Chapter 1). The time series of daily convective and stratiform precipitation amounts were obtained using the algorithm proposed and evaluated in Chapter 1. Because the algorithm subdivides precipitation into three categories (convective, stratiform and mixed), the mixed precipitation amounts were split in two halves that were added to the convective and stratiform amounts, respectively (on the daily basis).

By contrast to previous chapter, we excluded the highest-elevated station (Lysá hora, 1322 m a.s.l.) from the analysis, for two main reasons: 1) it is located on a summit of a relatively isolated mountain, i.e. in a location that is not well represented in RCMs with the given resolution; 2) the mean altitude of grid boxes and stations over the study area is much closer when the highest-elevated station is excluded, which allows for a more fair comparison of spatially averaged or pooled data (see also below).

We note that the comparison of convective and stratiform precipitation characteristics against RCMs cannot be carried out for gridded station data, as there are no other SYNOP stations with high-quality and relatively complete records in the study area, and the subdivision into two basic types of precipitation cannot be carried out in common rain-gauge data that have a much denser network of measuring sites but other variables auch as the weather state or cloud type are not observed.

3.2.2 Regional climate model (RCM) simulations

The RCM simulations originate from the ENSEMBLES project (http://www.ensembles-eu.org) database. We examine runs driven at the lateral boundaries by meteorological fields from the ERA-40 reanalysis (Uppala et al., 2005), forcing the atmospheric motion to be close to the observations. Details of the 11 examined RCMs are given in Table 3.1. Horizontal resolution of all simulations is 25 km (0.22°) and the number of grid boxes in the studied area ranges from 148 to 174.

Table 3.1: RCM simulations examined.

Acronym	Institute	Reference	Grid type	No. of grids	Mean altitude [m]
CLM	ETHZ (Swiss Federal Institute of Technology Zürich)	Jaeger et al. (2008)	Rotated lon-lat	174	456
HIRHAM	DMI (Danish Meteorological Institute)	Christensen et al. (1996)	Rotated lon-lat	174	456
RACMO	KNMI (Royal Netherlands Meteorological Institute)	Lenderink et al. (2003)	Rotated lon-lat	174	456
RCA	SMHI (Swedish Meteorological and Hydrological Institute)	Kjellström et al. (2005)	Rotated lon-lat	174	456
RCA_C4I	C4I (Community Climate Change Consortium for Ireland)	Kjellström et al. (2005)	Rotated lon-lat	174	457
REMO	MPI (Max-Planck Institute)	Jacob (2001)	Rotated lon-lat	174	456
Aladin	CNRM (National Centre for Meteorological Research)	Radu et al. (2008)	Lambert conformal	165	447
Aladin_CZ	CHMI (Czech Hydrometeorological Institute)	Farda et al. (2007)	Lambert conformal	166	446
RegCM	ICTP (International Centre for Theoretical Physics)	Giorgi et al. (2004)	Lambert conformal	148	443
PROMES	UCLM (University of Castilla-La Mancha)	Sanchéz et al. (2004)	Lambert conformal	154	452
GEMLAM	EC (Environment Canada)	Zadra et al. (2008)	Rotated lon-lat	174	456
OBS				10	509

Despite the same horizontal resolution, orography differs among the models (examples are shown in Figure 3.1). The largest difference is between RegCM on one hand, in which orography is most smoothed (with no grid boxes exceeding 700 m a.s.l.), and CLM on the other, with most realistic orography (Figure 3.1). Differences between model and real altitude are largest in mountain regions: While 4 highest mountain ranges in the Czech Republic exceed 1300 m a.s.l. and the highest mountain reaches 1602 m a.s.l., the altitude of grid boxes does not excess 1000 m a.s.l. in most of the RCMs. Hence differences in altitude between mountain summits and covering grid boxes may far exceed 500 m a.s.l., which would make comparison between station and related grid box data biased.

Therefore, we focus on comparison of characteristics which are spatially averaged and/or pooled (in the form of boxplots across stations and grid boxes) and do not discuss features related to locations of individual stations or differences between regions of the Czech Republic.

Because observed data span 1982–2010 while the RCM runs cover the 1961–2000 period, we analyse the 19-year overlapping period (1982–2000) common to all datasets.

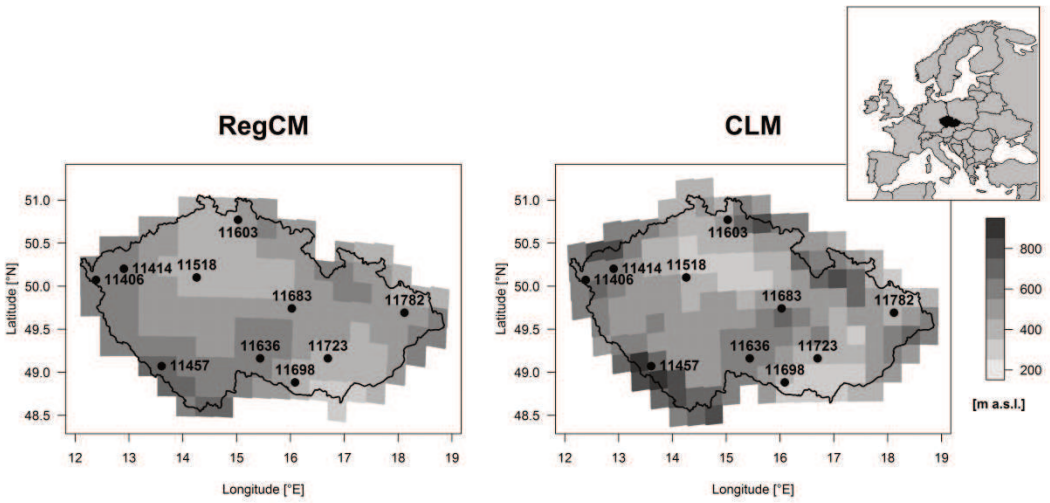

Figure 3.1: Locations of stations (black dots) and examples of orography in RCMs: RegCM (left) and CLM (right).

3.2.3 Precipitation characteristics and methods

Examined are the following characteristics of convective and stratiform precipitation, computed at the ten stations and in all grid boxes in the area of the Czech Republic in individual RCMs:

- mean annual cycle of monthly precipitation amounts, number of wet days (defined as days with precipitation of a given origin >= 0.5 mm) and rain intensity index (RII, defined as mean precipitation amount on wet days; cf. Klein Tank et al., 2002);
- proportion of convective and stratiform precipitation on total amounts for individual seasons;
- dependence of mean annual precipitation amounts on altitude; and
- mean annual maxima and 20-year return values of daily precipitation amounts.

The characteristics are computed for convective (subgrid), stratiform (large-scale) and total precipitation. Note that the term ‘wet day’ may refer either to convective, stratiform or total precipitation. Dependence of precipitation amounts on altitude is analysed using the least-squares regression with *t*-test (e.g., Wilks, 1995).

For estimatinf high quantiles of precipitation amounts (corresponding to 20-year return values), the Generalized Extreme Value (GEV) distribution (Coles, 2001) is fitted to samples of annual maxima of daily precipitation amounts. We use the

method of L-moments, which is more suitable for smaller samples than are methods based on maximum likelihood (Hosking and Wallis, 1997). A GEV parameterization in which positive values of the shape parameter correspond to heavy-tailed (unbounded) GEV distribution is used. Uncertainty for individual stations and grid boxes is large (due to relatively small sample size), so we avoid discussing location-specific results and focus on general tendencies when comparing the mean annual maxima, the estimated shape parameter of the GEV distribution, and the 20-year return values for observed and RCM-simulated data (in terms of boxplots across stations/grid boxes).

3.2.4 Effects of areal averaging on extremes

The interpretation of differences between characteristics of grid box and station maxima is not straightforward since grid box maxima represent an areal average rather than a point value. The effect of areal averaging on the magnitude of extremes is typically summarized by the area reduction factors (ARFs) representing the ratio between the areal average and point rainfall extreme for a given area, temporal aggregation and exceedance probability (see e.g., Svensson and Jones, 2010b for a comprehensive overview). In some studies, the effect of the latter is, however neglected. Based on 6 years of radar data, Řezáčová et al. (2005b) derived relations for the upper envelope of the observed ratios between areal average and point rainfall for the Czech Republic for various temporal aggregations. For the daily data and area corresponding to a grid box (625 km^2) the maximum ARF value is 0.84. This value is not directly applicable, however, to mean annual maxima and/or 20-year return values. In a more general study and using 11 years of radar data, Overeem et al. (2010) derived functional relations between area, temporal aggregation and parameters of a GEV model for precipitation maxima in the Netherlands. These relations result in ARFs of 0.88 and 0.77 for mean annual and 20-year precipitation maxima, respectively, and the shape parameter drops from 0.17 to 0.09. Although these semiempirical relations were derived for a different region than that studied here, we consider them to be more relevant for the discussion of our results as they account for dependence on the return level. Therefore, the ARFs and the areal dependence of the shape parameter given by Overeem et al. (2010) are further

considered in addition to the characteristics obtained from the station data to reflect the area reduction.

The reported ARFs were derived from total precipitation. Several studies have shown (Huff and Shipp, 1969; Skaugen, 1997), however, that the reduction of magnitude especially applies to convective events than in contrast to large-scale frontal rainfall. We therefore assume that the ARFs are relevant only for total and convective precipitation.

3.3 Results

3.3.1 Mean annual cycle of precipitation characteristics

While observed convective precipitation has a clear annual cycle of precipitation amounts, intensity and number of wet days, with a maximum during the summer months, observed stratiform precipitation has an annual cycle with a maximum in summer only for intensity of precipitation (Figure 3.2). Observed stratiform precipitation amounts are almost evenly distributed throughout year, and the number of wet days is slightly larger in winter. The annual cycle of observed total precipitation characteristics is dominated by the convective precipitation.

All RCMs reproduce the basic behaviour of the annual cycle of convective precipitation characteristics (Figure 3.2, left column). The summer peak of convective precipitation amounts and the number of wet days is too high in several RCMs, mainly Aladin and Aladin_CZ. These two RCMs simulate 20–25 days with convective precipitation ≥0.5 mm in summer months (averaged over grid boxes), which is almost twice as much as in observations. The peak in the annual cycle of convective precipitation tends to occur too early in most RCMs (mostly in June but already in May in RCA_C4I). Intensity of convective precipitation is reproduced most poorly, as all RCMs substantially underestimate it in the warm half-year (April–September). In cold half-year (October–March), intensity of convective precipitation is better simulated but several RCMs produce almost no convective precipitation in winter, which contradicts observations as well.

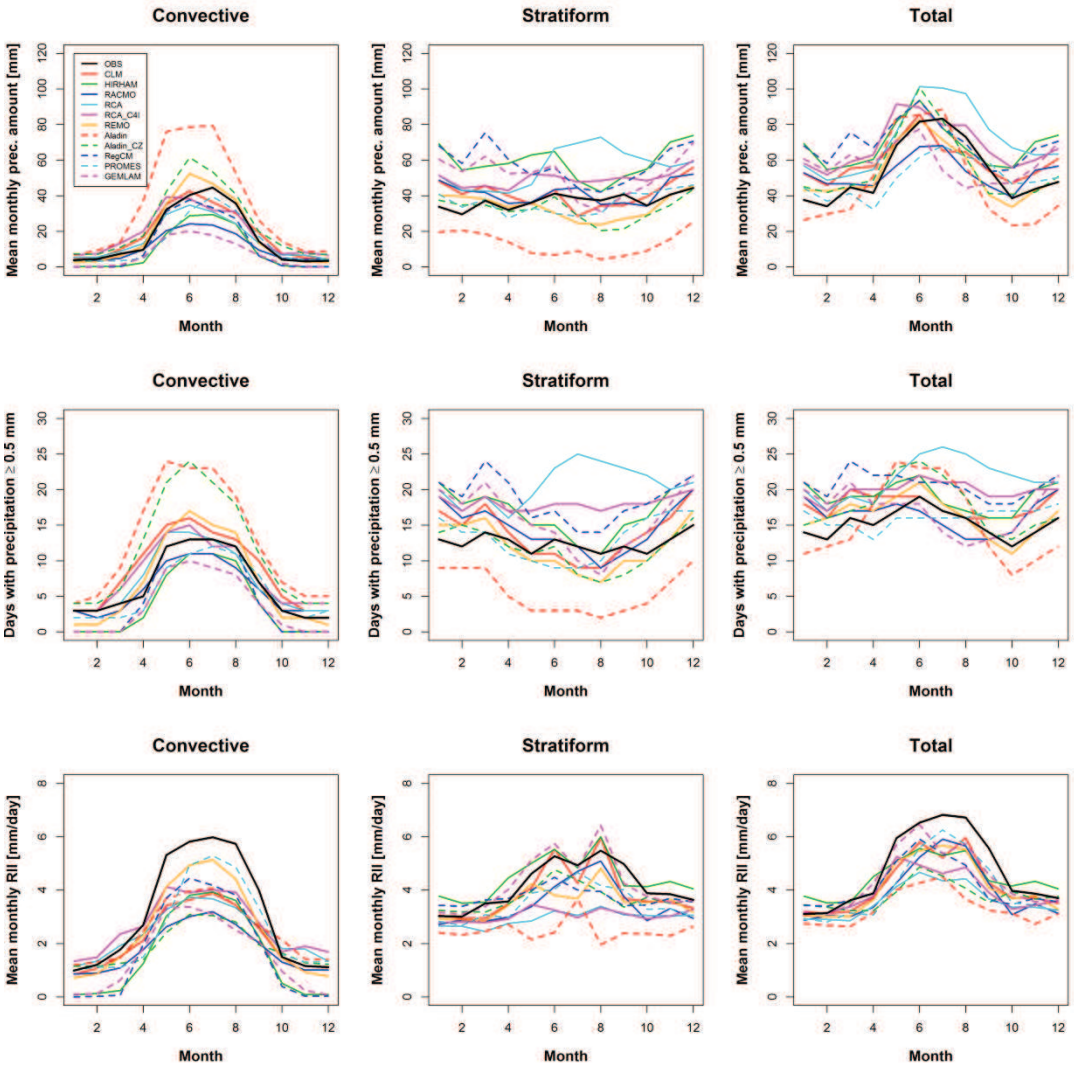

Figure 3.2: Mean annual cycle of monthly precipitation amount (top), number of wet days (with precipitation ≥0.5 mm, middle), and rain intensity index (RII, bottom), averaged over all stations and grid boxes in the area of the Czech Republic.

Most RCMs tend to underestimate also intensity of stratiform precipitation, mainly in summer and autumn (Figure 3.2, middle column). The stratiform precipitation amount and the number of wet days are reproduced better. Large differences exist among the individual RCMs, however, and the RCMs tend to overestimate stratiform precipitation in the cold half-year. An unrealistic annual cycle of stratiform precipitation and the number of wet days is simulated in RCA, with maximum in late summer and autumn (when the number of wet days is overestimated by a factor of 2). Stratiform precipitation is severely underestimated in Aladin (i.e. in the RCM with the largest overestimation of convective precipitation).

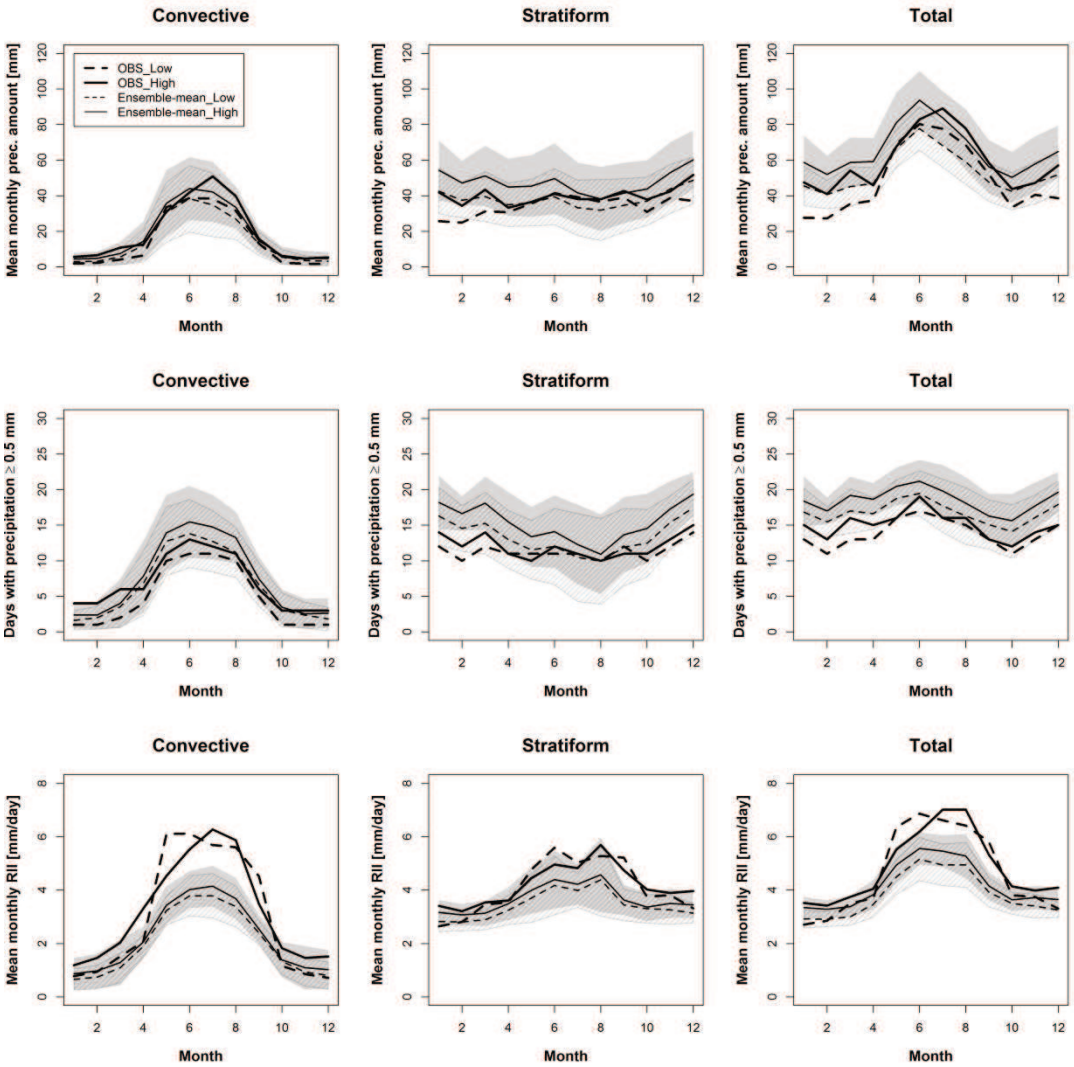

Figure 3.3: Mean annual cycle of monthly precipitation amount (top), number of wet days (middle) and rain intensity index (bottom) for stations and grid boxes with altitude ≤450 m a.s.l. (dashed lines) and >450 m a.s.l. (solid lines). Thicker lines show the observed annual cycle while thinner lines the RCMs' ensemble mean. The shaded area indicates the spread among RCMs expressed in terms of standard deviation (the striped-shaded area refers to lower-elevated grid boxes while the solid shaded area to higher-elevated grid boxes).

The annual cycle of total precipitation is dominated by convective precipitation also in the RCMs (Figure 3.2, right column), except for RCA in which it is governed by the unrealistic annual cycle of the stratiform component. In some RCMs, mainly in Aladin, biases in characteristics of convective and stratiform precipitation compensate for one another to some extent, and hence the total precipitation characteristics are much better simulated than are the individual components. The main features of the annual cycles of convective and stratiform precipitation

characteristics are similar at lowland (≤450 m a.s.l.) and higher-elevated (>450 m a.s.l.) locations in both observed and RCM data (Figure 3.3).

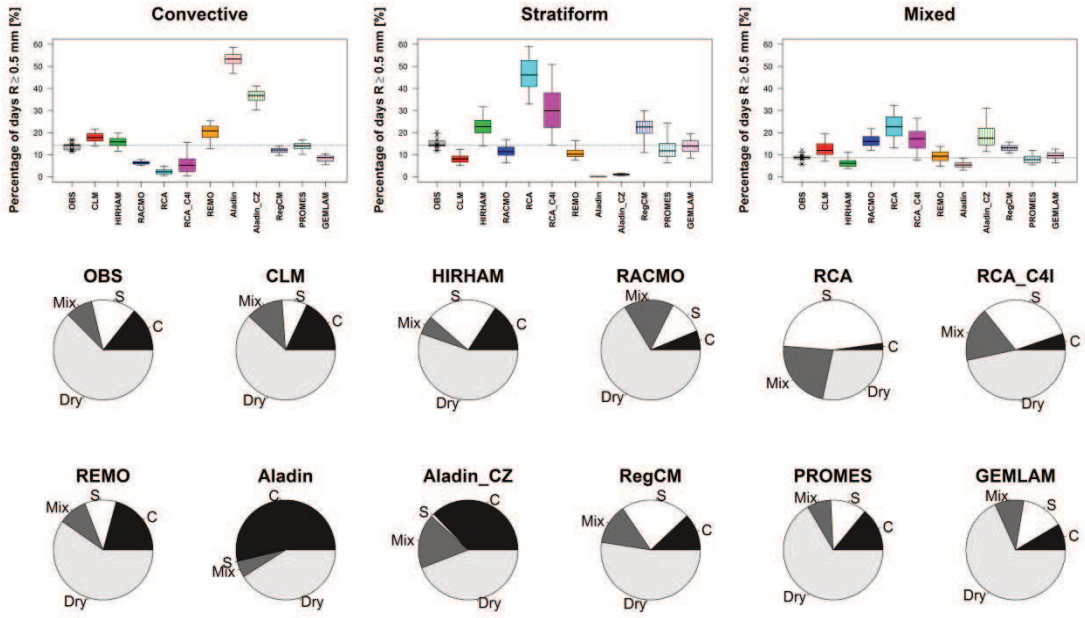

Figure 3.4: Frequency of wet days in summer (JJA) according to the origin of precipitation: convective (convective precipitation ≥0.5 mm while stratiform <0.5 mm), stratiform (stratiform precipitation ≥0.5 mm while convective <0.5 mm) and mixed (both convective and stratiform precipitation ≥0.5 mm). The boxplots (top) are calculated across grid boxes or stations. The bottom and top of the box are the first and third quartiles, and the band inside the box shows the median. The whiskers represent the 5 and 95% quantiles. For observed data, individual station values are depicted by crosses. The grey dotted line shows the median of observed values. In pie charts (bottom), dry days are the days with both convective and stratiform precipitation <0.5 mm. C (S) denotes convective (stratiform) origin.

The distribution of wet days according to the origin of precipitation is further scrutinized by splitting all wet days in summer into those of convective origin (with convective precipitation ≥ 0.5 mm while stratiform < 0.5 mm), stratiform origin (vice versa) and mixed (both components ≥ 0.5 mm). In the observed data, the frequency of convective and stratiform wet days is balanced (around 15%), and mixed wet days occur less often (around 8% of summer days; Figure 3.4). A good reproduction of the distribution of wet days according to convective, stratiform and mixed origin of precipitation is found for several RCMs, mainly PROMES (in which the frequency of wet days of each origin agrees with observations almost perfectly), RegCM, REMO and HIRHAM. In Aladin and Aladin_CZ, significant stratiform precipitation occurs only on days when convective precipitation is also significant. An opposite

pattern (significant convective precipitation usually associated with stratiform precipitation occurrence) appears for RCA, RCA_C4I and RACMO. Most RCMs overestimate the number of wet days in which both components are important.

3.3.2 Proportion of convective precipitation in total amounts

Percentage of precipitation amounts that fall in the form of convective precipitation is shown for individual seasons in Figure 3.5. In observed data, the proportion of convective precipitation is highest in summer, when it is close to 50%, followed by spring (~30%) and autumn (~15%).

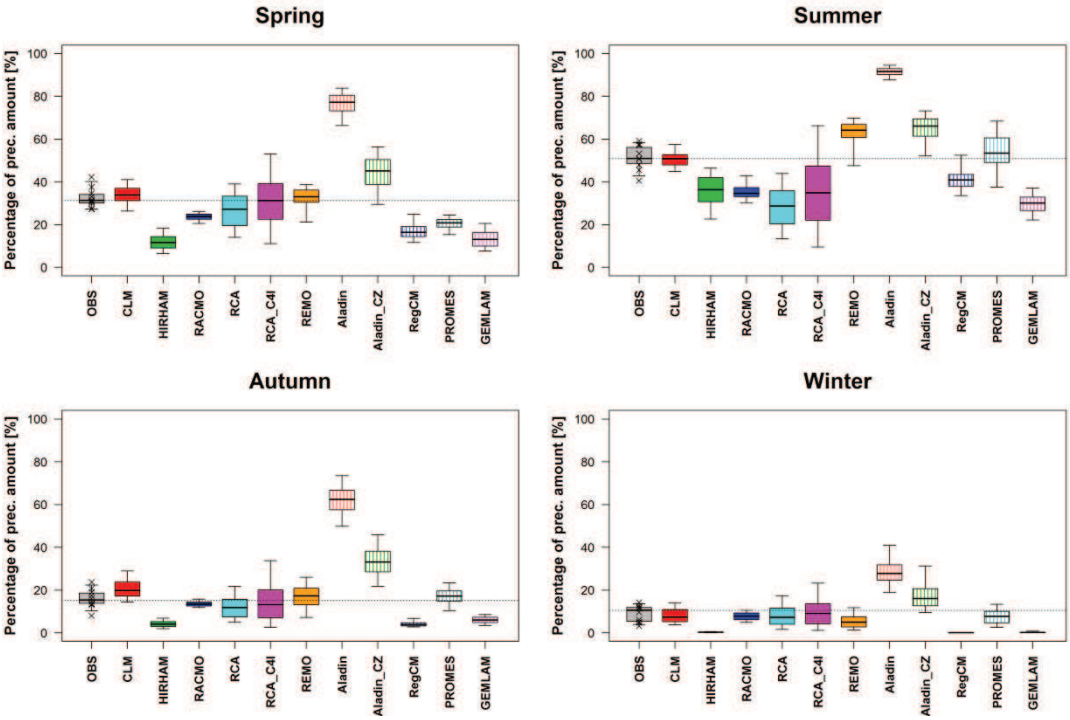

Figure 3.5: Percentage of convective precipitation in total amounts for individual seasons. The boxplots are calculated across grid boxes or stations. The bottom and top of the box are the first and third quartiles, and the band inside the box shows the median. The whiskers represent the 5 and 95% quantiles. For observed data, individual station values are depicted by crosses. The grey dotted line shows the median of observed values.

The proportion of convective precipitation in summer is captured best by CLM (Figure 3.5). A very large spread among the RCMs is found, with values of the median (across grid boxes) ranging from 29 to 92% in summer. CLM is also the only RCM in which proportions of convective precipitation are reasonably reproduced in all four seasons. Two RCMs (Aladin and Aladin_CZ) suffer from large

overestimation of the proportion of convective precipitation in all seasons, while in some other RCMs (HIRHAM, RegCM, GEMLAM), this proportion is underestimated throughout the year. The latter RCMs simulate no convective precipitation in winter and almost no in autumn, which also contradicts observations. Unrealistically high proportions of convective precipitation in Aladin are particularly suspicious in autumn (~62%) but this RCM is clearly an outlier from the ensemble in all seasons (possible reasons are discussed in section 3.4.5). In most other RCMs, on the other hand, the fractions of convective precipitation in total amounts in winter and autumn are captured well.

3.3.3 Dependence on altitude

In observed data, both convective and stratiform precipitation amounts increase with altitude, and the slope is larger for the latter (Table 3.2).

Table 3.2: Slopes of dependence of convective, stratiform and total precipitation amounts on altitude, expressed as changes of precipitation amount in mm/100 m.

	Convective		**Stratiform**		**Total**	
OBS	14.8 *		39.1 *		53.9 *	
CLM	9.7 *		39.2 *		48.9 *	
HIRHAM	15.7 *		151.7 *	N	167.4 *	N
RACMO	13.2 *		52.6 *		65.8 *	
RCA	51.0 *	N	47.0 *		98.0 *	N
RCA_C4I	91.4 *	N	46.2 *		137.5 *	N
REMO	–11.5 *	N	-0.2	N	–11.7 *	N
Aladin	21.7 *	N	27.0 *		48.7 *	
Aladin_CZ	5.2 *	N	61.5 *		66.7 *	
RegCM	–6.0 *	N	40.1 *		44.2 *	
PROMES	–2.5	N	41.0 *		38.5 *	
GEMLAM	0.3	N	70.7 *		71.1 *	

* Denotes statistical significance at the 0.05 level; N denotes RCMs' estimated slopes that fall outside the 95% confidence interval of the observed slope

Most RCMs reproduce the magnitude of the increase with altitude reasonably well for stratiform and total precipitation. For convective precipitation, RCA and RCA_C4I have unrealistically large slopes of dependence (overestimated by a factor of 3–6), while three RCMs (REMO, RegCM and PROMES) produce negative dependence on altitude. Only in three RCMs (CLM, RACMO and HIRHAM) do the estimated slopes of the dependence for convective precipitation lie within the 95% confidence interval of the observed one (Table 3.2).

For stratiform precipitation, the estimated slope lies within the 95% confidence interval of the observed slope in 9 out of the 11 RCMs, and the spread among the RCMs is much smaller (Table 3.2). REMO (zero slope) and HIRHAM (largest overestimation of the slope) are the least realistic (Figure 3.6). All RCMs except for RCA and RCA_C4I also agree with observed data on the fact that the dependence on altitude is stronger for stratiform than convective precipitation.

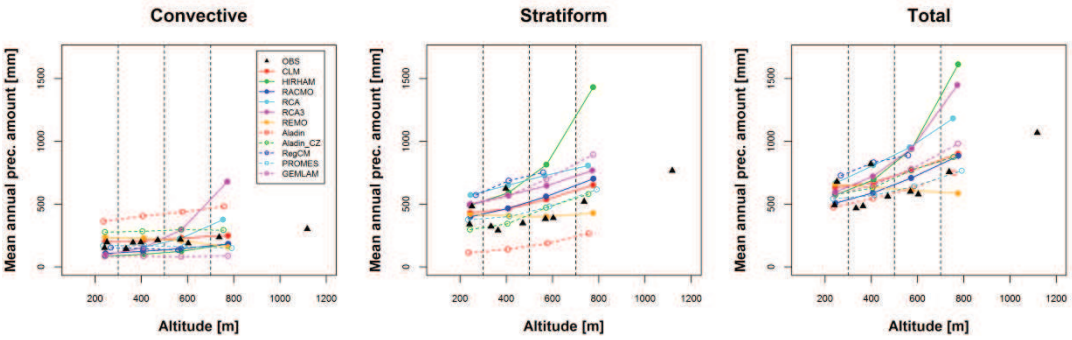

Figure 3.6: Dependence between mean annual precipitation amount and altitude for convective (left), stratiform (middle) and total (right) precipitation. For RCMs, mean values in elevation bins (≤300 m, 301–500 m, 501–700 m, and >700 m) are plotted; for observed data, station values are shown.

For total precipitation amounts, the RCMs' slope is close to that for the observed data except in cases of those RCMs that suffer from substantial bias in one or both components (RCA, RCA_C4I – overestimated dependence of convective precipitation; HIRHAM – overestimated dependence of stratiform precipitation; REMO – underestimated dependence of both; Figure 3.7, Table 3.2). In several RCMs, biases compensate for each other: underestimated dependence for convective amounts together with overestimated dependence for stratiform amounts result in good reproduction of the slopes for total precipitation amounts in Aladin_CZ, GEMLAM and RegCM. It is also noteworthy that unrealistic (in)dependence of precipitation on altitude in REMO is not manifested in a large bias in spatially-averaged precipitation amounts (cf. annual cycles for REMO in Figure 3.2), although it is obvious that spatial precipitation patterns (that are governed mainly by orography) cannot be realistic in this RCM.

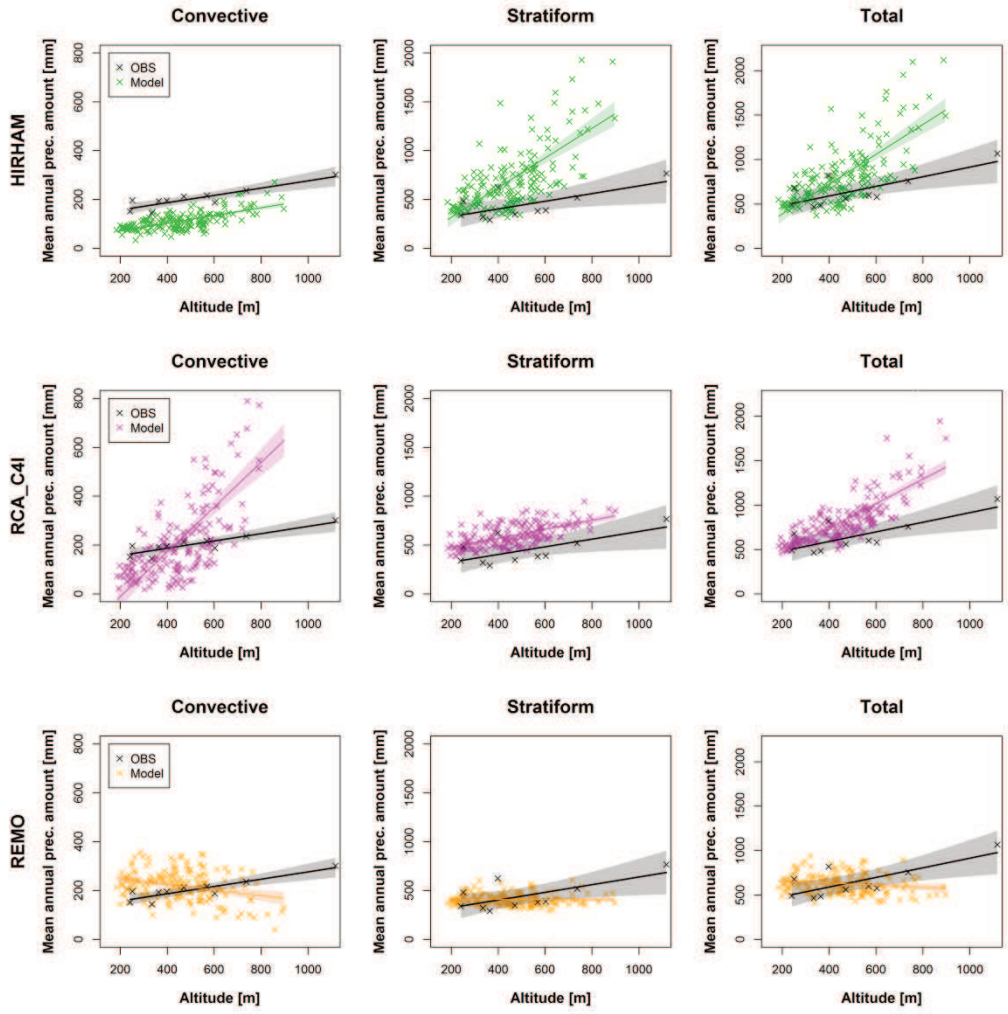

Figure 3.7: Examples of dependence between mean annual precipitation amount and altitude for convective (left), stratiform (middle) and total (right) precipitation in three RCMs with the largest biases, in comparison to observed data. Trends estimated by the linear regression and their 95% confidence bounds are plotted.

In general, CLM and RACMO simulate realistic dependence of both convective and stratiform precipitation amounts on altitude. In all other RCMs, the slope of the dependence lies outside the 95% confidence interval of that for the observed data for one or both precipitation components. The main conclusions concerning comparison of the RCMs and observed data do not change when the highest-elevated station (11457 Churáňov) is excluded from the data. The above-reported results refer to annual data but similar patterns appear also in individual seasons (not shown).

3.3.4 Extremes

Similarly to the study of the proportion of convective precipitation, we evaluate spatially pooled mean annual maxima, the shape parameter of the fitted GEV distribution (which governs the tail of the GEV distribution), and the estimated 20-year precipitation maxima in terms of boxplots (Figure 3.8). Mean annual maxima are underestimated for convective precipitation and, with the exceptation of CLM, also for total precipitation. If a reduction due to ARF is considered (Overeem et al., 2010), however, the mean annual maxima of total precipitation are reproduced reasonably well. For stratiform precipitation, both negative and positive biases appear with the latter being more frequent. Aladin is the only RCM suffering from large underestimation of both convective and stratiform mean annual maxima.

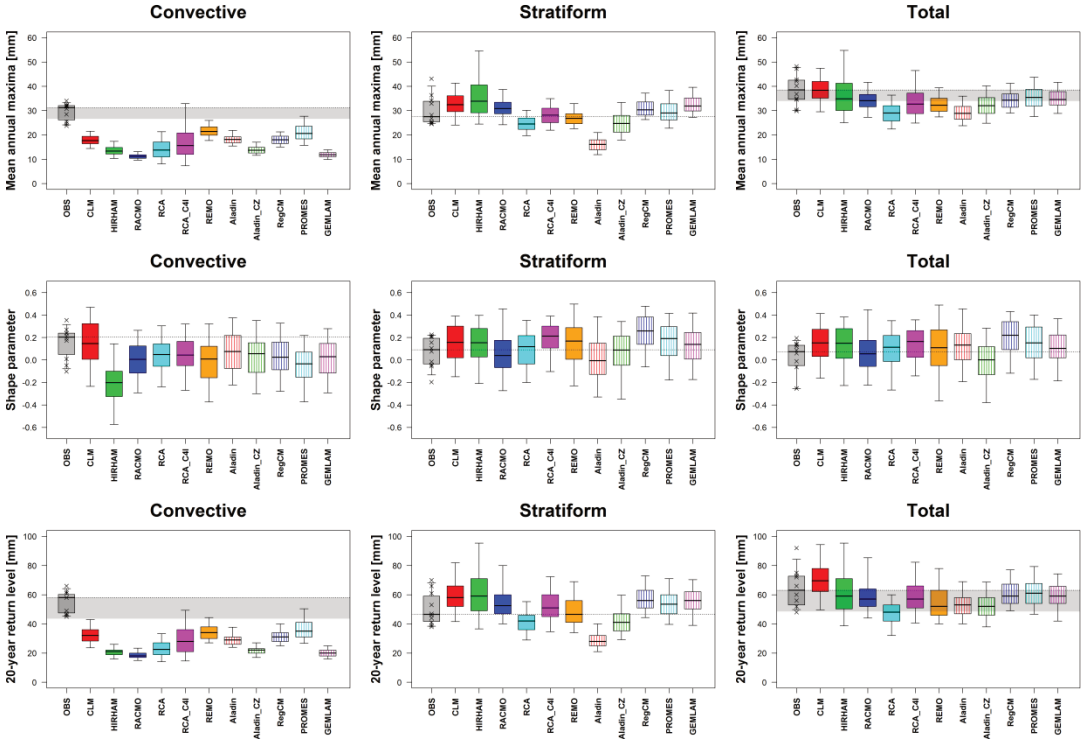

Figure 3.8: Mean annual maxima of daily precipitation amounts (top), shape parameter of the GEV distribution (middle) and 20-year return levels of annual maxima of daily precipitation amounts (bottom). The bottom and top of the box are the first and third quartiles, and the band inside the box shows the median. The whiskers represent the 5 and 95% quantiles. For observed data, individual station values are depicted by crosses. The lower boundary of the shaded area for extremes of total precipitation corresponds to the median of observed data after correction using ARFs from Overeem et al. (2010); for convective extremes, the same reduction (in mm) as for total precipitation was applied.

As mean annual maxima are mostly due to stratiform precipitation in the RCMs (in contrast to observations in which they are comparable for convective and stratiform precipitation, Figure 3.9), the shape parameter of the GEV distribution is similar for total and stratiform precipitation. Positive values of the shape parameter (corresponding to heavy tails) prevail, and the GEV distribution has a slightly heavier tail for total and stratiform precipitation in most RCMs compared to observations. For simulated convective precipitation, by contrast, the shape parameter tends to be smaller than in observed data and mostly close to zero. The exceptions are again CLM, which is the only RCM capturing the heavy-tailed behaviour also for convective extremes, and HIRHAM with clearly negative values corresponding to a right-bounded GEV distribution. Considering the decrease in the shape parameter with increasing area (from station to grid box) indicated by Overeem et al. (2010), the bias in the shape parameter for convective precipitation extremes is likely small for most of the RCM simulations. For total precipitation, however, similar reduction increases the tendency to positive bias of the shape parameter.

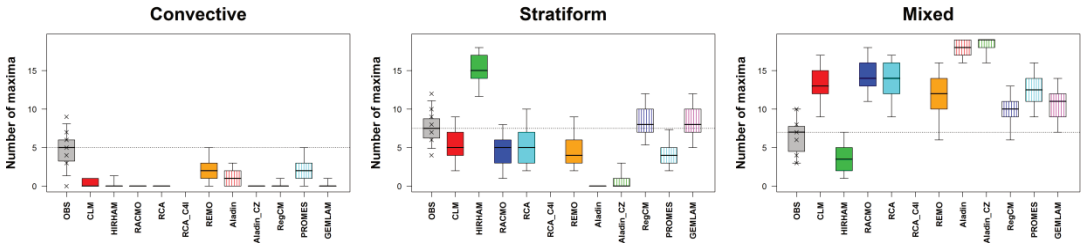

Figure 3.9: Number of annual maxima (in total 19) of convective (left), stratiform (middle) or mixed (right) origin. Annual maxima are considered to be of convective origin when the daily amount of stratiform precipitation is <0.5 mm, and vice versa. Mixed cases correspond to both components ≥0.5 mm.

A similar pattern as for mean annual maxima appears also for 20-year return values. These are severely underestimated for convective precipitation (even after consideration of the ARF, Figure 3.8), which is related not only to the underestimated annual maxima but also to the suppressed heavy-tailed behaviour of convective extremes in the RCMs, and they are slightly overestimated in most RCMs for stratiform precipitation. This results in a tendency towards slight underestimation of the 20-year return values of total precipitation amounts, which is found in most RCMs. The reproduction of extremes in total precipitation is much better compared

to that for the two components evaluated separately, however, and the tendency towards underestimating the 20-year total precipitation disappears when the reduction of the station values by the ARF from Overeem et al. (2010) is considered.

3.4 Discussion

3.4.1 Simulation of 'mean' characteristics

In general, the RCMs show a relatively good agreement with observed data for mean annual cycles of convective and stratiform precipitation characteristics. They tend to reproduce the pronounced annual cycle of convective precipitation with a single maximum in summer and a minimum in winter while stratiform precipitation is almost constant throughout the year. The convective component governs also the annual cycle of total precipitation in both observed data and the RCMs. The main and rather general deficiencies with respect to annual cycles are the shift of the peak of convective precipitation to early summer or late spring, and overestimation of stratiform precipitation in the cold half-year. The former could be related to more general problems with parameterization of convection in climate models, which often report too-early onset (and maximum) of convection in the diurnal cycle (Dai and Trenberth, 2004; Lee et al., 2007; Brockhaus et al., 2008). The latter may be related to overestimated flow strength in some RCMs (Plavcová et al., 2013). Many RCMs also simulate too many wet days (cf. Noguer et al., 1998; Déqué et al., 2007; Rauscher et al., 2010), particularly for stratiform precipitation in the cold half-year, and most RCMs overestimate the percentage of those wet days in which both convective and stratiform precipitation are important. A maximum in early summer (June) was found also in ERA-40 precipitation data for the nearby Danube basin (Hagemann et al. 2005) but a dry bias prevailed throughout the year, especially in the cold half-year. ERA-40 uses a convective parameterization based on the Tiedtke (1989) acheme, similarly to several RCMs (CLM, HORHAM, RACMO and REMO; see also section 3.4.5). Except for RACMO, these RCMs simulate a rather pronounced peak in the annual cycle of precipitation in July–August (Figure 3.2). A dry bias in the cold half-year is simulated only in Aladin. Due to very different

resolutions, other characteristics are difficult to compare between ERA-40 and the examined RCMs.

The increase with altitude is captured better for stratiform than convective precipitation amounts in most of the RCMs. Several RCMs simulate unrealistically strong or weak dependence on altitude, especially for convective precipitation. A decline of convective precipitation amounts with altitude in REMO – found also for total precipitation – is particularly suspicious and suggests a severe bias with respect to links between orography and precipitation in this RCM.

In some RCMs the biases in convective and stratiform precipitation characteristics are found to partly offset one another. This can be attributed to the fact that excessive moisture which is not converted to precipitation in the convection scheme is at least partly removed from the atmosphere by the large-scale scheme and vice versa, and illustrates that the model separation of the two components may be difficult to interpret since it is prone to design and formulation errors (cf. Williamson, 2013). This in turn can severely affect the whole model performance. Although such compensation effect may result in mean (climatological) characteristics of precipitation that are in good agreement with observations, it is likely that the spatial and temporal structure of precipitation, which is related to the underlying processes and is crutial, for example, with respect to the hydrological response, is misrepresented in those cases.

3.4.2 Simulation of extremes

The main limitation of the RCMs is found for extremes of convective precipitation, which are severely underestimated. However, this bias has to be interpreted with caution. First, the RCM (grid box) data are compared against station (point) data, so they represent precipitation at a different spatial scale. The convection parameterization schemes are not designed to represent individual storms and local rainfall events, but they describe the average properties of convection over a model grid box. Moreover, these schemes were usually designed for coarse-resolution (>50 km) models and for tropical convection, and they are less appropriate for higher resolutions and outside the tropics (Swann, 2001; Kendon et al., 2012). The daily amounts of convective precipitation rarely exceed some specific threshold in RCMs (Durman et al., 2006; Li et al., 2011; Kendon et al., 2012) and contribute little to

extreme total precipitation at the tail of the distribution. The effect of areal averaging – as estimated by the ARFs from Overeem et al. (2010) – is nevertheless small in comparison to the identified biases, so the underestimation of convective extremes in the RCMs is not only due to spatial smoothing. Suppressed heavy-tailed behaviour of extremes leads to even larger biases for 20-year return values of convective precipitation than for mean annual maxima.

Second, one has to take into account that, at the given 25 km resolution, large (mesoscale) convective systems affect multiple grid boxes simultaneously, and precipitation associated with them may be simulated as partly large-scale and partly subgrid in climate models whereas it is usually classified as convective in station data. This is a direct consequence of the fact that mesoscale systems and precipitation associated with them are only partially captured in model simulations with 25 km grid spacing.

The origin of annual maxima of daily precipitation in observed and RCM data is summarized in Figure 3.9. In most RCMs, the annual maxima are never or almost never solely of convective origin, and convective maxima are underrepresented compared to observations also in all remaining RCMs (this remains the case also when the threshold allowed for the stratiform component increases from 0.5 to 1 ar 5 mm). The same behaviour has been reported by Kendon et al. (2012) for the Met Office Hadley Centre Global Environmental Model. By contrast, all RCMs except for HIRHAM overestimate the proportion of annual maxima of mixed origin, i.e. when both convective and stratiform amounts play a role (which holds true also for the higher thresholds). In HIRHAM, most maxima are of stratiform (large-scale) origin, while in Aladin and Aladin_CZ, almost all maxima are mixed. The latter relates to the pronounced overestimation of convective precipitation and the number of days with convective precipitation in these two RCM simulations. Even in these RCMs, however, the annual maxima of daily precipitation are rarely (Aladin) or never (Aladin_CZ) of solely convective origin.

Extremes of stratiform precipitation are reproduced better than those of convective precipitation, with a tendency towards overestimation in most RCMs. Because the two biases (in convective and stratiform precipitation) compensate for each other to some degree, extremes of total precipitation are usually simulated better than are the individual components, and there is only slight tendency towards underestimation.

Generally good representation of (total) daily precipitation maxima was also concluded by Hanel and Buishand (2010) for the Netherlands. Although convective precipitation was not examined separately, the authors concluded from the severe biases in the simulated hourly precipitation extremes that convective processes may not be properly represented in some RCMs.

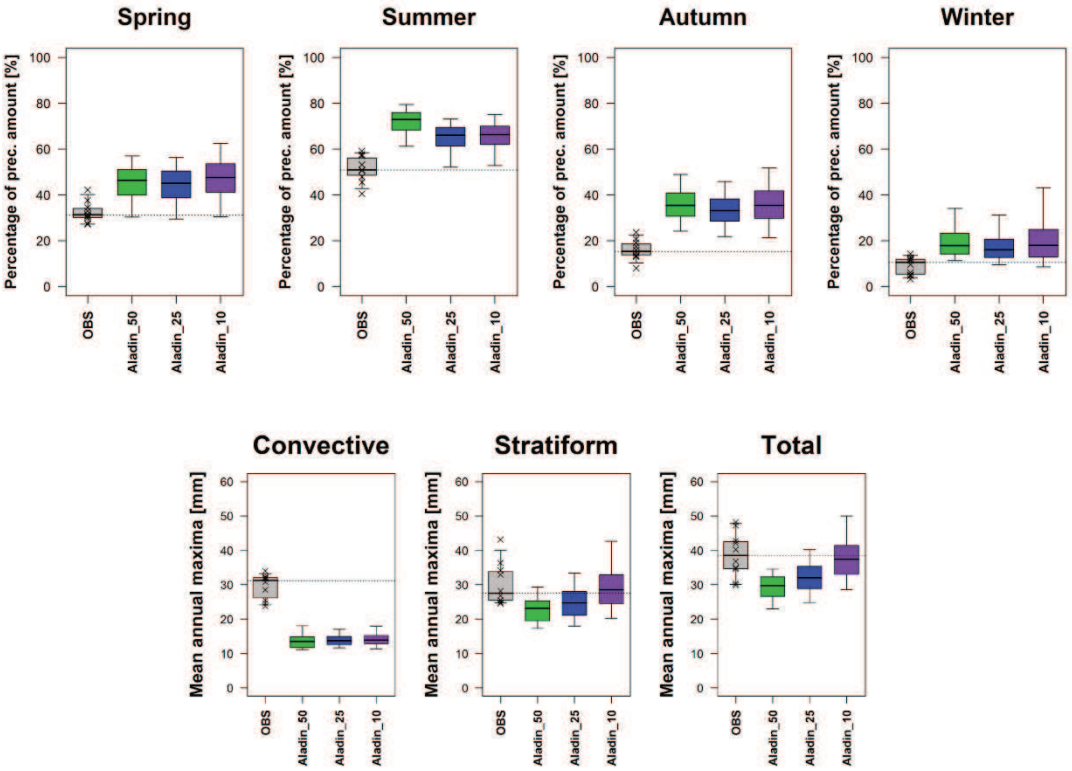

Figure 3.10: Percentage of convective precipitation in total amounts for individual seasons (top) and mean annual maxima of daily precipitation amounts (bottom) in three simulations of Aladin_CZ with 50, 25 and 10 km horizontal resolution.

3.4.3 Possible effects of horizontal resolution

Preliminary results concerning the influence of horizontal resolution on convective and stratiform precipitation based on three simulations of Aladin_CZ with 50, 25 and 10 km resolution (Skalák et al., 2014) show no important differences in characteristics of mean convective and stratiform precipitation, including the proportion of convective precipitation in the total amounts (Figure 3.10, upper panel). The horizontal resolution has a stronger effect on extremes (Figure 3.10, lower panel), which is in agreement with findings reported by Boyle and Klein (2010) and Li et al. (2011). Extremes of convective precipitation depend little on the

horizontal resolution in these Aladin_CZ simulations, however, while extremes of stratiform precipitation increase and become more realistic. This suggests that the biases in convective precipitation persist within a range of horizontal resolutions under which current RCMs are typically run and that better simulation of precipitation characteristics with increasing resolution (Boberg et al., 2010; Rauscher et al., 2010; Larsen et al., 2013) is mainly due to improved large-scale precipitation in relation to better representation of topography.

Convection-permitting models, commonly used in numerical weather prediction but computationally very costly for extended time scales in climatological studies, were reported to improve the diurnal cycle of convection (Hohenegger et al., 2008), hourly extremes (Wakazuki et al., 2008), and the spatial and temporal structure of rainfall in general (Kendon et al., 2012), so they probably represent a more promising route towards realistic representation of precipitation of convective precipitation in climate models.

3.4.4 Comparison of RCMs

CLM is the only RCM that does not suffer from a large bias in any examined characteristic of convective and stratiform precipitation. In several aspects, including proportion of convective precipitation, dependence of both convective and stratiform precipitation amounts on altitude, and heavy-tailed behaviour of convective extremes, this RCM performs best in the examined ensemble. The finding of CLM's good performance is in line with results of previous studies that evaluated performance of the ENSEMBLES RCMs over Europe with respect to various characteristics of surface climate (e.g., Christensen et al., 2010; Holtanová et al., 2012).

Severe biases in some precipitation characteristics appear in most other RCMs. Again, these may be to some extent compensated for in total amounts. Nevertheless, the biases point to drawbacks in the reproduction of precipitation processes that should be taken into account when interpreting the RCM data, in particular, in further developing and improving the RCMs.

3.4.5 Parameterizations in RCMs

Although different parameterizations of deep convection and large-scale precipitation are applied in the RCMs, they often are based on similar approaches. Convective parameterizations in most of the RCMs examined are formulated as bulk mass flux schemes. Nevertheless, no similarity was found in the behaviour of convective or stratiform precipitation in such RCMs having similar parameterizations, except for RCA and RCA_C4I which are almost identical. For example, CLM, HIRHAM, REMO and RACMO apply a similar parameterization of convection which is based on the mass flux scheme by Tiedtke (1989). Characteristics of convective precipitation, however, differ substantially amongst these models (cf. Figure 3.5 and 3.8). This finding is in line with a recent study by Fischer et al. (2015), who analysed modelled precipitation types in ENSEMBLES RCMs that were driven by GCMs instead of ERA-40.

Aladin and Aladin_CZ, which have the largest proportion of convective precipitation (Figure 3.5), use a deep convection scheme according to Bougeault (1985) that was designed for the "grey zone" with many differences from other common convection schemes (Gerard and Geleyn, 2005). This may contribute to the fact that Aladin stands out in many simulated characteristics and also to a strong compensating tendency of biases in characteristics of convective and stratiform precipitation in this RCM. Nevertheless, implementation of the convective parameterization differs as to the model cycle between Aladin and Aladin_CZ, and the two versions differ also in other specific parameterizations applied (Farda et al., 2010). This may contribute to rather large differences between Aladin and Aladin_CZ.

The last set of RCMs with a similar parameterization of convective clouds and subgrid precipitation is RCA, RCA_C4I, GEMLAM and PROMES, in which parameterization based on the Kain and Fritsch (1993) scheme is applied. The differences among these RCMs in convective precipitation characteristics are again large, and they are pronounced also for the dependence on altitude (Table 3.2). As pointed out by Fischer et al. (2015), differences in land-surface schemes and simulated land-surface characteristics, particularly soil moisture, probably contribute to the variability in precipitation composition among models. It should also be noted that some typical errors relating to parameterization of convection, such as too-early

onset of convection, have been reported to depend only slightly on the particular convection scheme (Brockhaus et al., 2008).

Precipitation is related to such other variables as atmospheric circulation, temperature and humidity, and their differences and biases affect the simulation of precipitation. On the other hand, biases in the convective and stratiform precipitation components may have large impacts on other aspects of the simulated climate because of their different effects on heat and mass transport (Dai, 2006). Representation of precipitation in climate models is therefore linked to atmospheric dynamics, land-atmosphere interactions and vertical profiles in a complex way. This may explain why RCMs with closely related parameterizations of precipitation processes differ in precipitation characteristics.

3.5 Summary

The present study evaluated biases in characteristics of convective (subgrid) and stratiform (large-scale) precipitation in an ensemble of 11 RCM simulations driven by the ERA-40 reanalysis in Central Europe. The main findings are summarized as follows:

- The RCMs on average reproduce the annual cycle of convective precipitation reasonably well but underestimate its intensity throughout the year. The peak tends to be shifted to early summer or even late spring.
- Stratiform precipitation tends to be overestimated in the cold half-year.
- The distribution of wet days according to convective, stratiform and mixed origin of precipitation is reproduced well in several RCMs, while some other RCMs substantially overestimate the proportion of wet days of convective or stratiform origin. Wet days when both components are important are too frequent in most RCMs.
- There is a large spread among the RCMs in the proportion of convective precipitation to total amounts; some of the RCMs consistently and substantially overestimate or underestimate this proportion throughout the year.

- Dependence on altitude is simulated better for stratiform and total precipitation than convective precipitation.
- Extremes (mean annual maxima, 20-year return values) are underestimated for convective precipitation while they tend to be slightly overestimated for stratiform precipitation. This results in a relatively good simulation of extremes in total precipitation amounts. For convective precipitation extremes, the effect of areal averaging (as estimated by the area reduction factor) is small in comparison to the identified biases.
- Characteristics of total precipitation are often better simulated than are those of the individual components, which is due to compensating biases in convective and stratiform precipitation. In REMO, the annual cycle and some other precipitation characteristics (including spatially averaged amounts) are simulated reasonably well in spite of an unrealistic negative dependence of precipitation amounts on altitude.
- There remains an open question why pair of closely related RCMs (Aladin and Aladin_CZ) that use a similar parameterization of convective precipitation and are run at the same resolution and with the same driving data produces very different results. Analogous differences are much smaller for another pair of simulations with the same RCM (RCA).
- Errors in precipitation characteristics in climate models are mainly related to drawbacks in the representation of convection.

Acknowledgements

The study was supported by the Czech Science Foundation under project 14-18675S, and the Charles University in Prague, student project GA UK No. 851713. The RCM data were obtained from the ENSEMBLES project database funded within the EU-FP6 (http://ensemblesrt3.dmi.dk/).

4 Convective and large-scale precipitation scenarios in the Czech Republic*

4.1 Introduction

Climate change observed in recent years is associated primarily with increasing global temperature, but there is evidence that the hydrological cycle is affected as well. Analyses of observed precipitation data show increases in mean precipitation in the tropics and high latitudes and decreases in the subtropics (Frich et al., 2002; Alexander et al., 2006), and intensification of precipitation even in regions where mean precipitation decreases (Alexander et al., 2006; Donat et al., 2013; Madsen et al., 2014; Dittus et al., 2015).

Because climate (including the precipitation regime) is affected by strong interannual and spatial variations (e.g., Pauling et al., 2006), which makes detection of significant trends in observed data almost impossible, climate models could better estimate possible future precipitation changes than can trend analyses based on a few decades of observations. From a theoretical point of view, we could expect changes in precipitation given by changes in the dynamics and thermodynamics of the atmosphere. The dynamic effects are associated with changes in large-scale circulation. Precipitation regimes in Europe may be affected by changing frequency and persistence of circulation types (e.g., Cahynová and Huth, 2010) and a shift of extratropical storm tracks to the north (e.g., Lehmann et al., 2014), although the relationships between precipitation and large-scale atmospheric circulation are rather weak in the warm season, when convective precipitation prevails (e.g., Huth and Kyselý, 2000). The thermodynamic effect is associated with changes in atmospheric humidity and stratification. Because the capacity of the atmosphere to hold water is governed by the Clausius–Clapeyron equation, intensification of precipitation is expected with increasing temperature (Trenberth et al., 2003). However,

* This chapter is based on:
Rulfová Z, Beranová R, Kyselý J. 2016. Climate change scenarios of convective and large-scale precipitation in the Czech Republic based on EURO-CORDEX data (submitted to *International Journal of Climatology*).

intensification of extreme precipitation depends not only on temperature but on moisture availability too (Panthou et al., 2014). Lenderink et al. (2011) have studied hourly precipitation extremes in Hong Kong and the Netherlands and found that precipitation intensity increases up to about 24 °C and then rises more slowly or even decreases, which is probably associated with moisture deficits.

All these aforementioned mechanisms, however, influence precipitation in different ways. Results of the analysed precipitation changes depend on precipitation indices (i.e. different results for mean vs. extreme precipitation) and on the time scale used for precipitation aggregations (e.g., Gaál et al., 2014). This is related especially to the different origin of precipitation. Convective precipitation increases with temperature faster than does stratiform precipitation, as shown, for example, in Berg et al. (2013) for observed data in Germany, and the ratio of seasonal convective precipitation amount to the total precipitation amount tends to be higher in the future climate in all seasons when convective precipitation plays an important role (i.e. spring, summer, and autumn), as shown by Fischer et al. (2015) for Switzerland.

Many studies focusing on European precipitation changes agree with the general intensification of precipitation, predominantly increasing trends in mean precipitation in northern Europe, and decreasing trends in the south (e.g., Frei et al., 2006; Boberg et al., 2010; Heinrich and Gobiet, 2012; Rajczak et al., 2013). Because Central Europe (and the Czech Republic) lies in the transition zone between increasing and decreasing precipitation, we focus our analyses on this region. Furthermore, we study convective and stratiform precipitation separately to gain a detailed view of projected precipitation changes.

We analyse here the output of four RCM projections from the EURO-CORDEX project (http://www.euro-cordex.net). The horizontal resolution of the RCMs (0.44° and 0.11°) allows one to analyse simulations with a finer resolution and to compare results of simulations with different horizontal resolutions. As shown in previous studies (e.g., Giorgi and Marinucci, 1996; Rauscher et al., 2010; Chan et al., 2013), model grid spacing influences precipitation characteristics simulated by climate models. RCMs with finer horizontal resolution better simulate spatial characteristics of mean and especially extreme precipitation, and these improvements are more visible in topographically complex regions. Casanueva et al. (2015) and Prein et al. (2016) confirm similar results for precipitation characteristics simulated by RCMs from the EURO-CORDEX project. Although both show benefits of the finer

horizontal resolution in spatial patterns of precipitation, Casanueva et al. (2015) found that this improvement is not statistically significant after bias correction.

The data and methods are introduced in section 4.2. The results of validation of RCMs and projected changes of convective and stratiform precipitation are presented in section 4.3. The discussion and summary of the results follow in sections 4.4 and 4.5, respectively.

4.2 Data and methods

The observed precipitation data analyzed in this study come from SYNOP reports at 10 stations (operated by the Czech Hydrometeorological Institute) during 1982–2010. The same dataset had been used to represent observations in Chapter 3 that examined the ability of ENSEMBLES RCMs to simulate convective and stratiform precipitation characteristics.

Table 4.1: Overview of the RCMs analysed and their parameterizations.

	CCLM	**HIRHAM**	**RACMO2**	**RCA4**
Institution	CLM Community (CLMCOM)	Danish Meteorological Institute (DMI)	Royal Netherlands Meteorological Institute (KNMI)	Swedish Meteorological and Hydrological Institute (SMHI)
Convection scheme	Tiedtke, 1989	Tiedtke, 1989	Tiedtke, 1989; Nordeng, 1994; Neggers et al., 2009	Kain and Fritsch, 1990; Kain, 2004
Microphysics scheme	Doms et al., 2011; Baldauf and Schulz, 2004	Lohmann and Roeckner, 1996	Tiedtke, 1993; Tompkins et al., 2007; ECMWF-IFS, 2007; Neggers, 2009	Rasch and Kristjánsson, 1998
Model references	Rockel and Geyer, 2008	Christensen et al., 2007	van Meijgaard et al., 2012	Samuelsson et al., 2011
EC-EARTH realisation	r12	r3	r1	r12

The RCM simulations originate from the EURO-CORDEX project (http://www.euro-cordex.net) database. We examine runs of four RCMs driven by the ERA-Interim reanalysis (Dee et al., 2011) and scenario simulations of the same RCMs driven by global climate models (GCMs). Table 4.1 provides details of the

examined RCMs. All simulations driven by the ERA-Interim reanalysis cover the 1989–2008 period and have grid resolutions of about 12 km (0.11° on a rotated grid) or 50 km (0.44° on a rotated grid). The 20-year overlapping period (1989–2008) common to the observed and RCM datasets was used for validation. Thirty-year time slices (1971–2000 and 2071–2100) are examined in analysing projected changes of precipitation characteristics. In this case, the RCMs with 0.11° horizontal resolution driven by GCMs and with two different RCP scenarios (RCP4.5 and RCP8.5, see van Vuuren et al., 2011) were used. All RCMs are driven by the EC-EARTH GCM, which is derived from a numerical weather prediction model and has a relatively high resolution compared to other models that participated in CMIP5 (Taylor et al., 2012). As a consequence it simulates atmospheric dynamics comparatively well (e.g., Zappa et al., 2013). The influence of the driving GCM on projected changes is discussed using four simulations of the CCLM RCM driven by different GCMs (EC-EARTH, MPI-ESM-LR, CNRM-CM5-LR, and HadGEM2-ES).

Because we evaluate runs of RCMs with different horizontal resolutions, orography differs slightly among the models and especially among resolutions (examples are shown in Figure 4.1). Orography is more realistic in RCMs with the horizontal resolution of 0.11°, although differences between model and real altitude are still large.

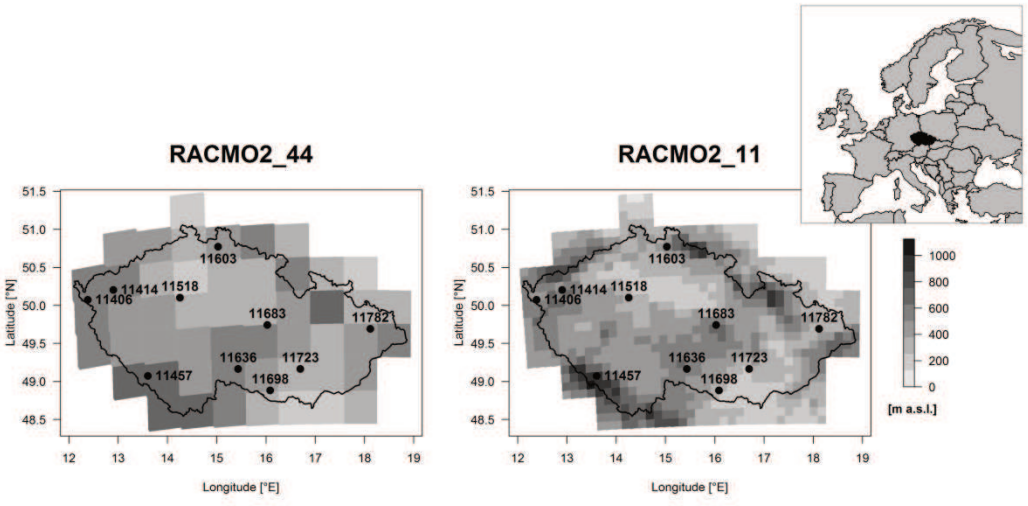

Figure 4.1: Locations of stations (black dots) and examples of orography in RACMO2 model with two horizontal resolutions: 0.44° (left) and 0.11° (right).

The following characteristics of convective, stratiform and total precipitation computed at the 10 stations and in all grid boxes in the area of the Czech Republic in individual RCMs are examined:

- mean seasonal precipitation amounts, number of wet days (defined as days with precipitation amount ≥0.5 mm), and rain intensity index (RII, defined as mean precipitation amount on wet days; cf. Klein Tank et al., 2002);
- proportion of convective and stratiform precipitation to total amounts for individual seasons; and
- mean annual maxima, 20- and 50-year return values of daily precipitation amounts.

High quantiles of precipitation amounts (corresponding to 20- and 50-year return values) are estimated by the generalized extreme value (GEV) distribution (Coles, 2001) fitted to samples of annual maxima of daily precipitation amounts. For estimating parameters of the GEV distribution, the method of L-moments is used (Hosking and Wallis, 1997).

4.3 Results

4.3.1 Validation of simulated precipitation characteristics for 1989–2008

Before assessing the climate change scenario simulations, it is important to evaluate the corresponding model performance over the region. Since reanalysis data provide a spatially coherent record of the actual historical atmospheric fields, the simulations driven by reanalysis are useful in determining biases of the RCMs themselves and thus without the influence of biases in the driving data.

Mean seasonal characteristics of convective, stratiform, and total precipitation are shown in Figure 4.2 (top row). All RCMs reproduce the basic behaviour of the annual cycle of convective precipitation amounts with maximum in summer and minimum in winter. Convective seasonal amount is underestimated by most RCMs, especially in summer, when the HIRHAM RCM simulates only about 50% of the observed value. Observed stratiform precipitation amounts are almost evenly distributed throughout the year, which is reproduced by most RCMs. In contrast to

convective precipitation, stratiform precipitation is predominantly overestimated by all models in all seasons except for summer. The annual cycle of total precipitation amounts is dominated by convective precipitation in observations as well as in the RCMs, but the RCMs rather generally simulate a flatter annual cycle with overestimated winter, spring, and autumn precipitation but underestimated summer precipitation. This means that total seasonal amounts are overestimated in all seasons when the stratiform component dominates.

The number of wet days and RII (Figure 4.2, middle and bottom rows) are slightly underestimated or overestimated in the RCMs for convective precipitation (with ensemble mean close to observations) while almost all RCM simulations overestimate these precipitation characteristics for stratiform and total precipitation. For characteristics of convective and stratiform precipitation, there is a larger difference between the RCMs than between any two single simulations of the same RCM with different (0.44° or 0.11°) resolutions. The HIRHAM model has the largest bias for the majority of studied characteristics of convective and stratiform precipitation. Since these biases compensate for one another to a large extent, the characteristics of total precipitation are simulated in HIRHAM similarly to how they are in the rest of the RCMs.

The percentage of precipitation amounts falling in the form of convective precipitation is shown for individual seasons in Figure 4.3. In the observed data, the proportion of convective precipitation is highest in summer (approximately 50%), followed by spring (~35%) and autumn (~15%). Models CCLM and HIRHAM tend to underestimate the percentage of convective precipitation in all seasons. In summer (and notwithstanding its resolution), HIRHAM simulates only 20% of convective precipitation. That is the lowest value across all studied RCMs. On the other hand, RACMO2 and RCA4 perform reasonably well in all seasons. All models except RCA4 underestimate the dispersion (interquartile range) of the simulated values. There are only slight differences between simulations of a single model with different horizontal resolutions.

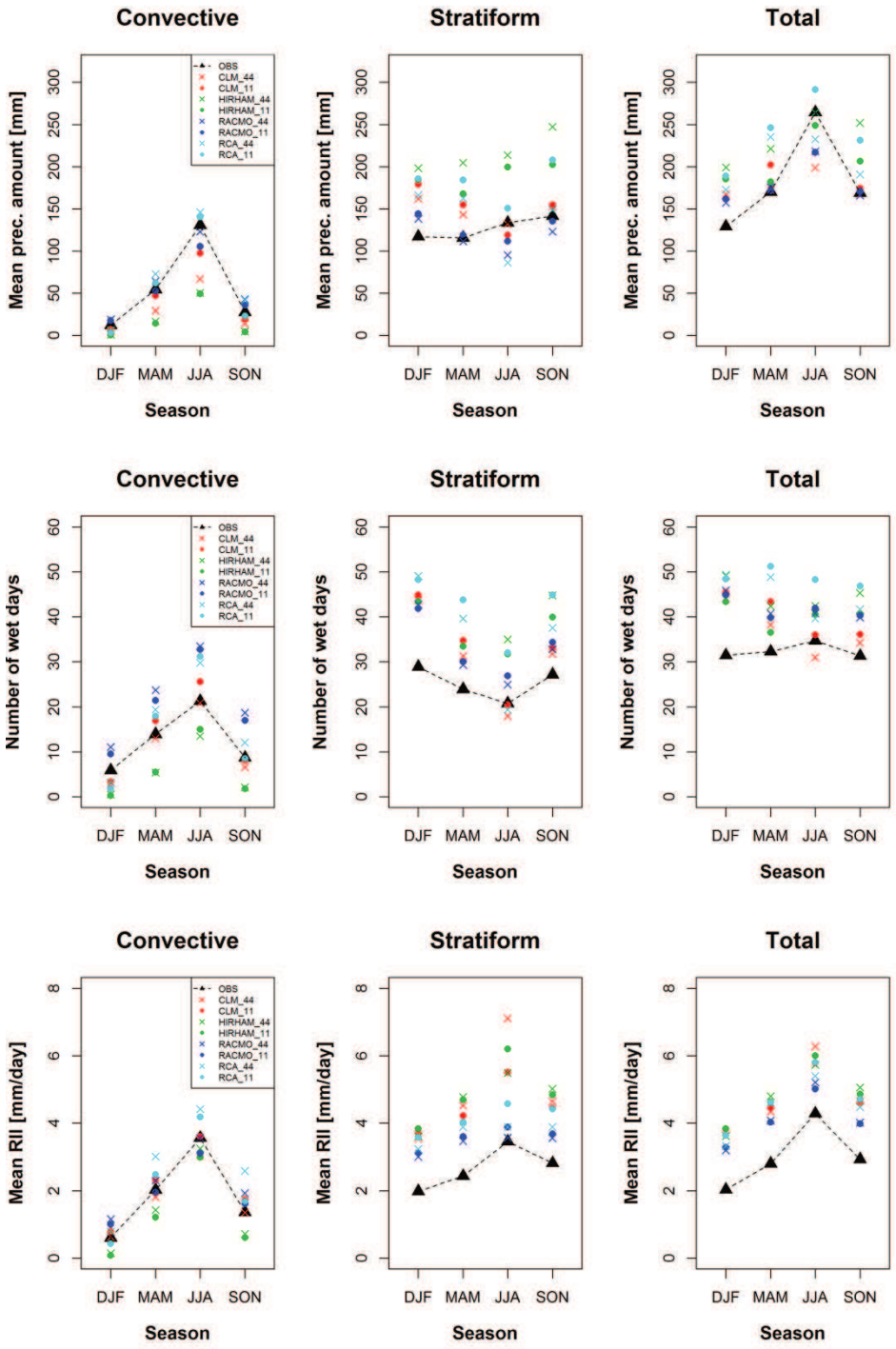

Figure 4.2: Mean seasonal precipitation amount (top row), number of wet days (with precipitation ≥0.5 mm, middle row), and rain intensity index (RII, bottom row) in the observed data (OBS) and RCM simulations (1989–2008), averaged across all stations or grid boxes in the area of the Czech Republic.

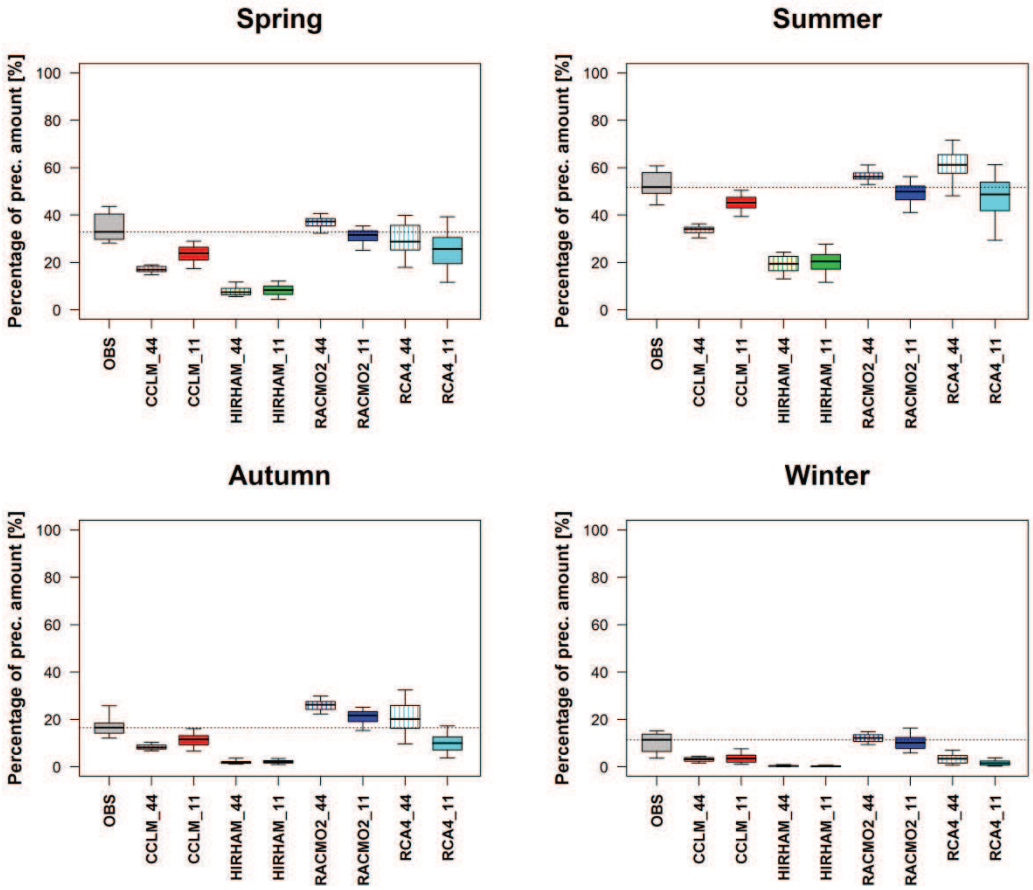

Figure 4.3: Percentages of convective precipitation in total amounts for individual seasons in the observed data (OBS) and RCM simulations (1989–2008). The boxplots are calculated across stations or grid boxes. The bottom and top of the box are the first and third quartiles, and the band inside the box shows the median. The whiskers represent the 5 and 95% quantiles. The grey dotted line shows the median of observed values.

Mean annual maxima of convective, stratiform, and total daily amounts are depicted in Figure 4.4. For comparison of grid box maxima, which represent areal averages, with station characteristics (point values), we use the area reduction factors (ARFs) representing the ratio between the areal average and point rainfall extreme for a given area, temporal aggregation, and exceedance probability (see e.g., Svensson and Jones, 2010b for a comprehensive overview). According to Overeem et al. (2010), we consider ARFs of 0.92 and 0.86 for mean annual maxima of total precipitation in RCMs with the 0.11° and 0.44° horizontal resolution, respectively. As the reduction of magnitudes applies especially to convective events in contrast to large-scale frontal precipitation (e.g., Huff and Shipp, 1969; Skaugen, 1997), we applied the same reduction (in mm) for convective precipitation as for total precipitation and no reduction for stratiform precipitation (cf. Chapter 3).

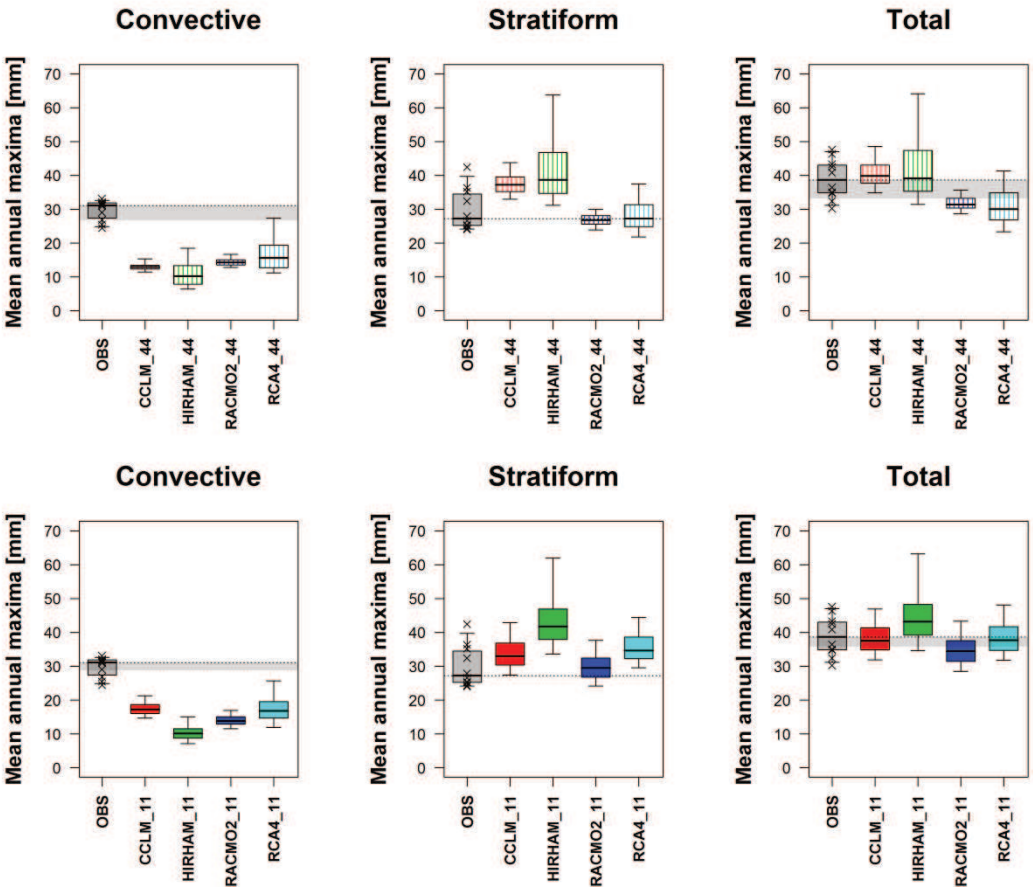

Figure 4.4: Mean annual maxima of daily precipitation amounts in the observed data (OBS) and RCM simulations (1989–2008) with horizontal resolution of 0.44° (top row) and 0.11° (bottom row). The boxplots are calculated across stations or grid boxes. The bottom and top of the box are the first and third quartiles, and the band inside the box shows the median. The whiskers represent the 5 and 95% quantiles. For observed data, individual station values are depicted by crosses. The lower boundary of the shaded area for extremes of total precipitation corresponds to the median of observed data after correction using areal reduction factor; for convective extremes, the same reduction (in mm) as for total precipitation was applied. The grey dotted line shows the median of observed values.

Although observed mean annual maxima of daily convective and stratiform precipitation are both about 30 mm, convective maxima simulated by the RCMs are markedly underestimated while stratiform maxima are predominantly overestimated. Convective maxima are underestimated slightly more in RCMs with the coarser 0.44° horizontal resolution, but the differences between the two resolutions are rather marginal and if the reduction due to ARF is considered, the biases are almost the same. Stratiform maxima are overestimated most by HIRHAM, in which, on the other hand, convective maxima are underestimated most. Total precipitation maxima

are reproduced reasonably well regardless of the biases for the convective and stratiform component in most RCMs. Although mean annual maxima are predominantly due to stratiform precipitation in the RCMs (in contrast to observations in which annual maxima originate almost equally from convective and stratiform precipitation), there is a tendency towards increase of mean annual maxima of convective precipitation in all models in the finer horizontal resolution (not shown).

In summary, characteristics of mean convective and stratiform precipitation are simulated reasonably well in all RCMs although the seasonal precipitation amount of convective precipitation is slightly underestimated and all characteristics of stratiform precipitation are predominantly overestimated. Extreme precipitation of convective origin is systematically underestimated and that of stratiform slightly overestimated, which results in a relatively good simulation of extreme total precipitation. For all precipitation characteristics, there is a tendency towards larger differences between RCMs than between two simulations of the same RCM with different horizontal resolutions (0.44° and 0.11°). Finally, the RACMO2 model seems to be the best in reproducing most characteristics of convective and stratiform precipitation.

4.3.2 Projected changes of precipitation characteristics for 2071–2100

In this section, we analyse RCM simulations driven by GCMs under RCP4.5 and RCP8.5 scenarios, and evaluate projected future changes (2071–2100) relative to the control runs of the RCMs (1971–2000). As shown in section 4.3.1, there are only small differences between RCM simulations with 0.11° and 0.44° horizontal resolutions. Because the spatial characteristics of precipitations are better captured in simulations with finer resolution, we analyse future projections for the RCMs using only the 0.11° (~12 km) horizontal resolution.

Changes of the mean annual precipitation cycle under RCP4.5 and RCP8.5 scenarios simulated by all RCMs driven by EC-EARTH are depicted in Figure 4.5 (top). The mean annual cycle of convective precipitation in future climate has still a maximum in summer and minimum in winter, but precipitation amounts tend to increase in all seasons, and especially in spring (RCP4.5: by 15%, RCP8.5: by 26%

relative to 1971–2000 on average) and summer (RCP4.5: by 10%, RCP8.5: by 6% relative to 1971–2000 on average). In these two seasons, there is a larger variance of the simulated changes between the RCMs. Stratiform precipitation amounts substantially increase in winter (RCP4.5: by 12%, RCP8.5: by 16% relative to 1971–2000 on average) and spring (RCP4.5: by 14%, RCP8.5: by 18% relative to 1971–2000 on average) while they slightly decrease in summer (RCP4.5: by −1%, RCP8.5: by −8% relative to 1971–2000 on average) and remain almost unchanged in autumn. Projected changes in stratiform precipitation amounts have a larger spread between the RCMs in all seasons except summer in comparison to convective precipitation. Changes of total precipitation amounts reflect changes in both convective and stratiform components although the stratiform precipitation plays a more important role in all seasons except for summer. The majority of RCMs simulate maximum in the annual cycle in summer and minimum in winter in the future climate regardless of the RCP scenario, but mean precipitation amounts tend to increase (in comparison to the control period) in all seasons except summer. The changes of convective, stratiform, and total seasonal precipitation amounts tend to be more pronounced under the RCP8.5 scenario.

The number of days with convective precipitation ≥0.5 mm is projected to increase in all seasons except summer while for stratiform precipitation this number tends to increase in winter and spring and decrease in summer and autumn (Figure 4.5, middle row). The number of wet days is usually smaller in the RCM simulations under the RCP8.5 scenario for both convective and stratiform precipitation. Total precipitation again reflects especially behaviour of the stratiform precipitation. Intensity of precipitation expressed by RII increases for both convective and stratiform precipitation in all seasons (Figure 4.5, bottom), and that increase is more pronounced in simulations under the RCP8.5 scenario. Larger increases are simulated for stratiform precipitation (by 2–3 times in absolute value) than for convective precipitation. The simulated intensity has also a larger spread between the RCMs for stratiform than convective precipitation. Increases in intensity of total precipitation are projected in all seasons by all RCMs under both RCP scenarios, and there is a clear tendency towards larger increases under the RCP8.5 scenario.

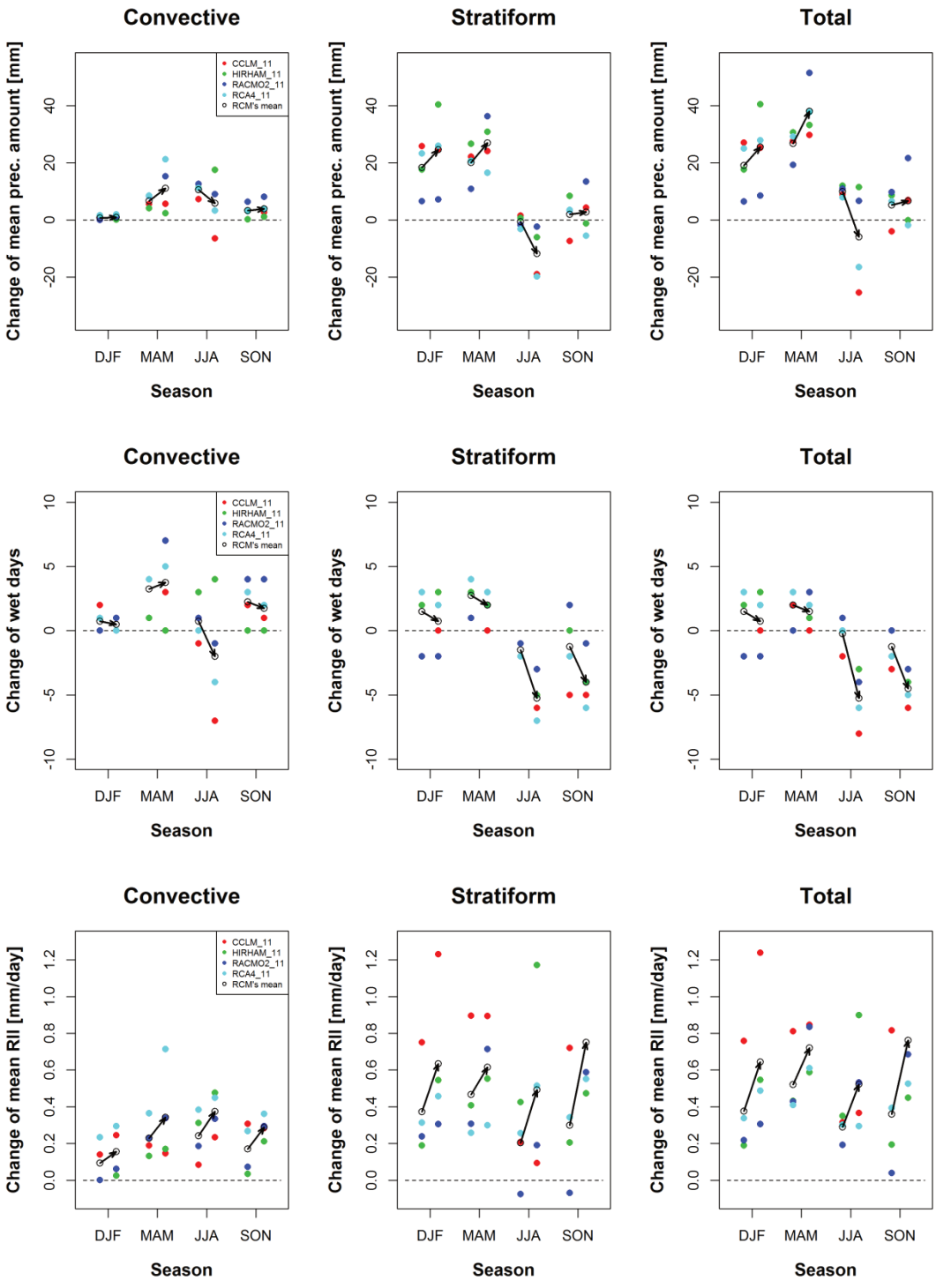

Figure 4.5: Projected changes of mean seasonal precipitation amount (top row), number of wet days (with precipitation ≥0.5 mm, middle row), and rain intensity index (RII, bottom row) in RCM simulations for 2071–2100 with respect to 1971–2000, averaged across all grid boxes in the area of the Czech Republic. For each season, the left (right) column refers to the RCP4.5 (RCP8.5) scenario. Arrows accentuate differences between changes of the studied characteristics (averaged over all RCMs) under the RCP4.5 and RCP8.5 scenarios.

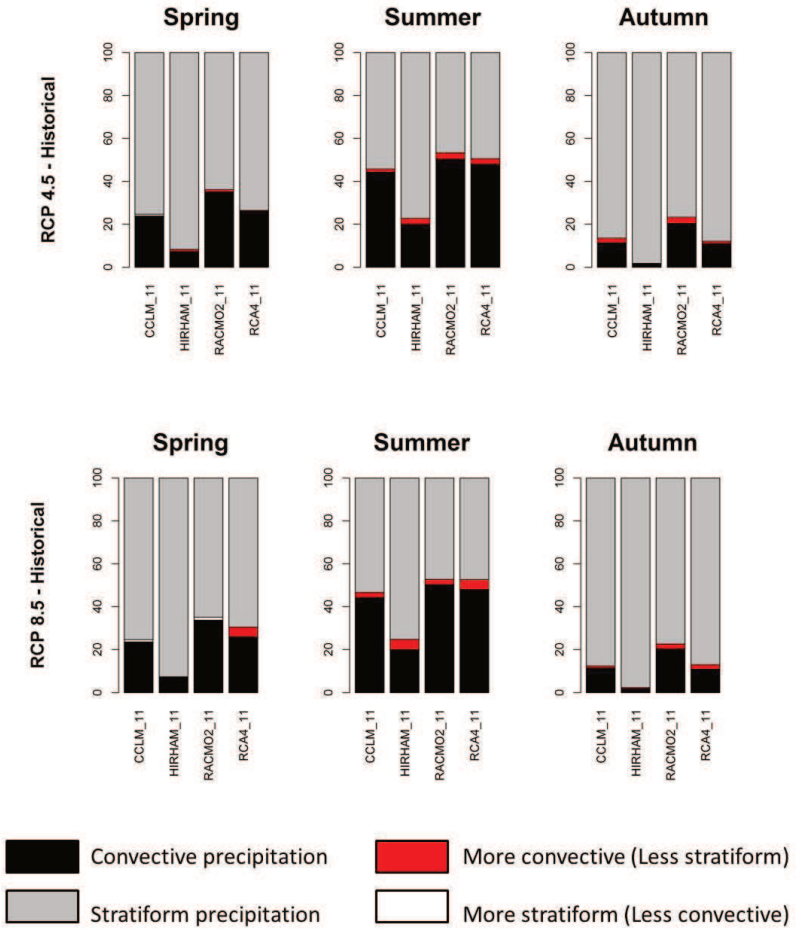

Figure 4.6: Percentages of convective (black) and stratiform (grey) precipitation in RCM simulations driven by the EC-EARTH GCM for spring, summer, and autumn. The red (white) coloured part represents the additional portion to which the convective (stratiform) fraction increases in the future climate (2071–2100) under the RCP4.5 (top) and RCP8.5 (bottom) scenarios against the 1971–2000 time slice.

The percentages of convective and stratiform precipitation amounts in the RCMs control period for spring, summer, and autumn (the convective component is negligible in winter) and their additional portions which are simulated for the future climate under RCP4.5 and RCP8.5 scenarios are shown in Figure 4.6. The increasing percentage of convective precipitation is most pronounced in summer, when the proportion of convective precipitation on seasonal totals is largest (see Figure 4.5). This increase is more pronounced in RCM simulations under the RCP8.5 scenario (increase by about 3–5% vs. 1–3% under RCP4.5). As both convective and stratiform precipitation amounts increase in spring and autumn in a majority of the RCMs (Figure 4.5), the change in the percentage of convective and stratiform precipitation

is smaller in these seasons. Increase in the percentage of convective precipitation still prevails in autumn under both RCP4.5 and RCP8.5, as well as in spring under RCP8.5.

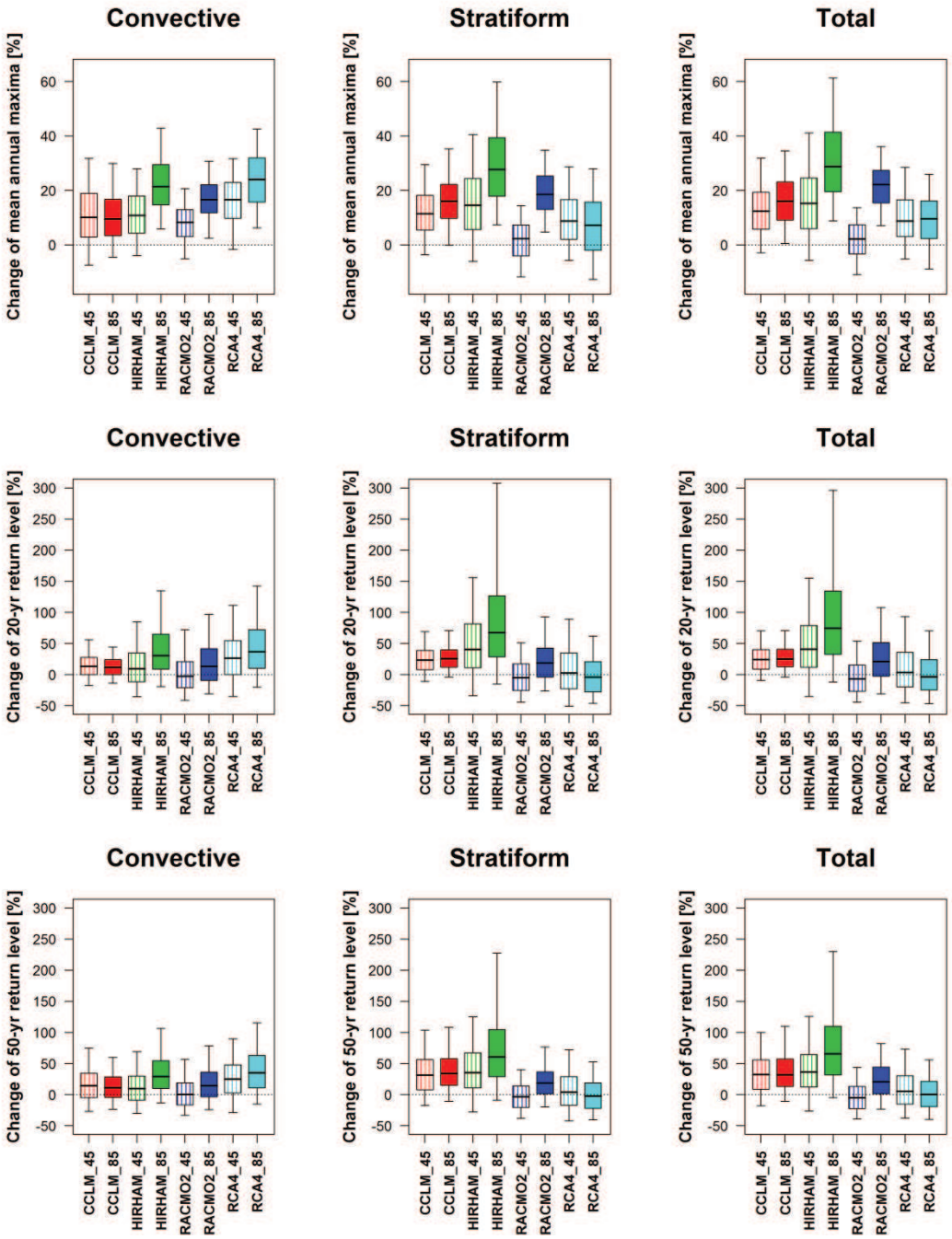

Figure 4.7: Projected changes of mean annual maxima (top row), 20-year return level (middle row), and 50-year return level (bottom row) of daily convective, stratiform, and total precipitation amounts in RCM simulations for 2071–2100 with respect to 1971–2000 under the RCP4.5 (_45) and RCP8.5 (_85) scenarios. The boxplots are calculated across grid boxes. The bottom and top of the box are the first and third quartiles, and the band inside the box shows the median. The whiskers represent the 5 and 95% quantiles.

Projected changes in mean annual maxima and 20- and 50-year return levels of daily convective and stratiform precipitation amounts are shown in Figure 4.7. Mean annual maxima tend to increase for both convective and stratiform precipitation in a similar way, and the changes tend to be more pronounced under the RCP8.5 scenario (an increase of about 20% vs. 10% under RCP4.5). Projected 20-year and 50-year return levels usually increase faster than do mean annual maxima (increase of about 15% and 35% for both return levels under RCP4.5 and RCP8.5, respectively). Although positive changes prevail on average across all RCMs for both convective and stratiform precipitation, the changes are spatially incoherent in magnitude and sign, especially for stratiform precipitation. In most RCMs, the precipitation extremes intensify more under the RCP8.5 than RCP4.5 scenario, and the difference between the two scenarios is particularly large for HIRHAM and RACMO2.

As all the aforementioned results of projected precipitation changes are based on RCM simulations driven by the EC-EARTH GCM, we repeated all analyses for single RCM (CCLM) simulations driven by four GCMs (a CCLM ensemble) for assessing possible uncertainty of the projected changes. The effect of GCM on simulated changes is larger for stratiform than for convective precipitation due to a closer connection of stratiform precipitation to the large-scale circulation. The CCLM ensemble mean of simulated changes in mean precipitation characteristics (Figure 4.8) is similar to the EC-EARTH-driven RCMs ensemble mean, and an increase in mean precipitation intensity and mean annual maxima of daily precipitation amounts and their return levels tends to prevail in both ensembles. Although the magnitude of the projected precipitation changes could differ in individual RCMs driven by different GCMs, the tendency towards positive or negative change seems to remain similar regardless of the GCM used.

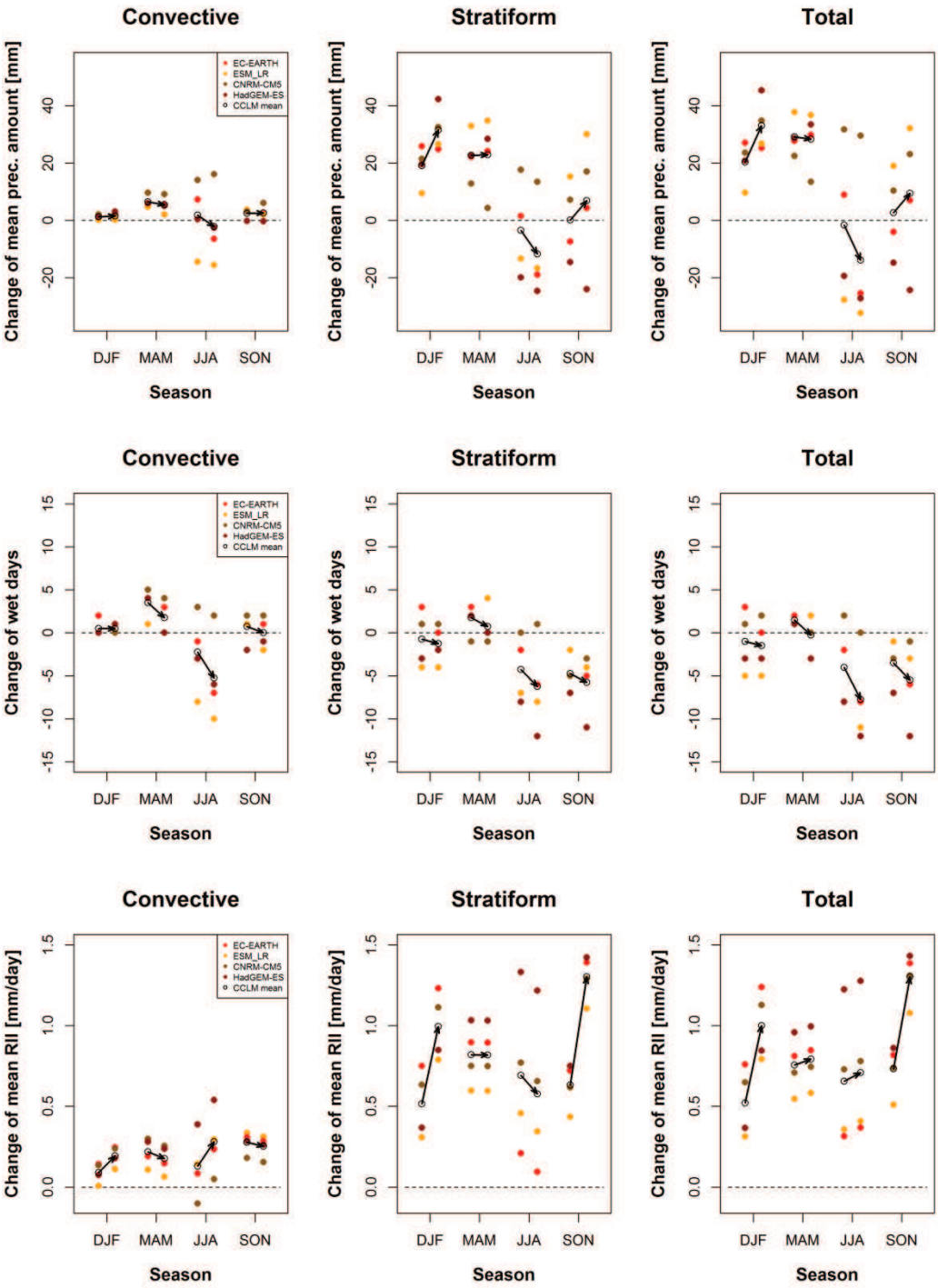

Figure 4.8: Projected changes of mean seasonal precipitation amount (top row), number of wet days (with precipitation ≥0.5 mm, middle row), and rain intensity index (RII, bottom row) in CCLM simulations driven by four GCMs for 2071–2100 with respect to 1971–2000, averaged across all grid boxes in the area of the Czech Republic. For each season, the left (right) column refers to the RCP4.5 (RCP8.5) scenario. Arrows accentuate differences between changes of the studied characteristics (averaged over all RCMs) under the RCP4.5 and RCP8.5 scenarios.

4.4 Discussion

All the studied EURO-CORDEX RCMs show reasonably good agreement with observations for mean annual cycle of convective and stratiform precipitation characteristics over 1989–2008. They reproduce the annual cycle of convective precipitation with a maximum in summer while stratiform precipitation amount is almost constant during the year. The main deficiency with respect to the annual cycle is an overestimation of stratiform precipitation amounts and the number of wet days, especially in the cold half of the year. The results are largely in line with the strengths and drawbacks of the ENSEMBLES RCMs identified in Chapter 3, and correspond also to results for total precipitation reported by Kotlarski et al. (2014) for a larger RCM ensemble from the EURO-CORDEX project.

The most important limitation of the RCMs appears for extremes of convective precipitation. Although the rain intensity index (RII) is simulated quite well, the mean annual maxima of convective precipitation are severely underestimated. As shown previously, the daily amounts of convective precipitation rarely exceed some specific threshold in RCMs (Durman et al., 2006; Li et al., 2011; Kendon et al., 2012) and contribute little to extreme total precipitation. After applying ARFs, which compensate the comparison of station (point) data and RCM (grid box) data, the identified biases of convective extremes are still large and cannot be explained merely by spatial smoothing. On the other hand, the RII of stratiform precipitation is overestimated and mean annual maxima of daily precipitation amounts are slightly overestimated. These biases in convective and stratiform precipitation maxima offset each other to some degree, which results in a good representation of total precipitation maxima with only a slight tendency towards underestimation (cf. Chaper 3).

The influence of horizontal resolution on convective and stratiform precipitation characteristics is more pronounced for extreme precipitation. Especially for convective precipitation, the RCMs with the 0.11° horizontal resolution simulate higher values for mean annual maxima of daily precipitation amounts. These results agree with findings of Casanueva et al. (2015) and Prein et al. (2016), who studied the influence of horizontal resolution of RCMs on precipitation characteristics in some parts of Europe and found that the resolution effects are more pronounced for

higher precipitation intensities and in regions with complex orography. They also concluded that the differences between simulations with the 0.44° and 0.11° horizontal resolutions could be reduced by spatial and temporal averaging or bias correction. For instance, our results show that the biases identified in the 0.11° and 0.44° simulations of mean annual maxima of daily convective precipitation amounts are almost the same after applying the ARFs (Figure 4.4), which compensate for spatial smoothing of climate model data. The simulations with finer horizontal resolution are nevertheless still preferred for analyses of daily and sub-daily precipitation amounts due to their better representation of orography and convection.

For the analysis of projected future precipitation patterns (2071–2100 against 1971–2000), we examined RCM simulations driven by GCMs under RCP4.5 and RCP8.5 scenarios. Mean seasonal amounts of total precipitation tend to increase in all seasons except summer. A similar pattern is found for stratiform precipitation while convective precipitation tends to increase throughout the year. The projected summer drying is associated mainly with a decrease of stratiform precipitation due to a decrease in the number of wet days. This decrease in the number of days with stratiform precipitation in summer (and autumn) could be caused by a decrease in the frequency of frontal systems reaching Central Europe due to a northwards shift of the Atlantic-European storm track (e.g., Lehmann et al., 2014).

The increase of convective precipitation and decrease of stratiform precipitation in summer result in an increasing proportion of convective precipitation to total precipitation amounts. The percentage of convective precipitation increases only slightly in autumn, and there is a negligible change in spring because both convective and stratiform precipitation amounts increase in these seasons. These findings largely agree with those of Fischer et al. (2015) for Switzerland, where the percentage of convective precipitation is projected to increase in all seasons when convective precipitation plays an important role (i.e. spring, summer, and autumn).

Expected intensification of total precipitation in Europe (e.g., Alexander et al., 2006; Giorgi and Coppola, 2009; Wagner et al., 2013; Rajczak et al., 2013; Jacob et al., 2014; Lehtonen et al., 2014; Fischer et al., 2015) is a consequence of intensification in both the convective and stratiform components. For all examined extremes (mean annual maxima of daily precipitation amounts and their 20- and 50-year return levels) of convective and stratiform precipitation, increases prevail over decreases. Most changes of precipitation characteristics tend to be more pronounced

in simulations driven by the RCP8.5 scenario, with a larger increase of temperature, and these changes are larger for precipitation with higher intensity.

4.5 Summary

We analysed precipitation characteristics over Central Europe in simulations of four RCMs from the EURO-CORDEX project. First we evaluated the ability of RCM simulations driven by the ERA-Interim reanalysis with two different horizontal resolutions (0.11° and 0.44°) to reproduce characteristics of convective (subgrid) and stratiform (large-scale) precipitation over 1989–2008. For the analysis of projected future precipitation patterns (2071–2100 against 1971–2000), we examined RCM simulations driven by GCMs under RCP4.5 and RCP8.5 scenarios.

The main findings can be summarized as follows:

- The RCMs capture relatively well the annual cycle of convective precipitation with its maximum in summer and minimum in winter.
- All characteristics of mean stratiform precipitation tend to be overestimated throughout the year.
- Extreme convective precipitation is systematically underestimated and stratiform slightly overestimated, which results in a relatively good simulation of extreme total precipitation.
- For all precipitation characteristics, there is a tendency towards larger differences between RCMs than between two simulations of the same RCM with different horizontal resolutions (0.44° and 0.11°).
- The increase of convective precipitation and decrease of stratiform precipitation in summer result in an increasing proportion of convective precipitation to total precipitation amounts. A tendency to increasing proportion of convective precipitation prevails also in autumn.
- Regardless of its convective or stratiform origin, there is a tendency towards intensification of extreme precipitation.
- Most changes of precipitation characteristics tend to be more pronounced in simulations driven by the RCP8.5 scenario, with a larger

increase of temperature, and these changes are larger for precipitation with higher intensity.

- Increasing proportion of convective precipitation in summer and generally increasing intensity of precipitation may have important consequences, e.g., for soil erosion, replenishment of soil moisture, and occurrence of flash floods and droughts.

Acknowledgements

The study was supported by the Czech Science Foundation under project GA14-18675S. The RCM data were obtained from the EURO-CORDEX project.

5 A two-component generalized extreme value distribution for precipitation frequency analysis*

5.1 Introduction

Extreme value theory (EVT) is the branch of probability theory and statistical science that deals with modelling and inference for extreme values (Coles, 2001). One of the main assumptions of EVT is that extremes belong to the same population (see Coles, 2001). However, this assumption is not fulfilled for extreme precipitation in mid-latitudes, which is caused by two different physical mechanisms (i.e. convective and stratiform precipitation).

Where observations are generated by two independent processes, the distribution function of the overall extremes is the product of the distribution functions $F_1(x)$ and $F_2(x)$ of the extremes from the separate processes (e.g., Gumbel, 1958; Canfield et al., 1980; Waylen and Woo, 1982; Tabony, 1983):

$$F(x) = F_1(x).F_2(x) \tag{5.1}$$

Gumbel (1958) suggested the use of such a two-component distribution to analyze floods arising from snow melt in spring and precipitation in autumn. Waylen and Woo (1982) fitted Gumbel distributions to the annual maxima of snowmelt and precipitation generated floods, and concluded that the resulting two-component Gumbel distribution provided a good fit to the overall annual maximum floods. The two-component Gumbel distribution has also been used for flood frequency modelling by Rossi et al. (1984), Strupczewski et al. (2012) and Kochanek et al. (2012), and for describing the distribution of extreme wind speeds (e.g., Gomes and Vickery, 1978; van den Brink et al., 2004; Escalante-Sandoval, 2008) and precipitation extremes for different durations (e.g., Caporali et al., 2008). In a number of these applications, however, the four parameters of the distribution were

* This chapter is based on:
Rulfová Z, Buishand A, Roth M, Kyselý J. 2016. A two-component generalized extreme value distribution for precipitation frequency analysis. *Journal of Hydrology* **534**: 659–668.

estimated jointly by fitting the distribution to the overall annual maxima, because an a priori subdivision of the observations according to the two generating mechanisms was not feasible. This leads in general to a larger standard error of quantile estimates (Strupczewski et al., 2012).

In this study, we analyze annual maxima of 6-hour precipitation amounts in the Czech Republic (Central Europe) over the period 1982–2010 using a two-component generalized extreme value (TCGEV) distribution, which consists of two generalized extreme value (GEV) distributions (e.g., Coles, 2001). As sub-daily precipitation extremes have usually a longer upper tail than the Gumbel distribution (e.g., Alila, 1999; Overeem et al., 2008), use of the GEV distribution as basis for a two-component model for extreme precipitation is more appropriate. For parameter estimation of the TCGEV distribution, we take advantage of a subdivision of observed precipitation into predominantly convective and stratiform type based on surface weather observations described in Chapter 1. The return levels from the TCGEV distribution are compared with those obtained by the common practice of fitting a GEV distribution to the overall annual maxima. We apply a regional frequency analysis, which assumes that the most uncertain distribution parameters are constant over the study area. The advantage of a regional frequency analysis is that sampling variations in the estimates of model parameters and high return levels can be substantially reduced compared to a single-site analysis (e.g., Lettenmaier et al., 1987; Cunnane, 1988, Stedinger et al., 1993). The homogeneity assumption is tested with a bootstrap procedure that takes spatial dependence into account. In addition, goodness-of-fit of the regional model is tested for each individual station and for all stations simultaneously, using the Anderson-Darling statistic.

After a short description of the data and precipitation patterns in the Czech Republic in section 5.2, the extreme value models and parameter estimation are discussed in section 5.3. Spatial homogeneity of distribution parameters and testing goodness-of-fit are dealt with in section 5.4. The return levels from the GEV and TCGEV distributions are compared in section 5.5. Section 5.6 presents a discussion and summary.

5.2 Data

The observed 6-hour precipitation data originate from SYNOP reports at 11 stations (operated by the Czech Hydrometeorological Institute) over 1982–2010. The time series of 6-hour convective and stratiform precipitation amounts were obtained using the algorithm proposed and evaluated in detail in Chapter 1. Extreme 6-hour precipitation classified as mixed comprises no more than one annual maximum at each station over the 29-year period (Table 5.1). These mixed maxima are taken into account in the analysis of the overall annual maxima but they are omitted from the analysis of the convective and stratiform components. As Eq. (5.1) assumes two independent processes, we tested the independence of the 6-hour annual maxima of convective and stratiform precipitation using Kendall's tau rank correlation coefficient (e.g., Wilks, 2006). No significant correlation at the 5% level was found.

Table 5.1: Percentage of the largest 6-hour precipitation amounts in each year originated from convective, stratiform and mixed precipitation.

Station	Convective	Stratiform	Mixed
11723	76	24	0
11782	55	41	3
11698	69	28	3
11518	83	17	0
11603	48	48	3
11406	62	38	0
11636	69	28	3
11414	62	38	0
11683	55	41	3
11457	69	31	0
11787	28	69	3

The Czech Republic is characterized by large spatial and temporal variability in precipitation (see Chapter 2). Sub-daily precipitation extremes occur in relation to thunderstorms (convective precipitation) or cloud belts associated with cyclones that usually originate in the Mediterranean area (stratiform precipitation, e.g., Štekl et al., 2001). Heavy precipitation at lowland stations is mostly of convective origin, while at high altitudes and at stations influenced by nearby mountains; intense stratiform precipitation becomes more important (Chapter 2). Box plots of the 6-hour annual maxima for convective and stratiform precipitation and the overall 6-hour annual maxima are depicted in Figure 5.1. The distributions are usually positively skewed

and the distribution of the overall 6-hour maxima is similar to that for convective precipitation especially at stations where more than 60% of the extremes come from convective precipitation (Table 5.1). Mountain station 11787 Lysá hora is the only station with predominantly stratiform extremes (69% of the annual extremes is of stratiform origin for that station).

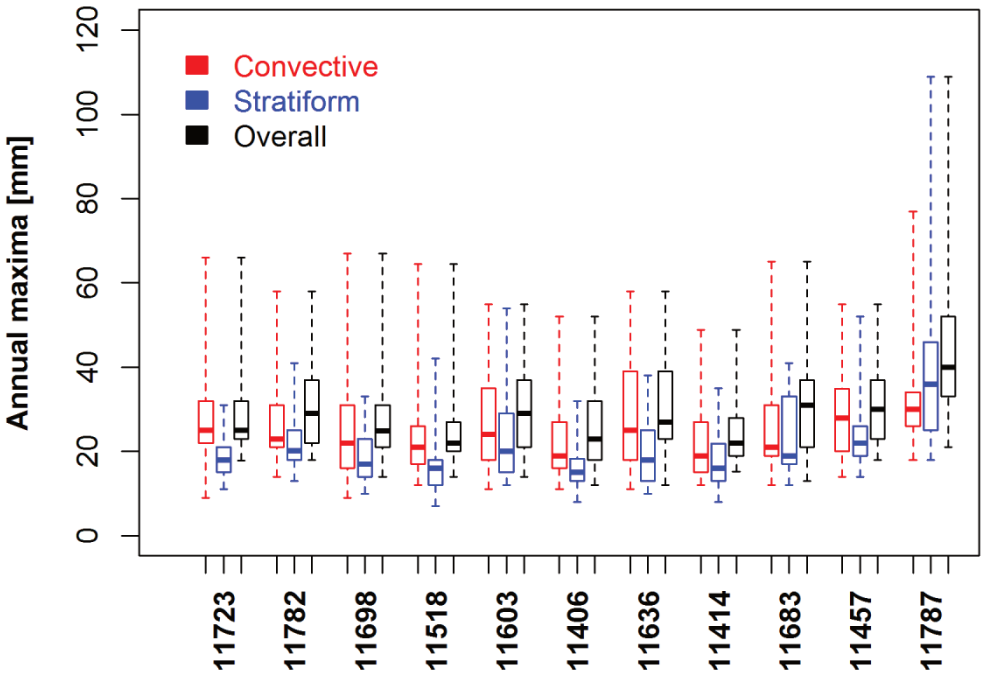

Figure 5.1. Distributions of the 6-hour annual maxima for convective and stratiform precipitation and the overall 6-hour annual maxima. The bottom and top of the box are the first and third quartiles, and the band inside the box is the median. The whiskers represent the minimum and maximum values.

5.3 The regional TCGEV distribution

The GEV distribution has been widely used to describe the distribution of annual maximum precipitation amounts (e.g., Schaefer, 1990; Alila, 1999; Overeem et al., 2008; Papalexiou and Koutsoyiannis, 2013). In a regional frequency analysis of 1-day and multi-day annual precipitation maxima in the Czech Republic (Kyselý and Picek, 2007), the GEV distribution was identified most frequently as the best three-parameter distribution using L-moment diagrams and a goodness-of-fit test. Moreover, the GEV distribution is based on asymptotic theory about the distribution

of maxima. It combines the three extreme value distributions (i.e., Gumbel, Fréchet, and reverse Weibull) into a single distribution. The cumulative distribution function is given by

$$F_{\mathrm{GEV}}(x) = \begin{cases} \exp\left\{-\left[1+\kappa\left(\frac{x-\mu}{\alpha}\right)\right]^{-\frac{1}{\kappa}}\right\}, \kappa \neq 0 \\ \exp\left\{-\exp\left[-\left(\frac{x-\mu}{\alpha}\right)\right]\right\}, \kappa = 0 \end{cases} \tag{5.2}$$

with μ, α and κ the location, scale, and shape parameter, respectively. The shape parameter controls the behavior of the tails of the distribution; $\kappa > 0$ implies a finite lower bound, $L = \mu - \alpha/\kappa$, and a heavy upper tail (Fréchet distribution), whereas for $\kappa < 0$ the distribution has a finite upper bound, $U = \mu - \alpha/\kappa$ (reverse Weibull distribution). For $\kappa = 0$ the GEV distribution reduces to the Gumbel distribution. In the subsequent regional analysis the ratio of the scale parameter to the location parameter, $\gamma = \alpha/\mu$, is considered. This dispersion coefficient is comparable with the coefficient of variation.

The use of the GEV distribution function in the right-hand side of Eq. (5.1) leads to the two-component generalized extreme value model:

$$\begin{aligned} F_{\mathrm{TCGEV}}(x) &= F_{\mathrm{C}}(x).F_{\mathrm{S}}(x) \\ &= \exp\left\{-\left[1+\kappa_{\mathrm{C}}\left(\frac{x-\mu_{\mathrm{C}}}{\alpha_{\mathrm{C}}}\right)\right]^{-\frac{1}{\kappa_{\mathrm{C}}}} - \left[1+\kappa_{\mathrm{S}}\left(\frac{x-\mu_{\mathrm{S}}}{\alpha_{\mathrm{S}}}\right)\right]^{-\frac{1}{\kappa_{\mathrm{S}}}}\right\},\ \kappa_{\mathrm{C}} \neq 0,\ \kappa_{\mathrm{S}} \neq 0, \end{aligned} \tag{5.3}$$

and max (L_C, L_S) < x < max (U_C, U_S). The subscripts C and S refer here to the convective and stratiform component, respectively, and L and U to the lower and upper bounds of the GEV distributions for these components. For $\kappa_C = 0$ and $\kappa_S = 0$, the TCGEV distribution reduces to the two-component Gumbel distribution.

The distribution has six unknown parameters, i.e., two sets of three GEV parameters. Because the observed precipitation data were subdivided into convective and stratiform precipitation, these two sets could be separately estimated from the annual maxima of each component.

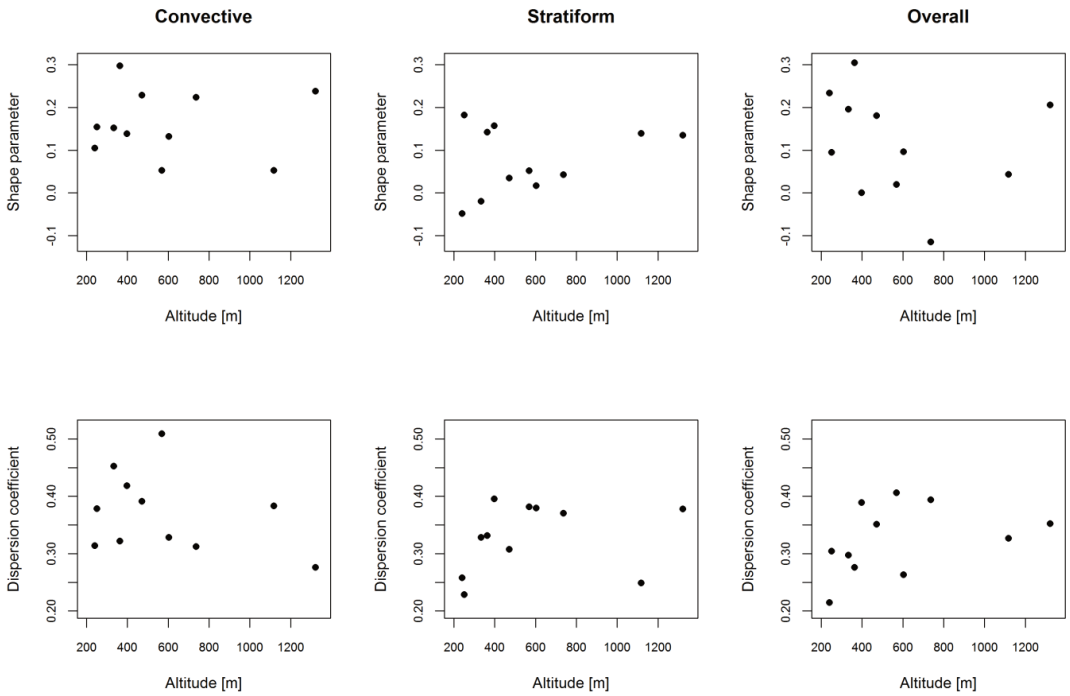

Figure 5.2: Dependence of the shape parameter and the dispersion coefficient on altitude for the 6-hour annual maxima of convective and stratiform precipitation and the overall 6-hour annual maxima.

Initially, the method of L-moments (Hosking and Wallis, 1997) was used to obtain estimates of the GEV parameters. Figure 5.2 shows the estimated shape parameters and dispersion coefficients for the 11 stations. A dependence on altitude is not observed. A difficulty with the at-site estimates in Figure 5.2 is that their standard errors are large owing to the limited sample size. To reduce the uncertainty in parameter estimates, a regional model is considered where both κ and γ are constant over the study area. These assumptions imply that the annual maximum distributions at the various sites are the same apart from a constant scaling factor (e.g., Hanel et al., 2009), which is a basic assumption in regional frequency analysis in hydrology (Hosking and Wallis, 1997). The parameters in the regional model are estimated simultaneously by maximizing the log-likelihood (e.g., Arnell and Gabriele, 1988; Buishand, 1991):

$$L(\boldsymbol{\theta}) = \sum_{i=1}^{n} L_i(\boldsymbol{\theta}) \tag{5.4}$$

where $L_i(\boldsymbol{\theta})$ is the log-likelihood for site i, $\boldsymbol{\theta}$ is the vector of GEV parameters and n is the number of sites. In our case this vector contains the common shape parameter,

the common dispersion coefficient and the location parameter for each site, thus 1+1+11=13 parameters for 11 sites. The resulting estimates of γ and κ will have a smaller standard error than the at-site estimates of these parameters, because they are based on more data. This results in more accurate estimates of return levels provided that the homogeneity assumption is met. The use of alternative regional models where the location parameter is related to the altitude or mean annual precipitation is explored.

The return levels from the regional TCGEV distribution are compared with those based on fitting a regional GEV distribution to the overall 6-hour annual maxima. The T-year return level x_T or (1–1/T) quantile of the annual maximum distribution $F(x)$ is given by $F(\mathrm{x}_T) = 1 - 1/T$ and can be expressed for the single GEV distribution as

$$x_T = \begin{cases} \mu - \frac{\alpha}{\kappa}\left[1 - \left(-\ln\left(1 - \frac{1}{T}\right)\right)^{-\kappa}\right], \kappa \neq 0, \\ \mu - \alpha \ln\left[-\ln\left(1 - \frac{1}{T}\right)\right], \kappa = 0 \end{cases} \tag{5.5}$$

Because an explicit form for the return levels of the TCGEV distribution does not exist, the inverse function F^{-1}_{TCGEV} must be found by an iterative technique. We use Newton's iterative method in this study. Note that the return levels of the TCGEV distribution are always larger than the return levels of the GEV distributions for the convective and stratiform components.

5.4 Homogeneity and goodness-of-fit tests

5.4.1 Homogeneity tests

The regional GEV model assumes that the dispersion coefficient and shape parameter are constant over the region. Estimated return levels may be seriously biased if this homogeneity assumption is not met. In the hydrological literature spatial homogeneity has often been tested by comparing the regional spread of L-moment ratios (Hosking and Wallis, 1997) or the estimated 10-year event (Lu and Stedinger, 1992) with the standard deviation of these statistics. Viglione et al. (2007)

showed that for highly skewed data the *n*-sample Anderson-Darling rank test has better performance than the Hosking and Wallis test based on the L-coefficient of variation (L-CV). A difficulty with these tests is that they assume that the annual maxima at different sites are independent. In our case this is not fulfilled for stratiform precipitation for which some weak dependence is observed (the average spatial correlation of the annual 6-hour maxima is 0.20). Castellarin et al. (2008) suggested a correction of the Hosking and Wallis L-CV test for spatial dependence, assuming a multivariate normal dependence structure. Van de Vyver (2012) accounted for spatial dependence using a bootstrap procedure to estimate the spatial correlation between estimated GEV parameters following Buishand et al. (2009). Here an alternative is considered, where the bootstrap is used directly to determine the significance of the statistic:

$$R = \sum_{i=1}^{n} \left(\hat{\theta}_i - \bar{\theta}\right)^2 \tag{5.6}$$

with $\hat{\theta}_i$ the estimate of the GEV parameter of interest (κ, γ or μ) for station i and $\bar{\theta} = \sum_{i=1}^{n} \hat{\theta}_i / n$ (see Attachment A.3). The null hypothesis is that the tested parameter is constant over the study area and the alternative hypothesis is that it is not constant, resulting in relatively large values of *R*. This method was used by Hanel et al. (2009) for testing for differences between GEV parameters of seasonal precipitation maxima for several sub regions of the Rhine basin. No assumptions on the underlying spatial dependence structure are needed.

Table 5.2: The *p*-values for testing spatial homogeneity of the GEV parameters (using the statistic *R* in Eq. (5.6)) and for testing the dependence of these parameters on altitude and mean annual precipitation amount for the annual maxima of convective and stratiform precipitation and the overall annual maxima.

	Homogeneity			Altitude			Amount		
	κ	γ	μ	κ	γ	μ	κ	γ	μ
Convective	0.941	0.223	0.121	0.936	0.158	0.009	0.984	0.346	0.012
Stratiform	0.965	0.153	0.000	0.468	0.240	0.000	0.318	0.498	0.000
Overall	0.601	0.182	0.000	0.614	0.130	0.000	0.546	0.116	0.000

Table 5.2 (first three columns) presents *p*-values of the test for homogeneity of the parameters κ, γ and μ over the study area. These *p*-values are based on 5000 simulations (see Attachment A.3). Because the *p*-values for κ and γ are higher than 0.1 for convective and stratiform precipitation as well as for the overall annual

maxima, these parameters can be considered to be constant over the study area. For the location parameter there is, however, strong evidence of spatial heterogeneity. The *p*-values are < 0.001 for stratiform precipitation and the overall annual maxima, and only for convective precipitation is the statistic not significant at the 10% level.

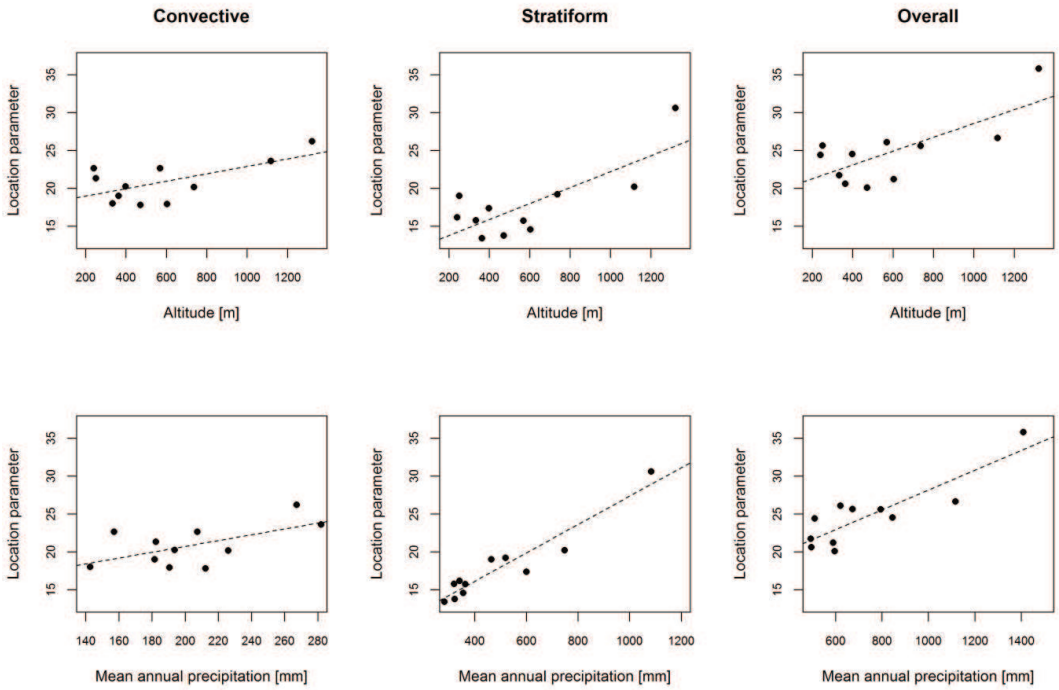

Figure 5.3: Linear dependence of the location parameter on altitude and mean annual precipitation amount for the 6-hour annual maxima of convective and stratiform precipitation and the overall 6-hour annual maxima.

In addition to the homogeneity test based on the statistic R, we tested the significance of a linear regression of the parameters κ, γ and μ on altitude and the mean annual precipitation amount. The null hypothesis is again that the tested parameter is constant over the study area, which implies that the slope is zero in the regression on altitude and mean annual precipitation amount. The alternative hypothesis is that the slope for κ and γ differs from zero and that the slope for μ is greater than zero both for altitude and mean annual precipitation amount. The *p*-values are presented in Table 5.2. These are based on the same bootstrap samples as those used for testing the significance of the statistic R (see Attachment A.3). The results for κ and γ confirm that these parameters can be considered to be constant over the study area. However, for the location parameter, the linear dependence on altitude and the mean annual precipitation amount is significant at the 10% level.

Figure 5.3 shows the increase of the location parameter with altitude and mean annual precipitation amount. For convective precipitation the increase is weaker than for stratiform precipitation and the overall annual maxima.

To test the adequacy of the regression, the statistic R was also calculated for the residuals of the least-squares fit. The null hypothesis in this test is that the location parameter depends linearly on altitude or mean annual precipitation amount and the alternative is that each station has a specific value for this parameter. The results are shown in Table 5.3. The regression on altitude is rejected at the 10% level for stratiform precipitation and the overall annual maxima. However, the regression on the mean annual precipitation amount is not rejected. In particular for stratiform precipitation, Figure 5.3 shows a reduction of the scatter around the regression line if the location parameter is related to the mean annual precipitation amount.

Table 5.3: The p-values for the test on the residuals from the regression of the location parameter on altitude or mean annual precipitation amount for the annual maxima of convective and stratiform precipitation and the overall annual maxima.

	Altitude	Amount
Convective	0.334	0.313
Stratiform	0.000	0.190
Overall	0.006	0.112

5.4.2 Anderson-Darling tests

The Anderson-Darling goodness-of-fit test (Anderson and Darling, 1952) is used to test whether a sample comes from a population with a specific distribution. It gives more weight to the tails of the distribution than the popular Kolmogorov-Smirnov test (Massey, 1951). The null hypothesis in the original Anderson-Darling test is that the data follow a fully specified distribution, $F_0(x)$, and the alternative is that the distribution $F(x)$ differs from $F_0(x)$. It is thus assumed that the parameters of $F_0(x)$ are known. Lower critical values should be used when these parameters are estimated from the sample. Though critical values of the Anderson-Darling test have been obtained for the GEV distribution with estimated parameters (Ahmad et al., 1988; Laio, 2004), these critical values cannot be used in the case of a regional GEV model with common parameters. Simulation from the fitted GEV model is then necessary to determine the critical value of the Anderson-Darling statistic. For this simulation exercise the annual maxima at the different sites were first transformed to standard

normal variables (Hanel et al., 2009). Samples from the multivariate standard normal distribution with the same average spatial correlation as the transformed annual maxima were then generated. These generated normal variables were subsequently transformed to GEV variables using the parameter estimates from the fitted regional model.

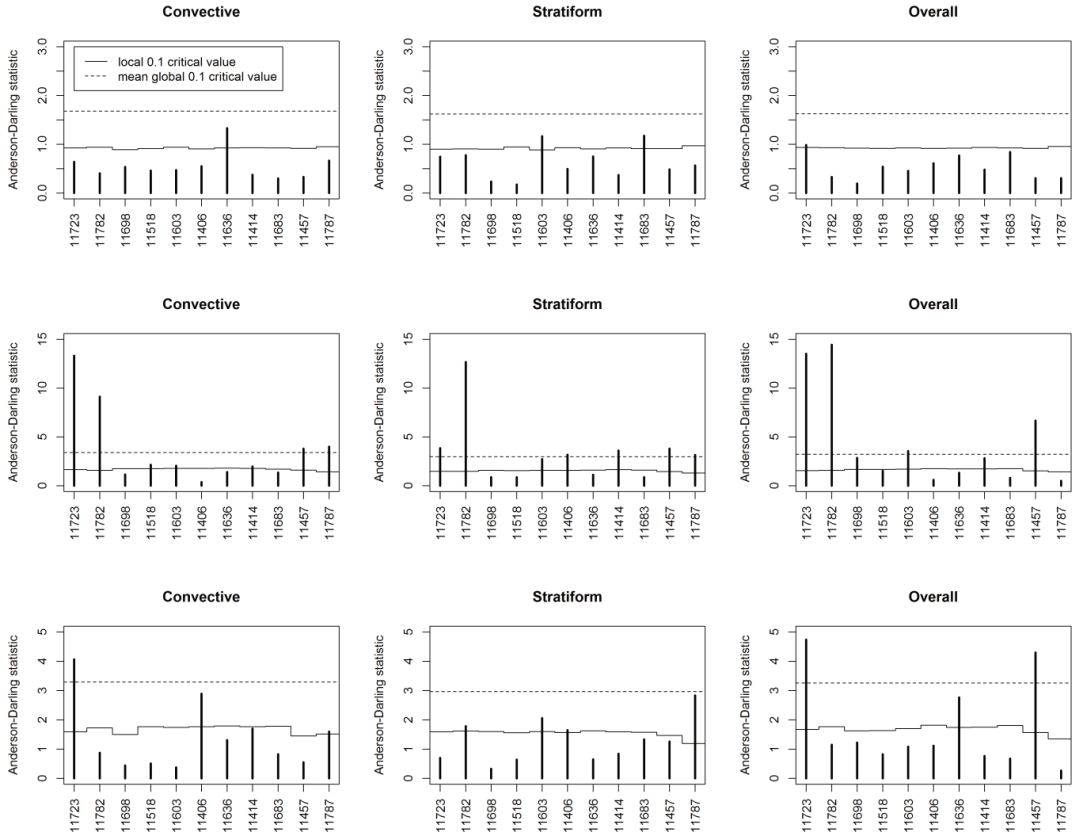

Figure 5.4: Values of the Anderson-Darling statistic for the regional model with a site specific location parameter (top), a linear dependence of the location parameter on altitude (middle) and a linear dependence of the location parameter on mean annual precipitation amount (bottom) for the 6-hour annual maxima of convective and stratiform precipitation and the overall 6-hour annual maxima.

Figure 5.4 gives values of the Anderson-Darling statistic for each station together with critical values for a test at the 0.1 significance level. Both the local critical values and the critical values of a global test at the 10% level are shown. The chance that one or more of the site-wise Anderson-Darling values exceed the latter is 10% in the case of an adequate fit. For the local critical values this chance is considerably larger, on average 10% of the Anderson-Darling values (1.1 value here) will exceed the local critical value if the model is true. The critical values in Figure 5.4 are based

on 3000 bootstrap samples. The global critical value is derived from the same bootstrap samples as the local critical values (see Hanel et al. (2009) for details).

For the regional model with a site-specific location parameter the Anderson-Darling statistic is significant for only one or two stations and the global critical value is not exceeded (Figure 5.4, top). The regional model with dependence of the location parameter on altitude is rejected at more than half of the stations for convective and stratiform precipitation as well as for the overall annual maxima, and the values of the Anderson-Darling statistic are often higher than the global critical value (Figure 5.4, middle). Better results are obtained for the regional model with dependence of the location parameter on mean annual precipitation amount (Figure 5.4, bottom). However, the global critical value is still exceeded at one station for convective precipitation and at two stations for the overall annual maxima. For stratiform precipitation, the Anderson-Darling statistic is locally significant at 4 stations, which is unsatisfactory (in only 2.2% of the bootstrap samples the statistic is locally significant at more than 3 stations). This result indicates that the assumption of a linear dependence of the location parameter on the mean annual precipitation amount is too restrictive. The Anderson-Darling statistic seems to have better performance to detect this than the statistic R. The Anderson-Darling statistic was also used to test the goodness of fit of the regional TCGEV distribution to the overall annual maxima, confirming the result that a spatial model with site-specific location parameter performs well and that a linear dependence of the location parameter on mean annual precipitation amount is less adequate. The regional model with site-specific location parameters is therefore chosen for the estimation of return levels of the regional TCGEV distribution and the comparison with the results obtained by the regional GEV distribution with site-specific parameter.

Table 5.4: Common shape parameter κ, common dispersion coefficient γ and site-specific location parameter for the annual maxima of convective and stratiform precipitation and the overall annual maxima.

	κ	γ	μ [mm]										
			11723	11782	11698	11518	11603	11406	11636	11414	11683	11457	11787
Convective	0.18	0.36	22.6	21.5	18.0	19.6	20.2	18.2	21.8	18.2	20.6	23.4	26.6
Stratiform	0.10	0.32	16.1	19.4	15.7	13.6	17.6	13.7	15.7	14.5	19.2	20.5	30.9
Overall	0.13	0.32	24.8	25.9	22.1	21.1	24.1	20.4	25.7	21.4	24.8	26.6	36.0

The common shape parameter, common dispersion coefficient and site-specific location parameter for convective and stratiform precipitation and the overall annual maxima are presented in Table 5.4. The GEV distribution for convective

precipitation is heavier tailed than the GEV distribution for stratiform precipitation. The location parameter is usually also larger for convective precipitation.

5.5 Comparison of return levels

Estimated return levels of the 6-hour annual maxima from the regional GEV and TCGEV distributions are shown for three stations in Figure 5.5. For long return periods the return levels from the TCGEV distribution are larger than those from the GEV distribution at the lowland station 11723 Brno–Tuřany, which is the result of the larger shape parameter and dispersion coefficient of the GEV distribution describing the convective component (Table 5.4). For T = 100 years, the difference is on average 6.1% (with respect to the estimate for the regional GEV distribution) for lowland stations with dominant convective precipitation. The differences between the estimated return levels of the overall annual maxima from the regional GEV and TCGEV distributions are even smaller (1.1% on average at the 100-year return period) at stations affected by mountains where stratiform precipitation becomes more dominant, e.g., station 11603 Liberec. Only at the highest station 11787 Lysá hora, where the return levels of the 6-hour annual maximum for convective and stratiform precipitation are comparable, are the estimated return levels from the regional TCGEV distribution smaller than those from the regional GEV distribution.

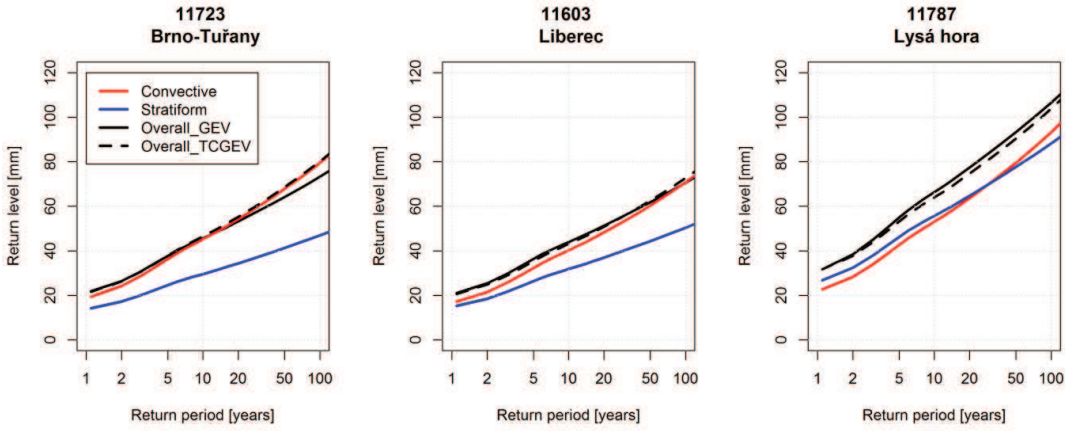

Figure 5.5: Return level plots for the overall 6-hour annual maxima as obtained by the regional GEV distribution and the regional TCGEV distribution together with the return levels for the convective and stratiform components.

Confidence intervals for return levels are usually constructed using the delta method, which relies on the covariance matrix of the estimated parameters (e.g., Coles, 2001). For spatially dependent data the covariance matrix should be based on the Godambe (or sandwich) information matrix rather than the Fisher information matrix (e.g., Blanchet and Lehning, 2010; Varin et al., 2011; Van de Vyver, 2012). However, it is difficult to estimate the Godambe information matrix in the case of many different location parameters. Therefore, the nonparametric and parametric bootstrap (e.g., Davison and Hinkley, 1997) are used in this study. While the nonparametric bootstrap is based on resampling with replacement from the given sample, the parametric bootstrap relies on randomly generated samples from a parametric model fitted to the data. In the latter, the effect of spatial dependence was accounted for in the same way as was done for the Anderson-Darling test making use of the multivariate normal distribution, whereas in the non-parametric bootstrap spatial dependence was preserved by resampling the data for a certain year simultaneously. Percentile confidence intervals were derived from 5000 samples for both the nonparametric and parametric bootstrap. Because of prevailing positive (negative) biases in the estimated return levels in the nonparametric (parametric) bootstrap, the confidence intervals were corrected for bias (Efron, 1987).

Examples of return level plots with 95%-confidence intervals are depicted in Figure 5.6. For the mountainous station 11787 Lysá hora the confidence intervals for the regional TCGEV distribution are narrower than those for the regional GEV distribution, in particular at long return periods, as a result of the relatively large influence of the stratiform component at this station. This reduces the sampling variability of return levels because of the relatively low value of the shape parameter and dispersion coefficient for stratiform precipitation. For the majority of the other stations the confidence intervals for the regional TCGEV distribution are slightly wider than those for the regional GEV distribution. The upper confidence limit from the parametric bootstrap is considerably higher compared to that from the nonparametric bootstrap in a number of cases. The parametric bootstrap results therefore on average in a wider confidence interval. For the GEV distribution the differences are on average 6.4% for T = 20 years and 15.4% for T = 100 years, and for the TCGEV distribution the differences are 12.0% and 28.8% for these return periods. The wider confidence intervals for the parametric bootstrap are in agreement

with the simulation results of Kyselý (2010) for univariate samples, where the use of the parametric bootstrap was advocated for extreme value data.

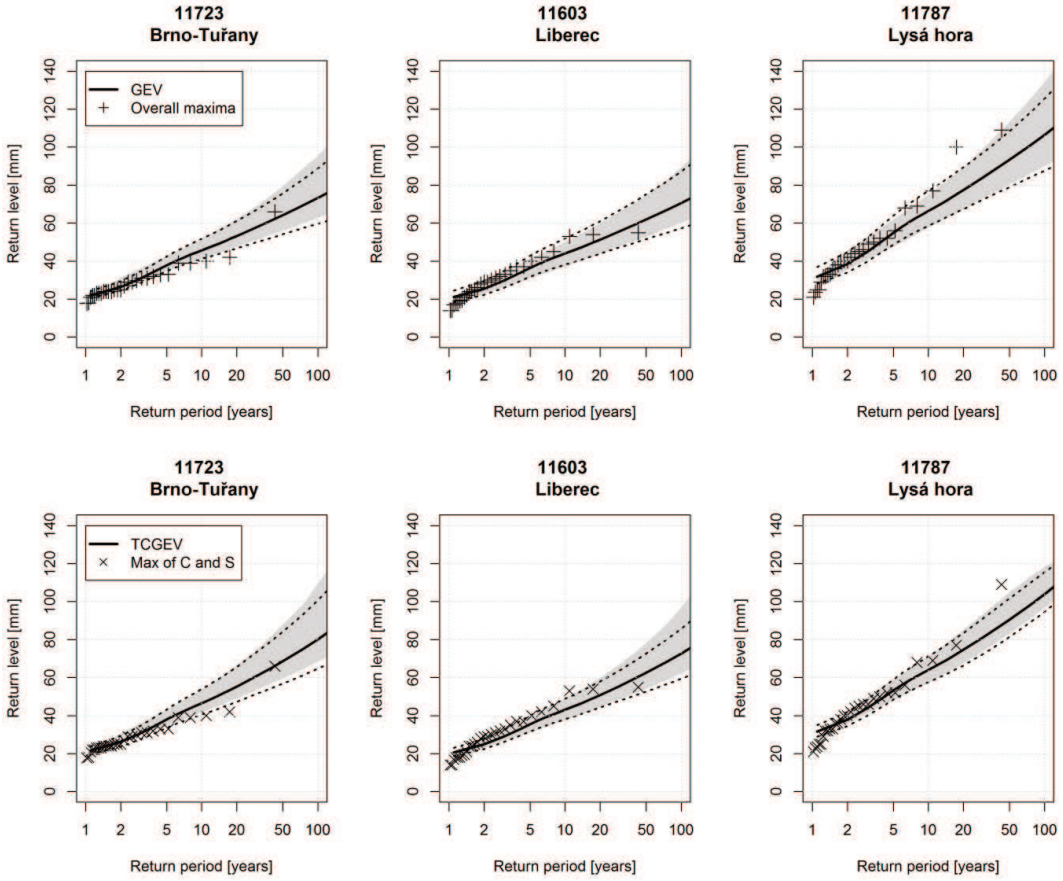

Figure 5.6: Return level plots for the overall 6-hour annual maxima from the regional GEV (top) and TCGEV (bottom) distributions. The observed overall annual maxima, including 6-hour events form mixed origin, are depicted by pluses and the maxima of convective and stratiform precipitation by crosses. The 95% confidence interval obtained by the parametric and the nonparametric bootstrap is depicted by the shaded area and the area between the two dotted lines, respectively.

The nonparametric bootstrap used here is based on the empirical distribution of 29 annual maxima for each site, which is subject to large sampling variability. Since the maxima from convective precipitation are almost independent, the bootstrap procedure for the convective component can be improved by resampling from the pooled sample of annual maxima, scaled by the at-site location parameter. This results on average in somewhat wider confidence intervals for the return levels from the regional TCGEV distribution. There remains, however, a considerable difference between those from the parametric bootstrap (9.0% and 21.8% for T = 20 and T = 100 years, respectively).

In the parametric bootstrap it was assumed that spatial dependence can be described by the multivariate normal distribution. To explore the sensitivity of the width of the confidence intervals to the assumed dependence structure, the parametric bootstrap was repeated with a multivariate Gumbel distribution of the logistic type (Stephenson, 2003). For the lowland stations the results were similar to those for the multivariate normal distribution because of the strong dominance of convective precipitation. But for the elevated stations the standard errors of the estimated 20-year and 100-year return levels increased by 12% and 20%, respectively, using the logistic-Gumbel dependence (for station 11787 Lysá hora even by 17% and 42%). This is caused by the stronger spatial association of large values in the logistic-Gumbel model. Diagnostic measures to distinguish between the two types of dependence models have been presented by Coles et al. (1999). These did not offer a clear conclusion for our data because of the large sampling variability due to the small sample size.

5.6 Discussion and summary

The two-component Gumbel distribution that has frequently been used to describe the distribution of extremes of environmental data, was generalized as a distribution having two GEV components, which is more suitable for precipitation extremes. This TCGEV distribution was used to analyze 6-hour precipitation maxima of convective and stratiform origin in the Czech Republic over 1982–2010. As the 6-hour precipitation amounts could be subdivided into predominantly convective and stratiform precipitation, the parameters of the underlying GEV distributions could be estimated for each component separately. To reduce the uncertainty in parameter estimates, a regional model with common shape parameter and common dispersion coefficient was considered for each precipitation type. The adequacy of a linear dependence of the location parameter on altitude or mean annual precipitation was explored using a homogeneity test on the residuals from a least-squares fit and the Anderson-Darling statistic. The latter showed that these models did not fit the observed annual maximum distributions well. The location parameter was therefore estimated for each site separately.

The return levels of the overall 6-hour maxima from the regional TCGEV distribution were compared with those obtained by fitting a regional GEV distribution to these maxima. The estimated return levels were quite similar. For T = 100 years the difference between the return levels from the TCGEV and GEV distributions is on average 6.1% and 1.1% at lowland and elevated stations, respectively. The larger values for the TCGEV distribution at low altitudes are due to the relatively high shape parameter and dispersion coefficient of the GEV distribution describing the maxima of convective precipitation. As a consequence, the common method of fitting a GEV distribution to the overall annual maxima may underestimate design values of precipitation extremes when convective precipitation is important. Another implication of the heavy upper tail of the convective extremes is that the return levels of the 6-hour annual maxima for convective precipitation can be larger than those from a GEV fit to the overall 6-hour annual maxima as is observed in Figure 5.5 for station 11723 Brno–Tuřany, which does not match reality because convective precipitation represents a part of the total precipitation. The use of the TCGEV distribution guarantees that the estimated return levels of the overall 6-hour annual maxima are larger than the values for the convective and stratiform component from the GEV distribution.

Confidence intervals for return levels were derived using the nonparametric and parametric bootstrap. For the majority of the stations the confidence intervals based on the TCGEV distribution are slightly wider than those based on the GEV distribution as a result of the relatively high value of the shape parameter and dispersion coefficient for the convective component. The confidence intervals from the parametric bootstrap are generally wider than those from the nonparametric bootstrap. This holds for both the GEV and TCGEV distribution. The wider confidence intervals for the parametric bootstrap are in line with the simulation results of Kyselý (2010) for univariate samples.

Acknowledgments

The study was supported by the Czech Science Foundation under project 14-18675S, and by the European Social Fund and the Ministry of Education of the Czech Republic under project CZ.1.07/2.3.00/20.0086. Part of the work was carried out during my Visiting Scientist position at KNMI.

Conclusions

An algorithm for subdivision of 6-hour precipitation amounts into predominantly convective and stratiform using station weather data was proposed and evaluated. In contrast to other studies, the new algorithm is not based on precipitation rates (usually taken from radar or satellite data) but makes use of information on weather state and cloud type reported in SYNOP data. The main advantages of this approach are that it makes use of precipitation data that are directly measured, rather than converted from radar reflectivity or other proxy variable, and that relatively long time series are available, which allows for analysing climatology of convective and stratiform precipitation and possible changes in their proportions over time.

The algorithm subdivides about 95% of precipitation amounts, and it performs better for moderate to heavy precipitation than light precipitation. This suggests that it may be particularly useful for analysis of precipitation extremes, which, in contrast to the assumptions of conventional extreme value models, obviously do not originate from a single process (distribution) at mid-latitudes. Sensitivity analysis showed that the time series and spatial patterns of convective and stratiform precipitation obtained using alternative versions of the algorithm (leading to 'strict' and 'maximum' subdivision) were very similar. Therefore, the particular setting of the algorithm has a rather small influence on results concerning basic characteristics of convective and stratiform precipitation.

The time series of convective and stratiform precipitation were used for evaluating climate models which simulate convective (subgrid) and stratiform (large-scale) precipitation separately through cumulus and large-scale precipitation parameterizations. The results based on comparison of observed and simulated precipitation characteristics from an ensemble of 11 RCMs from the ENSEMBLES project driven by the ERA-40 reanalysis showed that characteristics of mean convective and stratiform precipitation are reproduced reasonably well in all RCMs. The main limitation of the RCMs is found for extremes of convective precipitation, which are severely underestimated. Errors in precipitation characteristics in climate models mainly relate to drawbacks in the representation of convection, which finding is in line with previous studies based upon biases in daily or hourly precipitation extremes, as well as with comparisons of climate models involving a convection

parameterization scheme with cloud-resolving/convection-permitting models explicitly representing convection.

Although the model separation of the two components must be interpreted with caution, the evaluation of their simulated characteristics may be useful for further improving the models inasmuch as the biases may point to erroneous representation of physical processes. As our results refer to still relatively coarse horizontal resolution of RCMs in which both convective and stratiform precipitation need to be parameterized, similar analyses with convection-permitting models (e.g., Kendon et al., 2012) are needed. High computational costs might nevertheless impede wider availability of these simulations in the near future.

As changes in precipitation regime are crucial for impact studies, and in particular those in hydrology and agriculture, we analysed projected future convective and stratiform precipitation patterns simulated by four RCMs from the EURO-CORDEX project driven by GCMs under RCP4.5 and RCP8.5 scenarios. The main results for the end of the century (2071–2100) are an increase of convective precipitation amounts and a decrease of stratiform precipitation amounts in summer, a tendency towards intensification of extreme precipitation regardless of its convective or stratiform origin, and a tendency to more pronounced changes, especially for precipitation extremes, in simulations driven by the RCP8.5 scenario (i.e., with a larger increase of temperature).

Our results imply a rising probability of extreme precipitation events and important changes in soil moisture characteristics, especially in summer. Stratiform precipitation is by its nature more important for agriculture, and a decrease of stratiform precipitation amounts in combination with higher temperatures can lead to larger soil moisture deficits. More frequent and intense precipitation, projected for the future climate, is not able fully to compensate the deficit of light and moderate precipitation because dry soil cannot absorb all water from intense precipitation events. Furthermore, extreme convective precipitation may cause flash floods and landslides, thus representing additional hazards and damages.

Because there is ongoing need for more accurate estimation as to frequency of precipitation extremes, we proposed a new methodology for extreme value analysis which takes advantage of information about the origin of precipitation extremes (i.e., convective or stratiform type). Return levels from a regional two-component generalized extreme value (TCGEV) distribution for observed data were compared

with those obtained using the common method of fitting a regional generalized extreme value (GEV) distribution to the overall annual maxima, thus ignoring their convective or stratiform origins. The differences are generally small, but they increase with return period and are larger at lowland stations where the proportion of convective precipitation extremes is greater. High return levels based on a GEV fit to the overall annual maxima for these stations tend to be smaller than are those for the convective component. This is due to the heavier upper tail of the distribution for convective extremes.

The proposed methodology requires that the precipitation data can be subdivided into convective and stratiform origin. Particularly when high return levels are of interest such a subdivision should be considered in order to avoid biases. It will generally not be feasible to use the TCGEV distribution if an a priori subdivision of the precipitation data cannot be made because of the large number of parameters.

This methodology may be suitable also for analysis of extreme precipitation in climate models. The majority of available precipitation data from RCMs, however, do not have appropriate spatial and temporal resolution to capture the behaviour of extreme convective (subgrid) precipitation. Mean annual maxima of daily precipitation amounts in the RCMs from the ENSEMBLES and EURO-CORDEX projects are mostly of stratiform (large-scale) origin (in contrast to observations in which extremes of convective and stratiform origin are comparable in Central Europe), and they are about two times larger for stratiform (large-scale) than convective (subgrid) precipitation in the RCMs on average.

Preliminary results based on daily precipitation amounts in RCMs show that the 20-year return levels of total precipitation obtained by the TCGEV distribution are similar (equal or slightly larger) to those for large-scale precipitation estimated by the GEV distribution and predominantly smaller than are those for total precipitation estimated by the GEV distribution. An explanation of the differences between estimated return levels of total precipitation from the TCGEV and GEV distributions in RCMs, and in particular to what extent the differences may be interpreted as a bias for the standard GEV distribution, is currently under investigation. With further improvements of climate models and development of convection-permitting RCMs, the proposed TCGEV distribution has potential to become a useful tool for analysing precipitation extremes in their outputs.

Bibliography

Ahmad MI, Sinclair CD, Spurr BD. 1988. Assessment of flood frequency models using empirical distribution function statistics. *Water Resources Research* **24**(8): 1323–1328.

Alder RF, Negri AJ. 1988. A satellite infrared technique to estimate tropical convective and stratiform rainfall. *Journal of Applied Meteorology* **27**: 30–51.

Alexander LV, Zhang X, Peterson TC, Caesar J, Gleason B, Klein Tank AMG, Haylock M, Collins D, Trewin B, Rahimzadeh F, Tagipour A, Ambenje P, Rupa Kumar K, Ravadekar J, Griffiths G, Vincent L, Stephenson DB, Burn J, Aguilar E, Brunet M, Taylor M, New M, Zhai P, Rusticucci M, Vazquez-Aguirre JL. 2006. Global observed changes in daily climate extremes of temperature and precipitation. *Journal of Geophysical Research: Atmospheres* **111**: D05109.

Alibegova ŽD. 1985. *Prostranstvenmo-vremennaja struktura polej židkich osadkov*. Gidrometizdat, Leningrad.

Alila Y. 1999. A hierarchical approach for the regionalization of precipitation annual maxima in Canada. *Journal of Geophysical Research: Atmospheres* **104**(D24): 31645–31655.

Allan RP, Soden BJ. 2008. Atmospheric warming and the amplification of precipitation extremes. *Science* **321**: 1481–1484.

Anagnostou EN. 2004. A convective/stratiform precipitation classification algorithm for volume scanning weather radar observations. *Meteorological Applications* **11**(4): 291–300.

Anderson TW, Darling DA. 1952. Asymptotic theory of certain "goodness of fit" criteria based on stochastic processes. *Annals of Mathematical Statistics* **23**(2): 193–212.

Arnell NW, Gabriele S. 1988. The performance of the two-component extreme value distribution in regional flood frequency analysis. *Water Resources Research* **24**(6): 879–887.

Austin PM, Houze RA Jr. 1972. Analysis of the structure of precipitation patterns in New England. *Journal of Applied Meteorology* **11**: 926–935.

Baldauf M, Schulz J-P. 2004. Prognostic precipitation in the Lokal-Modell (LM) of DWD. *COSMO Newsletter* **4**: 177–180.

Bek S, Ježek J, Bližňák V. 2010. Spatial relationship of heavy rains in the Czech Republic. *Advances in Geosciences* **25**: 85–90.

Berg P, Moseley C, Haerter JO. 2013. Strong increase in convective precipitation in response to higher temperatures. *Nature Geoscience* **6**: 181–185.

Bissolli P, Karsten F, Rapp J, Ziese M. 2011. Flooding in eastern central Europe in May 2010 – reasons, evolution and climatological assessment. *Weather* **66**: 147–153.

Blanchet J, Lehning M. 2010. Mapping snow depth return levels: smooth spatial modeling versus station interpolation. *Hydrology and Earth System Sciences* **14**: 2527–2544.

Boberg F, Berg P, Thejll P, Gutowski WJ, Christensen JH. 2010. Improved confidence in climate change projections of precipitation further evaluated using daily statistics from ENSEMBLES models. *Climate Dynamics* **35**(7–8): 1509–1520.

Bougeault P. 1985. A simple parameterization of the large-scale effects of cumulus convection. *Monthly Weather Review* **113**: 2108–2121.

Boyle J, Klein SA. 2010. Impact of horizontal resolution on climate model forecasts of tropical precipitation and diabatic heating for the TWP-ICE period. *Journal of Geophysical Research: Atmospheres* **115**: D23112.

Brázdil R, Štekl J. 1986. *Cirkulační procesy a atmosférické srážky v ČSSR*. Univerzita J. E. Purkyně, Brno (in Czech).

Brockhaus P, Lüthi D, Schär C. 2008. Aspects of the diurnal cycle in a regional climate model. *Meteorologische Zeitschrift* **17**(4): 433–443.

Buishand TA. 1991. Extreme rainfall estimation by combining data from several sites. *Hydrological Sciences Journal* **36**(4): 345–365.

Buishand TA, Jilderda R, Wijngaard JB. 2009. *Regionale verschillen in extreme neerslag*. Scientific Report WR 2009-01, KNMI, De Bilt, Netherland (in Dutch).

Cahynová M, Huth R. 2010. Circulation vs. climatic changes over the Czech Republic: A comprehensive study based on the COST733 database of atmospheric circulation classifications. *Physics and Chemistry of the Earth* **35**(9–12): 422–428.

Canfield RV, Olsen DR, Hawkins RH, Chen TL. 1980. Use of extreme value theory in estimating flood peaks from mixed populations. *Reports*. Paper 577.

Caporali E, Cavigli E, Petrucci A. 2008. The index rainfall in the regional frequency analysis of extreme events in Tuscany (Italy). *Environmetrics* **19**(7): 714–724.

Casanueva A, Kotlarski S, Herrera S, Fernández J, Gutiérrez JM, Boberg F, Colette A, Christensen OB, Goergen K, Jacob D, Keuler K, Nikulin G, Teichmann C, Vautard R. 2015. Daily precipitation statistics in a EURO-CORDEX RCM ensemble: added value of raw and bias-corrected high-resolution simulations. *Climate Dynamics*, in press. doi:10.1007/s00382-015-2865-x.

Castellarin A, Burn DH, Brath A. 2008. Homogeneity testing: How homogeneous do heterogeneous cross-correlated regions seem? *Journal of Hydrology* **360**(1–4): 67–76.

Chan SC, Kendon EJ, Fowler HJ, Blenkinsop S, Ferro CAT, Stephenson DB. 2013. Does increasing the spatial resolution of a regional climate model improve the simulated daily precipitation? *Climate Dynamics* **41**(5–6): 1475–1795.

Christensen JH, Christensen OB, Lopez P, van Meijgaard E, Botzet M. 1996. *The HIRHAM4 regional atmospheric climate model*. Scientific Report 96–4. Danish Meteorological Institute: Copenhagen, Denmark.

Christensen JH, Kjellström E, Giorgi F, Lenderink G, Rummukainen M. 2010. Weight assignment in regional climate models. *Climate Research* **44**(2–3):179–194.

Christensen OB, Drews M, Christensen JH, Dethloff K, Ketelsen K, Hebestadt I, Rinke A. 2007. *The HIRHAM Regional Climate Model Version 5 (beta)*. Technical Report 06–17. Danish Meteorological Institute: Copenhagen, Denmark.

Churchill DD, Houze RA Jr. 1984. Development and structure of winter monsoon cloud cluster on 10 December (1978). *Journal of the Atmospheric Sciences* **41**: 933–960.

Coles S. 2001. *An Introduction to Statistical Modeling of Extreme Values*. Springer: London, UK.

Coles S, Heffernan J, Tawn J. 1999. Dependence measures for extreme value analyses. *Extremes* **2**(4): 339–365.

Cunnane C. 1988. Methods and merits of regional flood frequency analysis. *Journal of Hydrology* **100**(1–3): 269–290.

Dai A. 2006. Precipitation characteristics in eighteen coupled climate models. *Journal of Climate* **19**: 4605–4630.

Dai A, Trenberth KE. 2004. The diurnal cycle and its depiction in the community climate system model. *Journal of Climate* **17**:930–951.

Davison AC, Hinkley DV. 1997. *Bootstrap methods and their application*. Cambridge University Press: Cambridge, UK.

Dee DP, Uppala SM, Simmons AJ, Berrisford P, Poli P, Kobayashi S, Andrae U, Balmaseda MA, Balsamo G, Bauer P, Bechtold P, Beljaars ACM, van de Berg L, Bidlot J, Bormann N, Delsol C, Dragani R, Fuentes M, Geer AJ, Haimberger L, Healy SB, Hersbach H, Hólm EV, Isaksen L, Kållberg P, Köhler M, Matricardi M, McNally AP, Monge-Sanz BM, Morcrette J-J, Park B-K, Peubey C, de Rosnay P, Tavolato C, Thépaut J-N, Vitart F. 2011. The ERA-interim reanalysis: configuration and performance of the data assimilation system. *Quarterly Journal of the Royal Meteorological Society* **137**(656): 553–597.

Déqué M, Rowell DP, Lüthi D, Giorgi F, Christensen JH, Rockel B, Jacob D, Kjellström E, de Castro M, van den Hurk B. 2007. An intercomparison of regional climate simulations for Europe: assessing uncertainties in model projections. *Climate Change* **81**:53–70

Dittus AJ, Karoly DJ, Lewis AC, Alexander LV. 2015. A multiregional assessment of observed changes in the areal extent of temperature and precipitation extremes. *Journal of Climate* **28**: 9206–9220.

Doms G, Förstner J, Heise E, Herzog H-J, Mironov D, Raschendorfer M, Reinhardt T, Ritter B, Schrodin R, Schulz J-P, Vogel G. 2011. *A Description of the Nonhydrostatic Regional COSMO Model. Part II: Physical Parameterization*. Deutscher Wetterdiens: Offenbach, Germany.

Donat MG, Alexander LV, Yang H, Durre I, Vose R, Dunn RJH, Willett KM, Aguilar E, Brunet M, Caesar J, Hewitson B, Jack C, Klein Tank AMG, Kruger AC, Marengo J, Peterson TC, Renom M, Oria Rojas C, Rusticucci M, Salinger J, Elrayah AS, Sekele SS, Srivastava AK, Trewin B, Villarroel C, Vincent LA, Zhai P, Zhang X, Kitching S. 2013. Updated analyses of temperature and precipitation extreme indices since the beginning of the twentieth century: The HadEX2 dataset. *Journal of Geophysical Research: Atmospheres* **118**(5): 2098–2118.

Durman CF, Gregory JM, Hassell DC, Jones RG, Murphy JM. 2006. A comparison of extreme European daily precipitation simulated by a global and a regional climate model for present and future climates. *Quarterly Journal of the Royal Meteorological Society* **127**(573): 1005–1015.

ECMWF-IFS. 2007. *IFS Documentation-Cy31r1. Part IV: Physical Processes.* ECMWF: Reading, UK.

Efron B. 1987. Bootstrap methods: Another look at the jackknife. *The Annals of Statistics* **7**(1): 1–26.

Escalante-Sandoval C. 2008. Bivariate distribution with two-component extreme value marginals to model extreme wind speeds. *Atmósfera* **21**(4): 373–387.

Farda A, Déqué M, Somot S, Horanyi A, Spiridonov V, Toth H. 2010. Model Aladin as regional climate model for Central and Eastern Europe. *Studia Geophysica et Geodaetica* **54**: 313–332.

Farda A, Štěpánek P, Halenka T, Skalák P, Belda M. 2007. Model Aladin in climate mode forced with ERA-40 reanalysis (coarse resolution experiment). *Meteorological Journal* **10**: 123–130.

Fischer AM, Keller DE, Liniger MA, Rajczak J, Schär C, Appenzeller C. 2015. Projected changes in precipitation intensity and frequency in Switzerland: A multi-model perspective. *International Journal of Climatology* **35**(11): 3204–3219.

Fowler HJ, Ekström M, Blenkinsop S, Smith AP. 2007. Estimating change in extreme European precipitation using a multimodel ensemble. *Journal of Geophysical Research: Atmospheres* **112**: D18104.

Frei C, Christensen J, Deque M, Jacob D, Jones R, Vidale P. 2003. Daily precipitation statistics in regional climate models: Evaluation and intercomparison for the European Alps. *Journal of Geophysical Research: Atmospheres* **108**(D3): 4124.

Frei C, Schär C. 1998. A precipitation climatology of the Alps from high-resolution rain-gauge observations. *International Journal of Climatology* **18**: 873-900.

Frei C, Schöll R, Fukutome S, Schmidli J, Vidale PL. 2006. Future change of precipitation extremes in Europe: Intercomparison of scenarios from regional climate models. *Journal of Geophysical Research: Atmospheres* **111**: D06105.

Frich P, Alexander LV, Della-Marta P, Gleason B, Haylock M, Klein Tank AMG, Peterson T. 2002. Observed coherent changes in climatic extremes during the second half of the twentieth century. *Climate Research* **19**(3): 193–212.

Gaál L, Beranová R, Hlavčová K, Kyselý J. 2014. Climate change scenarios of precipitation extremes in the Carpathian region based on an ensemble of regional climate models. *Advances in Meteorology* **2014**: ID 943487.

Gerard L, Geleyn J-F. 2005. Evolution of a subgrid deep convection parametrization in a limited-area model with increasing resolution. *Quarterly Journal of the Royal Meteorological Society* **131**: 2293–2312.

Giorgi F, Bi X, Pal JS. 2004. Mean, interannual variability and trends in a regional climate change experiment over Europe. I. Present day climate (1961–1990). *Climate Dynamics* **22**: 733–756

Giorgi F, Coppola E. 2009. Projections of twenty-first century climate over Europe. *The European Physical Journal Conferences* **1**: 29–46.

Giorgi F, Marinucci MR. 1996. An investigation of the sensitivity of simulated precipitation to model resolution and its implications for climate studies. *Monthly Weather Review* **124**: 148–166.

Gomes L, Vickery BJ. 1978. Extreme wind speeds in mixed wind climates. *Journal of Wind Engineering and Industrial Aerodynamics* **2**(4): 331–344.

Gregersen IB, Sørup HJD, Madsen H, Rosbjerg D, Mikkelsen PS, Arnbjerg-Nielsen K. 2013. Assessing future climatic changes of rainfall extremes at small spatio-temporal scales. *Climate Change* **118**: 783–797.

Gregory D, Guichard F. 2002. Aspects of the parametrization of organized convection: contrasting cloud-resolving model and single-column model realizations. *Quarterly Journal of the Royal Meteorological Society* **128**(580): 625–646.

Guichard F, Petch JC, Redelsperger J-L, Bechtold P, Chaboureaou J-P, Cheiner S, Grabowski W, Grenier H, Jones CG, Köhler M, Piriou J-M, Tailleux R, Tomasini M. 2004. Modelling the diurnal cycle of deep precipitating convection over land with cloud-resolving models and single-column models. *Quarterly Journal of the Royal Meteorological Society* **130**(604): 3139–3172

Gumbel EJ. 1958. *Statistics of Extremes*. Columbia University Press: New York, USA.

Haerter JO, Berg P. 2009. Unexpected rise in extreme precipitation caused by a shift in rain type? *Nature Geoscience* **2**(6): 372-373.

Hagemann S, Arpe K, Bengtsson L. 2005. *Validation of the hydrological cycle of ERA40*. Reports on Earth System Science 10, Max-Planck-Institute for Meteorology: Hamburg, Germany.

Hanel M, Buishand TA. 2010. On the value of hourly precipitation extremes in regional climate model simulations. *Journal of Hydrology* **393**(3–4): 265–273,

Hanel M, Buishand TA, Ferro CAT. 2009. A nonstationary index flood model for precipitation extremes in transient regional climate model simulations. *Journal of Geophysical Research: Atmospheres* **114**(D15): D15107.

Hanslian D, Brázdil R, Štekl J, Kakos V. 2000. The effect of cyclones of Mediterranean origin on high daily precipitation totals at Mt. Milešovka and Mt. Lysá hora in the period 1961-1995. *Meteorological Bulletin* **53**(2): 33-41 (In Czech).

Heinrich G, Gobiet A. 2012. The future of dry and wet spells in Europe: A comprehensive study based on the ENSEMBLES regional climate models. *International Journal of Climatology* **32**(13): 1951–1970.

Herrera S, Fita L, Fernández J, Gutiérrez JM. 2010. Evaluation of the mean and extreme precipitation regimes from the ENSEMBLES regional climate

multimodel simulation over Spain. *Journal of Geophysical Research: Atmospheres* **115**: D21117.

Hohenegger C, Brockhaus P, Schär C. 2008. Towards climate simulations at cloud-resolving scales. *Meteorologische Zeitschrift* **17**(4): 383–394.

Holtanová E, Mikšovský J, Kalvová J, Pišoft P, Motl M. 2012. Performance of ENSEMBLES regional climate models over Central Europe using various metrics. *Theoretical and Applied Climatology* **108**(3): 463–470.

Hosking JRM, Wallis JR. 1997. *Regional Frequency Analysis. An Approach Based on L-moments*. Cambridge University Press: Cambridge, UK.

Houze RA Jr. 1973. A climatological study of vertical transport by cumulus-scale convection. *Journal of the Atmospheric Sciences* **30**: 1112-1123.

Houze RA Jr. 1993. *Cloud dynamics*. International Geophysics Series 53, Academic Press: San Diego, USA.

Houze RA Jr. 1997. Stratiform precipitation in regions of convection: A meteorological paradox? *Bulletin of the American Meteorological Society* **78**: 2179–2196

Hu L, Li Y, Song Y, Deng D. 2011. Seasonal variability in tropical and subtropical convective and stratiform precipitation of the East Asian monsoon. *Science China Earth Science* **54**: 1595–1603.

Huff FA, Shipp WL. 1969. Spatial correlations of storm, monthly, and seasonal precipitation. *Journal of Applied Meteorology* **8**: 542–550.

Huth R, Kyselý J. 2000. Constructing site-specific climate change scenarios on a monthly scale using statistical downscaling. *Theoretical and Applied Climatology* **66**(1): 13–27.

Jacob D. 2001. A note to the simulation of the annual and inter-annual variability of the water budget over the Baltic Sea drainage basin. *Meteorology and Atmospheric Physics* **77**: 61–73.

Jacob D, Bärring L, Christensen OB, Christensen JH, de Castro M, Déqué M, Giorgi F, Hagemann S, Hirschi M, Jones R, Kjellström E, Lenderink G, Rockel B, Sánchez E, Schär C, Seneviratne SI, Somot S, van Ulden A, van den Hurk B.

2007. An inter-comparison of regional climate models for Europe: Model performance in present-day climate. *Climate Change* **81**: 31–52.

Jacob D, Petersen J, Eggert B, Alias A, Christensen OB, Bouwer LM, Braun A, Colette A, Déqué M, Georgievski G, Georgopoulou E, Gobiet A, Menut L, Nikulin G, Haensler A, Hempelmann N, Jones C, Keuler K, Kovats S, Kröner N, Kotlarski S, Kriegsmann A, Martin E, van Meijgaard E, Moseley C, Pfeifer S, Preuschmann S, Radermacher C, Radtke K, Rechid D, Rounsevell M, Samuelsson P, Somot S, Soussana J-F, Teichmann C, Valentini R, Vautard R, Weber B, Yiou P. 2014. EURO-CORDEX: New high-resolution climate change projections for European impact research. *Regional Environmental Change* **14**(2): 563–578.

Jaeger E, Anders I, Luthi D, Rockel B, Schär C, Seneviratne S. 2008. Analysis of ERA40-driven CLM simulation for Europe. *Meteorologische Zeitschrift* **17**(4): 349–367.

Kain JS. 2004. The Kain-Fritsch convective parameterization: An update. *Journal of Applied Meteorology* **43**: 170–181.

Kain JA, Fritsch JM. 1990. A one-dimensional entraining/detraining plume model and its application in convective parameterization. *Journal of Atmospheric Sciences* **47**(23): 2784–2802.

Kain JS, Fritsch JM. 1993. Convective parameterization for mesoscale models: The Kain-Fritsch scheme. The representation of cumulus convection in numerical models. Meteorological Monographs 24, American Meteorological Society, 165–170.

Karagiannidis AF, Karacostas T, Maheras P, Makrogiannis T. 2012. Climatological aspects of extreme precipitation in Europe, related to mid-latitude cyclonic systems. *Theoretical and Applied Climatology* **107**: 165-174.

Kendall M. 1975. *Multivariate Analysis*. Charles Griffin & Company: London, UK.

Kendon EJ, Roberts NM, Fowler HJ, Roberts MJ, Chan SC, Senior C. 2014. Heavier summer downpours with climate change revealed by weather forecast resolution model. *Nature Climate Change* **4**: 570–576.

Kendon EJ, Roberts NM, Senior CA, Roberts MJ. 2012. Realism of rainfall in a very high-resolution regional climate model. *Journal of Climate* **25**(17): 5791–5806.

Kjellström E, Bärring L, Gollvik L, Hansson U, Jones C, Samuelsson P, Rummukainen M, Ullerstig A, Willén U, Wyser K. 2005. *A 140-year simulation of European climate with the new version of the Rossby Centre regional atmospheroc climate model (RCA3)*. SMHI reports meteorology and climatology 108, SMHI, SE-60176. Norrköping, Sweden.

Kjellström E, Boberg F, Castro M, Christensen JH, Nikulin G, Sanchéz E. 2010. Daily and monthly temperature and precipitation statistics as performance indicators for regional climate models. *Climate Research* **44**: 135–150.

Klein Tank AMG, Wijngaard JB, Können GP, Böhm R, Demarée G, Gocheva A, Mileta M, Pashiardis S, Hejkrlik L, Kern-Hansen C, Heino R, Bessemoulin P, Müller-Westermeier G, Tzanakou M, Szalai S, Pálsdóttir T, Fitzgerald D, Rubin S, Capaldo M, Maugeri M, Leitass A, Bukantis A, Aberfeld R, van Engelen AFV, Forland E, Mietus M, Coelho F, Mares C, Razuvaev V, Nieplova E, Cegnar T, Antonio López J, Dahlström B, Moberg A, Kirchhofer W, Ceylan A, Pachaliuk O, Alexander LV, Petrovic P. 2002. Daily dataset of 20th-century surface air temperature and precipitation series for the European Climate Assessment. *International Journal of Climatology* **22**(12): 1441–1453.

Kochanek K, Strupczewski WG, Bogdanowicz E. 2012. On seasonal approach to flood frequency modelling. Part II: flood frequency analysis of Polish rivers. *Hydrological Processes* **26**(5): 717–730.

Kotlarski S, Keuler K, Christensen OB, Colette A, Déqué M, Gobiet A, Goergen K, Jacob D, Lüthi D, van Meijgaard E, Nikulin G, Schär C, Teichmann C, Vautard R, Warrach-Sagi K, Wulfmeyer V. 2014. Regional climate modeling on European scales: A joint standard evaluation of the EURO-CORDEX RCM ensemble. *Geoscientific Model Development* **7**(4): 1297–1333.

Kurejko IA. 1978. O radzeleniji a livnevych a obložnych osadkov. Trudy. UkrNIGMI 161: 97–102.

Kyselý J. 2009. Trends in heavy precipitation in the Czech Republic over 1961-2005. *International Journal of Climatology* **29**: 1745-1758.

Kyselý J. 2010. Coverage probability of bootstrap confidence intervals in heavy-tailed frequency models, with application to precipitation data. Theoretical and Applied Climatology **101**(3): 345–361.

Kyselý J, Beguería S, Beranová R, Gaál L, López-Moreno JI. 2012. Different patterns of climate change scenarios for short-term and multi-day precipitation extremes in the Mediterranean. *Global and Planetary Change* **98–99**: 63–72.

Kyselý J, Picek J. 2007. Regional growth curves and improved design value estimates of extreme precipitation events in the Czech Republic. *Climate Research* **33**(3): 243–255.

Kyselý J, Rulfová Z, Farda A, Hanel M. 2016. Convective and stratiform precipitation characteristics in an ensemble of regional climate model simulations. *Climate Dynamics* **46**(1): 227–243.

Laio F. 2004. Cramer–von Mises and Anderson-Darling goodness of fit tests for extreme value distributions with unknown parameters. *Water Resources Research* **40**(9): W09308.

Lam HY, Luini L, Din J, Capsoni C, Panagopoulos AD. 2010. Stratiform and convective rain discrimination for equatorial region. In: Proceedings of the 2010 IEEE Student Conference on Research and Development – Engineering: Innovation and Beyond, SCOReD 2010, 112–116.

Larsen MAD, Thejll P, Christensen JH, Refsgaard JC, Jensen KH. 2013. On the role of domain size and resolution in the simulations with the HIRHAM region climate model. *Climate Dynamics* **40**: 2903–2918.

Lee M-I, Schubert SD, Suarez MJ, Held IM, Kumar A, Bell TL, Schemm JKE, Lau NC, Ploshay JJ, Kim HK, Yoo SH. 2007. Sensitivity to horizontal resolution in the AGCM simulations of warm season diurnal cycle of precipitation over the United States and northern Mexico. *Journal of Climate* **20**: 1862–1881.

Lehmann J, Coumou D, Frieler K, Eliseev AV, Levermann A. 2014. Future changes in extratropical storm tracks and baroclinicity under climate change. *Environmental Research Letters* **9**(8): 084002.

Lehtonen I, Ruosteenoja K, Jylhä K. 2014. Projected changes in European extreme precipitation indices on the basis of global and regional climate model ensembles. *International Journal of Climatology* **34**(4): 1208–1222.

Lenderink G, Mok HY, Lee TC, van Oldenborgh GJ. 2011. Scaling and trends of hourly precipitation extremes in two different climate zones - Hong Kong and the Netherlands. *Hydrology and Earth System Sciences* **15**(9): 3033–3041.

Lenderink G, van der Hurk B, van Meijgaard E, van Ulden A, Cuijpers H. 2003. Simulation of present day climate in RACMO2: first results and model developments. Technical Report 252, KNMI: De Bilt, Netherlands.

Lenderink G, van Mejgaard E. 2008. Increase in hourly precipitation extremes beyond expectations from temperature changes. *Nature Geoscience* **1**: 511-514.

Lenderink G, van Mejgaard E. 2010. Linking increases in hourly precipitation extremes to atmospheric temperature and moisture changes. *Environmental Research Letters* **5**(2): 025208 (9pp).

Lettenmaier DP, Wallis JR, Wood EF. 1987. Effect of regional heterogeneity on flood frequency estimation. *Water Resources Research* **23**(2): 313–323.

Li F, Collins WD, Wehner MF, Williamson DL, Olson JG, Algieri C. 2011. Impact of horizontal resolution on simulation of precipitation extremes in an aqua-planet version of Community Atmospheric Model (CAM3). *Tellus* **63A**(5): 884–892.

Lohmann U, Roeckner E. 1996. Design and performance of a new cloud microphysics scheme developed for the ECHAM general circulation model, *Climate Dynamics* **12**(8): 557–572.

Loriaux JM, Lenderink G, De Roode SR, Pier Siebsma A. 2013. Understanding convective extreme precipitation scaling using observations and an entraining plume model. *Journal of the Atmospheric Sciences* **70**(11): 3641–3655.

Lu L-H, Stedinger JR. 1992. Sampling variance of normalized GEV/PWM quantile estimators and a regional homogeneity test. *Journal of Hydrology* **138**(1–2): 223–245.

Madsen H, Lawrence D, Lang M, Martinkova M, Kjeldsen TR. 2014. Review of trend analysis and climate change projections of extreme precipitation and floods in Europe. *Journal of Hydrology* **519**: 3634–3650.

Mann HB. 1945. Nonparametric tests against trend. *Econometrica* **13**(3) 245–259.

Mapes BE, Houze RA Jr. 1995. Diabatic divergence profiles in western Pacificmesoscaleconvectivesystems. *Journal of the Atmospheric Sciences* **52**: 1807–1828.

Maraun D, Osborn TJ, Rust HW. 2012. The influence of synoptic airflow on UK daily precipitation extremes. Part II: regional climate model and E-OBS data validation. *Climate Dynamics* **39**: 287–301.

Massey FJ. 1951. The Kolmogorov-Smirnov test for goodness of fit. *Journal of the American Statistical Association* **46**(253): 68–78.

May W. 2007. The simulation of the variability and extremes of daily precipitation over Europe by the HIRHAM regional climate model. *Global and Planetary Change* **57**: 59–82.

Moberg A, Jones PD. 2005. Trends in indices for extremes in daily temperature and precipitation in central and western Europe, 1901–99. *International Journal of Climatology* **25**: 1149–1171.

Molinari J, Dudek M. 1992. Parameterization of convective precipitation in mesoscale numerical models: a critical review. *Monthly Weather Review* **120**: 326–344.

Molnar P, Fatichi S, Gaál L, Szolgay J, Burlando P. 2015. Storm type effects on super Clausius–Clapeyron scaling of intense rainstorm properties with air temperature. *Hydrology and Earth System Sciences* **19**: 1753–1766.

Neggers RAJ. 2009. A dual mass flux framework for boundary layer convection. Part II: Clouds. *Journal of Atmospheric Sciences* **66**: 1489–1506.

Neggers RAJ, Köhler M, Beljaars ACM. 2009. A dual mass flux framework for boundary layer convection. Part I: Transport. *Journal of Atmospheric Sciences* **66**: 1465–1487.

Noguer M, Jones RG, Murphy JM. 1998. Sources of systematic errors in the climatology of a regional climate model over Europe. *Climate Dynamics* **14**: 691–712

Nordeng TE. 1994. *Extended version of the convection parameterization scheme at ECMWF and their impact upon the mean climate and transient activity of the*

model in the tropics. Research Department Technical Memorandum No. 206, ECMWF: Reading, UK.

Orlova EM. 1979. *Kratkosrocnyj prognoz atmosfernych osadkov*. Gidrometeoizdat Leningrad.

Overeem A, Buishand A, Holleman I. 2008. Rainfall depth-duration-frequency curves and their uncertainties. *Journal of Hydrology* 348(1–2): 124–134.

Overeem A, Buishand TA, Holleman I, Uijlenhoet R. 2010. Extreme value modeling of areal rainfall from weather radar. *Water Resources Research* **46**: W09514.

Panthou G, Mailhot A, Laurence E, Talbot G. 2014. Relationship between surface temperature and extreme rainfalls: A multi-time-scale and event-based analysis. *Journal of Hydrometeorology* **15**: 1999–2011.

Papalexiou SM, Koutsoyiannis D. 2013. Battle of extreme value distributions. A global survey on extreme daily rainfall. *Water Resources Research* **49**(1): 187–201.

Pauling A, Luterbacher J, Casty C, Wanner H. 2006. Five hundred years of gridded high-resolution precipitation reconstructions over Europe and the connection to large-scale circulation. *Climate Dynamics* **26**(4): 387–405.

Plavcová E, Kyselý J, Štěpánek P. 2013. Links between circulation types and precipitation in Central Europe in the observed data and regional climate model simulations. *International Journal of Climatology* **34**(9): 2885–2898.

Prein AF, Gobiet A, Truhetz H, Keuler K, Goergen K, Teichmann C, Fox Maule C, van Meijgaard E, Déqué M, Nikulin G, Vautard R, Colette A, Kjellström E, Jacob D. 2016. Precipitation in the EURO-CORDEX 0.11° and 0.44° simulations: High resolution, high benefits? *Climate Dynamics* **46**(1): 383–412.

Radu R, Déqué M, Somot S. 2008. Spectral nudging in a spectral regional climate model. *Tellus* **60A**(5): 898–910

Rajczak J, Pall P, Schär C. 2013. Projections of extreme precipitation events in regional climate simulations over Europe and the Alpine Region. *Journal of Geophysical Research: Atmospheres* **118**(9): 3610–3626.

Rasch PJ, Kristjánsson JE. 1998. A comparison of the CCM3 model climate using diagnosed and predicted condensate parameterizations. *Journal of Climate* **11**: 1587–1614.

Rauscher SA, Coppola E, Piani C, Giorgi F. 2010. Resolution effects on regional climate model simulations of seasonal precipitation over Europe. *Climate Dynamics* **35**(4): 685–711.

Řezáčová D, Kašpar M, Müller M, Sokol Z, Kakos V, Hanslian D, Pešice P. 2005a. A comparison of the flood precipitation episode in August 2002 with historic extreme precipitation events on the Czech territory. *Atmospheric Research* **77**: 354–366.

Řezáčová D, Pešice P, Sokol Z. 2005b. An estimation of the PMP for river basins in the Czech Republic. *Atmospheric Research* **77**: 407–421.

Rockel B, Geyer B. 2008. The performance of the regional climate model CLM in different climate regions, based on the example of precipitation. *Meteorologische Zeitschrift* **17**(4): 487–498.

Rossi F, Fiorentino M, Versace P. 1984. Two-component extreme value distribution for flood frequency analysis. *Water Resources Research* **20**(7): 847–856.

Ruiz-Leo AM, Hernández E, Queralt S, Maqueda G. 2013. Convective and stratiform precipitation trends in the Spanish Mediterranean coast. *Atmospheric Research* **119**: 46–55.

Rulfová Z, Beranová R, Kyselý J. 2016. Climate change scenarios of convective and large-scale precipitation in the Czech Republic based on EURO-CORDEX data (submitted to *International Journal of Climatology*).

Rulfová Z, Buishand A, Roth M, Kyselý J. 2016. A two-component generalized extreme value distribution for precipitation frequency analysis. *Journal of Hydrology* **534**: 659–668.

Rulfová Z, Kyselý J. 2013. Disaggregating convective and stratiform precipitation from station weather data. *Atmospheric Research* **134**: 100–115.

Samuelsson P, Jones CG, Willén U, Ullerstig A, Gollvik S, Hansson U, Jansson C, Kjellström E, Nikulin G, Wyser K. 2011. The Rossby centre regional climate model RCA3: Model description and performance. *Tellus* **63A**(1): 4-23.

Sanchéz E, Gallardo C, Gaertner MA, Arribas A, Castro M. 2004. Future climate extreme events in the Mediterranean simulated by a regional climate model: a first approach. *Global and Planetary Change* **44**: 163–180.

Schaefer MG. 1990. Regional analyses of precipitation annual maxima in Washington State. *Water Resources Research* **26**(1): 119–131.

Schumacher C, Houze RA Jr. 2003. Stratiform rain in the tropics as seen by the TRMM precipitation radar. *Journal of Climate* **16**: 1739–1756.

Sempere-Torres D, Sanchez-Diezma R, Zawadzki I, Creutin JD. 2000. Identification of stratiform and convective areas using radar data with application to the improvement of DSD analysis and Z-R relations. *Physics and Chemistry of the Earth* **25**(10-12): 985–990.

Sen PK. 1968. Estimates of the regression coefficient based on Kendall's tau. *Journal of the American Statistical Association* **63**: 1379–1389.

Sevruk B. 1997. Regional dependency of precipitation-altitude relationship in the Swiss Alps. *Climatic Change* **36**(3–4): 355–369.

Skalák P, Déqué M, Belda M, Farda A, Halenka T, Csima G, Bartholy J, Caian M, Spiridonov V. 2014. CECILIA regional climate simulations for present climate – validation and inter-comparison. *Climate Research* **60**: 1–12.

Skaugen T. 1997. Classification of rainfall into small- and large-scale events by statistical pattern recognition. *Journal of Hydrology* **200**(1–4): 40–57.

Sokol Z, Bližňák V. 2009. Areal distribution and precipitation-altitude relationship of heavy short-term precipitation in the Czech Republic in the warm part of the year. *Atmospheric Research* **94**: 652–662.

Stedinger JR, Vogel RM, Foufoula-Georgiou E. 1993. *Frequency analysis of extreme events*. Handbook of Hydrology, edited by D.R. Maidment, McGraw-Hill: New York, USA.

Steiner M, Houze RA Jr, Yuter SE. 1995. Climatological characterization of three-dimansional storm structure from operational radar and rain gauge data. *Journal of Applied Meteorology* **34**: 1978–2007.

Štekl J, Brázdil R, Kakos V, Jež J, Tolasz R, Sokol Z. 2001. *Extreme daily precipitation on the territory of the Czech Republic in the period 1879-2000 and their synoptic causes*. Czech Hydrometeorological Institute: Prague, Czech Republic.

Stephenson A. 2003. Simulating multivariate extreme value distributions of logistic type. *Extremes* **6**(1): 49–59.

Stewart EJ, Reed DW, Faulkner DS, Reynard NS. 1999. The FORGEX method of rainfall growth estimation I: Review of requirement. *Hydrology and Earth System Sciences* **3**(2): 187–195.

Strupczewski WG, Kochanek K, Bogdanowicz E, Markiewicz I. 2012. On seasonal approach to flood frequency modelling. Part I: Two-component distribution revised. *Hydrological Processes* **26**(5): 705–716.

Svensson C, Jones DA. 2010a. Review of rainfall frequency estimation methods. *Journal of Flood Risk Management* **3**(4): 296–313.

Svensson C, Jones DA. 2010b. Review of methods for deriving areal reduction factors. *Journal of Flood Risk Management* **3**(3): 232–245.

Swann H. 2001. Evaluation of the mass-flux approach to parametrizing deep convection. *Quarterly Journal of the Royal Meteorological Society* **127**(574): 1239–1260.

Tabony RC. 1983. Extreme value analysis in meteorology. *Meteorological Magazine* **12**: 77–98.

Tao W-K, Simpson J. 1984. Modeling study of a tropical squall-type convective line. *Journal of the Atmospheric Sciences* **46**: 177–202.

Tao W-K, Simpson J, Sui S-H, Ferrier B, Lang S, Scala J, Chou M-D, Pickering K. 1993. Heating, moisture, and water budgets of tropical and midlatitude squall lines: Comparisons and sensitivity to longwave radiation. *Journal of the Atmospheric Sciences* **50**: 673–690.

Tao W-K, Lang S, Simpson J, Olson WS, Johnson D, Ferrier B, Kummerow C, Adler R. 2000. Vertical profiles of latent heat release and their retrieval for TOGA COARE convective systems using a cloud resolving model, SSM/I, and ship-borne radar data. *Journal of Meteorological Society of Japan* **78**: 333–355.

Taylor KE, Stouffer RJ, Meehl GA. 2012. An overview of CMIP5 and the experiment design. *Bulletin of the American Meteorological Society* **93**: 485–498.

Thurai M, Gatlin PN, Bringi VN. 2016. Separating stratiform and convective rain types based on the drop size distribution characteristics using 2D video disdrometer data. *Atmospheric Research* **169**: 416–423.

Tiedtke M. 1989. A comprehensive mass flux scheme for cumulus parameterization in large-scale models. *Monthly Weather Review* **117**: 1779–1800.

Tiedtke M. 1993. Representation of clouds in large-scale models. *Monthly Weather Review* **121**: 3040–3061.

Tolasz R, Brázdil R, Bulíř O, Dobrovolný P, Dubrovský M, Hájková L, Halásová O, Hostýnek J, Janouch M, Kohut M, Krška K, Křivancová S, Květoň V, Lepka Z, Lipina P, Macková J, Metelka L, Míková T, Mrkvica Z, Možný M, Nekovář J, Němec L, Pokorný J, Reitschläger JD, Richterová D, Rožnovský J, Řepka M, Semerádová D, Sosna V, Stříž M, Šercl P, Škáchová H, Štěpánek P, Štěpánková P, Trnka M, Valeriánová A, Valter J, Vaníček K, Vavruška F, Voženílek V, Vráblík T, Vysoudil M, Zahradníček J, Zusková I, Žák M, Žalud Z. 2007. *Climate Atlas of Czechia*, Czech Hydrometeorological Institute and Palacký University: Prague and Olomouc, Czech Republic.

Tompkins AM, Gierens K, Rädel G. 2007. Ice supersaturation in the ECMWF integrated forecast system. *Quarterly Journal of Royal Meteorological Society* **133**(622): 53–63.

Tremblay A. 2005. The stratiform and convective components for surface precipitation. *Journal of the Atmospheric Sciences* **62**: 1513–1528.

Trenberth KE, Dai A, Rasmussen RM, Parsons DB. 2003. The changing character of precipitation. *Bulletin of the American Meteorological Society* **84**: 1205–1217.

Ungewitter G. 1970. Studien über tägliche Niederschlagssummen für das Gebiet der Bundesrepublik Deutschland. *Meteorologische Rundschau* **23**(4): 114–117.

Uppala SM, Kallberg PW, Simmons AJ, Andrae U, Bechtold VDC, Fiorino M, Gibson JK, Haseler J, Hernandez A, Kelly GA, Li X, Onogi K, Saarinen S, Sokka N, Allan RP, Andersson E, Arpe K, Balmaseda MA, Beljaars ACM, van de Berg L, Bidlot J, Bormann N, Caires S, Chevallier F, Dethof A, Dragosavac M, Fisher M, Fuentes M, Hagemann S, Hólm E, Hoskins BJ, Isaksen L, Janssen PAEM, Jenne R, Mcnally AP, Mahfouf J-F, Morcrette J-J, Rayner NA, Saunders RW, Simon P, Sterl A, Trenberth KE, Utch A, Vasiljevic D, Vuterbo P, Woollen J. 2005. The ERA-40 re-analysis. *Quarterly Journal of Royal Meteorological Society* **131**(612): 2961–3012.

van de Vyver H. 2012. Spatial regression models for extreme precipitation in Belgium. *Water Resources Research* **48**(9): W09549.

van den Brink HW, Können GP, Opsteegh JD. 2004. Statistics of extreme synoptic-scale wind speeds in ensemble simulations of current and future climate. *Journal of Climate* **17**(23): 4564–4574.

van Meijgaard E, van Ulft LH, Lenderink G, de Roode SR, Wipfler EL, Boers R, Timmermans RMA. 2012. *Refinement and Application of a Regional Atmospheric Model for Climate Scenario Calculations of Western Europe*. Programme Office Climate changes Spatial Planning: Nunspeet, Netherlands.

van Vuuren DP, Edmonds J, Kainuma M, Riahi K, Thomson A, Hibbard K, Hurtt GC, Kram T, Krey V, Lamarque J-F, Masui T, Meinshausen M, Nakicenovic N, Smith SJ, Rosse SK. 2011. The representative concentration pathways: An overview. *Climatic Change* **109**: 5–31.

Varin C, Reid N, Firth D. 2011. An overview of composite likelihood methods. *Statistica Sinica* **21**: 5–42.

Viglione A, Laio F, Claps P. 2007. A comparison of homogeneity tests for regional frequency analysis. *Water Resources Research* **43**(3): W03428.

Wagner S, Berg P, Schädler G, Kunstmann H. 2013. High resolution regional climate model simulations for Germany: Part II–projected climate changes. *Climate Dynamics* **40**(1): 415–427.

Wakazuki Y, Nakamura M, Kanada S, Muroi C. 2008. Climatological reproducibility evaluation and future climate projection of extreme precipitation events in the

baiu season using a high-resolution non-hydrostatic RCM in comparison with an AGCM. *Journal of the Meteorological Society of Japan* **86**: 951–967

Wang XL, Swail VR. 2001. Changes in extreme wave haights in northern hemisphere oceans and related atmospheric circulation regimes. *Journal of Climate* **14**: 2204–2221.

Waylen P, Woo M-K. 1982. Prediction of annual floods generated by mixed processes. *Water Resources Research* **18**(4): 1283–1286.

Westra S, Fowler HJ, Evans JP, Alexander LV, Berg P, Johnson F, Kendon EJ, Lenderink G, Roberts NM. 2014. Future changes to the intensity and frequency of short-duration extreme rainfall. *Reviews of Geophysics* **52**: 522–555.

Wilks DS. 1995. *Statistical Methods in the Atmospheric Science*. Academic Press: San Diego, USA.

Wilks DS. 2006. *Statistical Methods in the Atmospheric Sciences*. 2d ed. Academic Press: San Diego, USA.

Williamson DL. 2013. The effect of time steps and time-scales on parametrization suites. *Quarterly Journal of the Royal Meteorological Society* **139**: 548–560.

Yu R, Yuan W, Fu J. 2010. Diurnal phase of late-night against late-afternoon of stratiform and convective precipitation in summer southern sontiguous China. *Climate Dynamics* **35**: 567–576.

Zadra A, Caya D, Cote J, Dugas B, Jones C, Laprise R, Winger K, Caron L-P. 2008. The next Canadian regional climate model. *Physics in Canada* **64**: 75–83

Zappa G, Shaffrey LC, Hodges KI, Sansom PG, Stephenson DB. 2013. A multimodel assessment of future projections of North Atlantic and European extratropical cyclones in the CMIP5 climate models. *Journal of Climate* **26**(16): 5846–5862.

Zhang X, Vincent LA, Hog WD, Niitsoo A. 2000. Temperature and precipitation trends in Canada during the 20th century. *Atmosphere-Ocean* **38**(3): 395–429.

List of Figures

List of Tables

List of Abbreviations

Aladin	Regional climate model operated by the CNRM
Aladin_CZ	Regional climate model operated by the CHMI
ARF	Areal reduction factor
BET	Background-exceeding technique
CC	Clausius–Clapeyron
CCLM, CLM	Regional climate model – climate version of the operational weather forecast model COSMO (Consortium for Small-scale Modeling), RCMs operated by the CLM Community and ETHZ
CHMI	Czech Hydrometeorological Institute
CNRM	National Centre for Meteorological Research
C4I	Community Climate Change Consortium for Ireland
DMI	Danish Meteorological Institute
EC	Environment Canada
ENSEMBLES	ENSEMBLES-based Predictions of Climate Changes and their Impacts
ERA-Interim, ERA-40	European Centre for Medium-Range Weather Forecasts reanalyses
ETHZ	Swiss Federal Institute of Technology Zürich
EURO-CORDEX	Coordinated Downscaling Experiment - European Domain
EVT	Extreme Value Theory
GCM	Global Climate Model
GEMLAM	Regional climate model operated by the EC
GEV	Generalized Extreme Value
HIRHAM	Regional climate model operated by the DMI

ICTP	International Centre for Theoretical Physics
KNMI	Koninklijk Nederlands Meteorologisch Instituut (Royal Netherlands Meteorological Institute)
MPI	Max-Planck Institute
OBS	Observations
PROMES	Regional climate model operated by the UCLM
RACMO, RACMO2	Regional climate model developed and operated by the KNMI
RegCM	Regional climate model developed at the National Center for Atmospheric Research and operated by the ICTP
REMO	Regional climate model operated by the MPI
RCA, RCA4	Regional climate model operated by the SMHI
RCA_C4I	Regional climate model operated by the C4I
RCM	Regional Climate Model
RII	Rain Intensity Index
SMHI	Swedish Meteorological and Hydrological Institute
SYNOP	Surface Synoptic Observations
TCGEV	Two-component Generalized Extreme Value
UCLM	University of Castilla-La Mancha

Attachments

Attachment A.1

Codes of weather state in the SYNOP reports characterizing convective and stratiform precipitation

Table A.1: Codes of weather state characterizing convective precipitation.

1. Non-precipitation events	**2. Precipitation within past hour but not at observation time**
17 thunderstorm but no precipitation falling at station	25 snow showers
18 squalls within sight but no precipitation falling at station	26 snow showers
	27 hail showers
19 funnel clouds within sight	29 thunderstorms
3. Showers	**4. Thunderstorms**
	91 thunderstorm in past hour, currently only light rain
80 light rain showers	
81 moderate to heavy rain showers	92 thunderstorm in past hour, currently only moderate to heavy rain
82 violent rain showers	
83 light rain and snow showers	93 thunderstorm in past hour, currently only light snow or rain/snow mix
84 moderate to heavy rain and snow showers	
85 light snow showers	94 thunderstorm in past hour, currently only moderate to heavy snow or rain/snow mix
86 moderate to heavy snow showers	
87 light snow/ice pellet showers	95 light to moderate thunderstorm
88 moderate to heavy snow/ice pellet showers	96 light to moderate thunderstorm with hail
	97 heavy thunderstorm
89 light hail showers	98 heavy thunderstorm with duststorm
90 moderate to heavy hail showers	99 heavy thunderstorm with hail

Table A.2: Codes of weather state characterizing stratiform precipitation.

1. Precipitation within past hour but not at observation time	**2. Drizzle**
20 drizzle	50 intermittent light snow
20 drizzle	51 continuous light drizzle
21 rain	52 intermittent moderate drizzle
22 snow	53 continuous moderate drizzle
23 rain and snow	54 intermittent heavy drizzle
24 freezing rain	55 continuous heavy drizzle
	56 light freezing drizzle
	57 moderate to heavy freezing drizzle
	58 light drizzle and rain
	59 moderate to heavy drizzle and rain
3. Rain (not in the form of showers)	**4. Snow (not in the form of showers)**
60 intermittent light rain	70 intermittent light snow
61 continuous light rain	71 continuous light snow
62 intermittent moderate rain	72 intermittent moderate snow
63 continuous moderate rain	73 continuous moderate snow
64 intermittent heavy rain	74 intermittent heavy snow
65 continuous heavy rain	75 continuous heavy snow
66 light freezing rain	76 diamond dust
67 moderate to heavy freezing rain	77 snow grains
68 light rain and snow	78 snow crystals
69 moderate to heavy rain and snow	79 ice pellets

Attachment A.2

Annual cycle of 6-hour convective and stratiform precipitation amount and their maxima

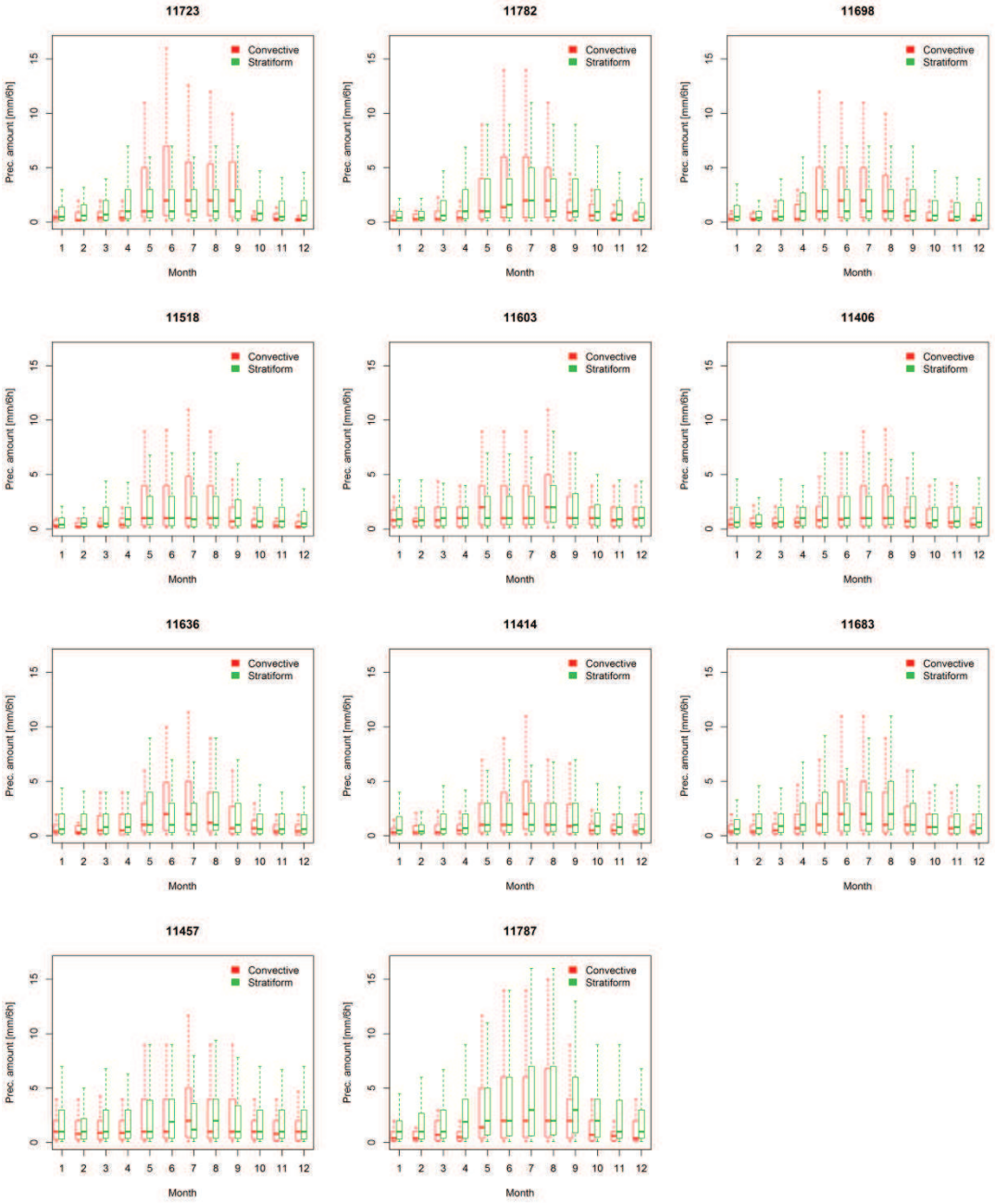

Figure A.1: Boxplots of all non-zero 6-hour convective and stratiform precipitation amount for each month.

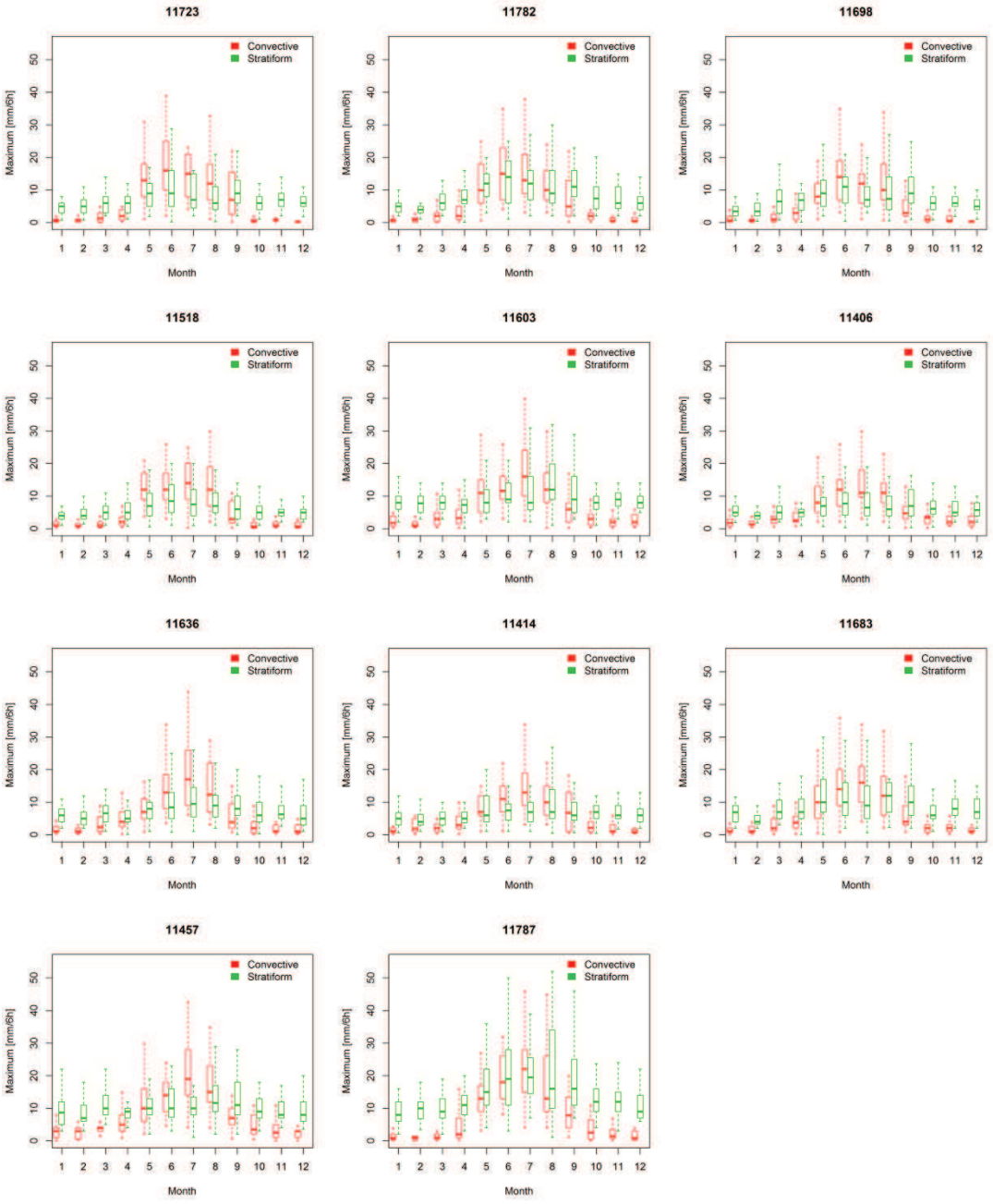

Fugire A.2: Boxplots of maximum monthly 6-hour convective and stratiform precipitation amount for each month.

Attachment A.3

Testing for homogeneity using the statistic *R*

In the bootstrap procedure the data are transformed to standard Gumbel residuals to remove spatial heterogeneities. These residuals are resampled with replacement and then transformed to GEV variables with parameters satisfying the homogeneity assumption. The statistic *R* is calculated for these simulated data and compared with the observed value of *R*.

For testing homogeneity of the shape parameter at *n* sites, i.e., $\kappa_1 = \kappa_2 = \ldots = \kappa_n$, the bootstrap procedure consists of the following steps:

1. Calculate standard Gumbel residuals:

$$\tilde{x}_{it} = \frac{1}{\hat{\kappa}_i} \ln\left[1 + \hat{\kappa}_i\left(\frac{x_{it} - \hat{\mu}_i}{\hat{\alpha}_i}\right)\right], \quad i = 1,...,n;\ t = 1,...,N \tag{A.1}$$

   where x_{it} is the annual maximum at site *i* for year *t*, *N* is the number of years, and $\hat{\kappa}_i, \hat{\alpha}_i$ and $\hat{\mu}_i$ are the L-moment estimates of the GEV parameters at site *i*.

2. Take the average $\bar{\kappa}$ of the estimated shape parameters as the estimate of the common shape parameter under the null hypothesis, and re-estimate α_i and μ_i by the method of L-moments, given $\kappa_1 = \kappa_2 = \cdots = \kappa_n = \bar{\kappa}$. Denote these estimates as $\hat{\alpha}_{i0}$ and $\hat{\mu}_{i0}$.

3. Draw a sample from the standard Gumbel residuals by resampling from the years 1,…,*N* with replacement. For each selected year *u* the Gumbel residuals $\tilde{x}_{iu}, i = 1, \ldots, n$ are entered in the bootstrap sample. This preserves spatial dependence.

4. Transform the resampled Gumbel residuals to GEV variables with a common shape parameter:

$$x^*_{iu} = \hat{\mu}_{i0} + \hat{\alpha}_{i0}\frac{\exp\left(\bar{\kappa}\tilde{x}_{iu}\right) - 1}{\bar{\kappa}}, \quad i = 1,...,n;\ u = 1,...,N. \tag{A.2}$$

5. Re-estimate κ for each site in the region, and recalculate the statistic *R*. The recalculated test statistic is denoted as *R**.

6. Repeat steps 3 to 5 until the desired number of bootstrap samples is obtained. The p-value is the fraction of R^* values larger than R.

In the test on homogeneity of the dispersion coefficient γ, common estimates $\hat{\kappa}_0$ and $\hat{\gamma}_0$ of the shape parameter and dispersion coefficient were used in the transformation (A.2). These estimates were derived in step 2 from the average L-moment ratios over the study area (Hosking and Wallis, 1997). In step 2 the location parameter was re-estimated assuming a constant shape parameter and dispersion coefficient.

For the test on the homogeneity of the location parameter μ, a common location parameter was estimated in step 2 as the average of the at-site estimates. In addition to the calculation of the statistic R in step 5, least squares regressions of the at-site locations parameters on altitude and mean annual precipitation amount were performed and the statistic R was calculated for the residuals of the regression. Note that for testing the adequacy of the regression, it is not necessary to include the fitted regression line in the transformation (A.2), because this does not affect the values of the least-squares residuals.